MICRODERMABRASION FOR TRANSDERMAL DRUG DELIVERY

A Thesis
Presented to
The Academic Faculty

by

Samantha N. Andrews

In Partial Fulfillment
of the Requirements for the Degree
Doctor of Philosophy in Biomedical Engineering
in the
The Wallace H. Coulter Department of Biomedical Engineering

Georgia Institute of Technology

December 2010

MICRODERMABRASION FOR TRANSDERMAL DRUG DELIVERY

Approved by:

Dr. Mark Prausnitz, Advisor
School of Chemical Engineering & Biomolecular Engineering
Georgia Institute of Technology

Dr. Julia Babensee
Wallace H. Coulter Department of Biomedical Engineering
Georgia Institute of Technology

Dr. Gilda Barabino
Wallace H. Coulter Department of Biomedical Engineering
Georgia Institute of Technology

Dr. Niren Murthy
Wallace H. Coulter Department of Biomedical Engineering
Georgia Institute of Technology

Dr. Richard Compans
Emory School of Medicine
Emory University

Dr. Eric Tomlinson
Altea Therapeutics

Date Approved: August 17, 2010

To my mother,
whose tireless sacrifices continue to inspire me everyday

ACKNOWLEDGEMENTS

I would like to thank my advisor, committee members, and funding sources for making it possible for me to carry out my thesis work. Thanks to Dr. Mark Prausnitz for serving as a great mentor and for guiding me through graduate school. I would also like to thank my thesis committee members, Dr. Barabino, Dr. Tomlinson, Dr. Murthy, Dr. Babensee, and Dr. Compans, for their support, feedback, and suggestions for my project.

Many thanks to all the members of the Prausnitz lab, past and present, for all their guidance, and support in help me to complete my project. I will cherish the great laughs, friendships, cultural lessons, lab socials, and conferences. Dr. Harvinder Gill was instrumental in getting me started on my project. His mentoring helped me to start a project in which I had no prior experience. Dr. Jeong Woo Lee and Dr. Seong-O Choi, my "Dream Team", were always willing to assist me with my in vivo studies and ELISA. Thanks to Dr. Yue-Chun Kim and Aritra Sengupta for helping with the in vitro delivery study and Dr. Tanicia Daley for supplying insulin. Dr. Vladimir Zarnitsyn was instrumental in helping me with designing and fabricating the masks for my project. Samir Patel was always willing to assist with the education outreach demos and tissue harvesting. I am sure we both scared a few kids out of science, at least not intentionally. Dr. Prerona Chakravarty and Ying Liu, my lab sisters, thanks for all the fun times we spent together from the road trips, to the trips to Vortex and Macy's, and of course teriyaki chicken. Thanks to Dr. Hyo-Jick Choi, Yoo Chun Kim, James Norman, Dr. Leonard Chu, Chris Edens, Dr. Saffar Moonsor, Dr. Robyn Schlicher, Dr. Jyoti Gupta, and Dr. Cetin Tas for your support and guidance during my time as a graduate student.

I would like to thank my undergraduate students Eunhye (Grace) Jeong, Brian Bondy, and Samantha Koncal for their assistance with my project. I appreciate their enthusiasm, dedication, and all their histology sectioning. Thanks to Brian Bondy for counting the hundreds of particle for the velocity measurements. It was a pleasure working with all of them.

I would like to extend gratitude to Donna Bondy, our lab assistant. Without her, our lab would be chaotic. Thanks to Donna for being organized, caring, and for baking goodies for the lab.

Thanks to the members of the Compans lab for their help with the in vivo vaccine study. Their research and assay expertise was invaluable in helping to carry out the experiment. Special thanks to Dr. Dimitrios Koutsonanos and Dr. Ioanna Skountzou for their advice and support of my thesis.

Thanks to Altea Therapeutics for enhancing my graduate school experience by allowing me to intern at the company. It was a good learning experience and provided a great introduction into preclinical research at a start up company. I am grateful for their support of my thesis work and for giving me an opportunity to work in an industrial position.

Thanks to the IBB staff and core facilities for their help in the completion of my project. Thanks to Tracey Couse and Aqua Ashberry for helping with histology. I appreciate their help in training, performing immunohistochemistry, and their friendship. Thanks to Steve Woodward for maintaining all the core facilities and for helping with training. Lastly I would like to thank the IBB administrative staff for their help with packages and letting me in the lab when I couldn't find my Buzz Card.

Thanks to my University of Florida engineering family. Dr. Jonathan F.K. Earle thanks for taking a chance on the girl from the Florida Panhandle and for making it your personal

mission to help UF minority engineering students complete their degrees. Thanks for making sure I did not get sidetracked at UF and for reminding me that engineering is an obligation, not a sacrifice. Thanks to UF NSBE, Mrs. Margie Williams, Mr. Earl Wade for encouraging me to attend graduate school and for their support during my time at Georgia Tech.

Last, but not least I would like to thank my family, especially my mother and brothers, for their prayers and words of encouragement. Thanks to my mother, Danita Sheffield, for being my biggest cheerleader during highs and lows of graduate and for reminding me that I can preserve through anything. Thanks to my brothers, Eddie, Cornelius, Quinn, and Quentin, for being great supporters and for not asking why graduate school takes so long to complete.

Table of Contents

LIST OF TABLES

LIST OF FIGURES

LIST OF SYMBOLS AND ABBREVIATIONS

ANOVA	Analysis of variance
D	Dermis
Da	Daltons
DNA	Deoxyribonucleic acid
ELISA	Enzyme-linked Immunosorbant Assay
ECM	Extracellular matrix
FDA	Food and Drug Administration
FITC	Fluorescein isothiocyanate
HAI	Hemagglutinin Inhibition Assay
H&E	Hematoxylin and eosin
H_3P0_4	Phosphoric Acid
IACUC	Institutional Animal Care and Use Committee
IM	Intramuscular injection
MMP	Matrix metalloproteinase
MDA	Microdermabrasion
MN	Microneedles
MVA	Modified Vaccina Ankara
MW	Molecular weight
NC	Negative control
OCT	Optimal Cutting Temperature
PET	Polyethylene terephthalate

PBS	Phosphate buffered saline
R18	Octadecyl rhodamine B chloride
RBCs	Red blood cells
SC	Stratum corneum
STZ	Streptozocin
SQ	Subcutaneous injection
SR	Sulforhodamine
BSA	Texas Red Bovine Serum Albumin
TEWL	Trans-epidermal water loss
U	Units of insulin
VE	Viable epidermis

SUMMARY

The skin serves as a semi-permeable barrier that protects the body from pathogens and water loss. The stratum corneum, the upper 10-15 μm layer of skin, controls the transport of substances into the body and is the primary barrier to transdermal drug delivery. Due to its structure, only drugs that are lipophilic and low molecular weight (<500 Da) can penetrate intact stratum corneum. This study examines the use of microdermabrasion as a method of removing the stratum corneum to increase the skin's permeability to hydrophilic molecules, proteins, and vaccines. Microdermabrasion is a FDA-approved cosmetic skin resurfacing procedure that removes the stratum corneum by bombarding it with abrasive particles under vacuum. The stratum corneum is not innervated or vascularized and is constantly being rejuvenated. Therefore, removing it does not cause pain, bleeding, or permanent damage. In this thesis we will determine for the first time if microdermabrasion can be optimize completely remove the stratum corneum, without damaging the viable epidermis, to allow delivery of large hydrophilic molecules, proteins, and vaccines into the skin.

The aims of this thesis are focused on optimizing the microdermabrasion conditions that will selectively remove stratum corneum with and with a mask, evaluating the transport of different sized molecules through abraded skin in vitro, and determining the efficacy of insulin delivered in vivo and the kinetics of stratum corneum recovery after treatment. The first aim was to evaluate selective removal of stratum corneum using microdermabrasion with and without a mask. Without the mask, large areas of stratum corneum were removed to increase the skin's permeability. A stainless steel mask was fabricated to further control the three dimensional removal of stratum corneum and limit the area of removal, which is important for safety. The

microdermbrasion machine parameters such as crystal flow rate and the effect of pressure and crystal flow on the degree of stratum corneum removal were also characterized. We found the degree of stratum corneum removal was more dependant on the exposure time the crystal flow rate and not as much on the pressure. Abraded through a mask allowed better control of the abrasion area and the mask could be designed to be self limiting feature to prevent damaging the viable epidermis.

For the second aim, sulforhodamine, Texas Red bovine serum albumin, insulin, and inactivated influenza vaccine were delivered to porcine and human skin in vitro that was abraded with and without a mask. The drugs were delivered for 1 to 54 hours. The drug delivery was assessed using horizontal and vertical diffusion cells and the drug concentration was quantified using fluorescence. In this aim, the affect of removing the viable epidermis was also evaluated. Removing the stratum corneum resulted in an increase in the skin permeability over unabraded skin. However, removing the viable epidermis allowed up to ten times higher penetration of the drugs than in the skin with stratum corneum removal.

The third aim evaluated in vivo microdermabrasion drug delivery with a mask and examined resealing of the skin after abrasion. Insulin was delivered to diabetic rats with stratum corneum or viable epidermis removal. For both cases there was a significant decrease in the blood glucose levels. The greatest differences in the two removal groups were the time lag and the magnitude of the blood glucose decrease. Removing only the stratum corneum resulted in a 4 hour time lag, while removing the epidermis resulted in a 30 min time lag. The maximum blood glucose decrease for the stratum corneum and viable epidermis was 43 and 147 mg/dL, respectively.

The resealing of the skin after abrasion was evaluated for 24 hr in hairless guinea pigs using electrical resistance, histology, and a hydrophilic dye to test the permeability of the skin. The affect of occlusive and non-occlusive coverings on the rate of stratum corneum recovery was also evaluated. Based on the electrical resistance data, we found that the non-occlusive skin resealed at a significantly higher rate than the occluded skin. Using histology data we found that the dye did not penetrate the skin 12 h after abrasion, which indicates that the stratum was recovered and functional. The difference in the results of the resistance and histology may be due to the occluded skin being permeable to ions, but not stratum corneum since it have not been fully resealed.

The results from this thesis show that microdermabrasion has the potential to further the field of transdermal drug delivery. In the future, the results from this project can be used to increase the number of effective topical drugs and vaccines to increase ease of delivery, increase patient compliance, and reduce the use of hypodermic needles.

CHAPTER 1
INTRODUCTION

Transdermal drug delivery is the transportation of drugs across the skin's surface and is a highly favorable delivery route since it does not involve the use of needles or cause pain and the drugs can avoid the first pass effect of the liver [1]. Despite the ease of drug delivery and the large availability of skin, only a few compounds can be administered using transdermal patches [1, 2]. The main barrier to transdermal drug delivery is the stratum corneum (SC), the outer most layer of skin. The SC is composed of dead flattened keratinocytes that are surrounded by a lipid extracellular matrix and its structure only allows low molecular weight (MW<500 Da) lipophilic compounds to penetrate intact skin [3].

Due to the difficulty of crossing the skin's surface, several techniques have been developed to overcome the SC barrier. These techniques include microneedles, thermal ablation, jet injectors, electroporation, iontophoresis, and abrasion. Microneedles are micron-size needles that penetrate the superficial dermis to deliver drugs and vaccines [4, 5]. They are not as painful as a hypodermic needle since they do not penetrate deep enough to stimulate the nerves in the dermis [6]. Thermal ablation uses heat generated by lasers or resistive heating to remove the SC and have been used to deliver vaccines and protein therapeutics [7-9]. The area of damage caused by ablation is often limited to the SC and viable epidermis (VE) to avoid pain and skin damage. Jet injectors use pressurized air to rapidly deliver therapeutics to the skin [10]. Electroporation and iontophoresis both use electrical current for drug delivery [1]. Abrasion uses abrasive particles, such as alumina, to remove the SC [11]. Abrasion can be carried out using sandpaper or microdermabrasion [12, 13]. The objective of this thesis is to study the use of

microdermabrasion as a method of selectively removing the SC to increase the skin's permeability for drug delivery.

Microdermabrasion (MDA) is a FDA-approved cosmetic technique that removes the skin layers using pressurized abrasive particles. Clinically, it is used to improve the skin's appearance by reducing the appearance of fine lines, wrinkles, and scars [14]. In most of the studies in the drug delivery literature, microdermabrasion has been used to partially abrade the SC to deliver small molecular weight hydrophilic compounds such as vitamin C (MW 176 Da) [7, 8, 13, 15]. Those studies did not completely remove the SC. If the SC is completely removed, then larger molecules, such as vaccines, can be delivered [12]. Though studies have used MDA to remove the SC, there are no studies that have examined the mechanics of abrasion or have characterized the MDA device. Studies are also needed to determine the range of drugs that can be delivered using MDA and the kinetics of skin healing after SC removal and the effect on drug delivery. The aims of this research will evaluate the use of MDA as a drug delivery technique, the efficacy of delivered drugs, and rate of skin healing after MDA.

Specific Aim 1 is to optimize the MDA conditions, using excised porcine skin, that will result in selective and complete SC removal, without removing the VE. The second part of the aim is to characterize the MDA device to quantify the settings and develop a skin abrasion model that correlates the settings to SC removal. **Specific Aim 2** is to conduct an in vitro drug delivery study to measure the flux of various compounds that are delivered using MDA. **Specific Aim 3** is to conduct an in vivo delivery experiment to deliver insulin and influenza to hairless rats and guinea pigs, respectively. This will determine if therapeutic levels of the drugs can be delivered using MDA. The kinetics of skin resealing was also examined in hairless guinea pigs to determine the time necessary for the SC to recover after removal and the effect on drug delivery.

CHAPTER 2
BACKGROUND

Transdermal Drug Delivery

The drug delivery field is ever evolving to design new technologies that efficiently and effectively deliver therapeutics. Currently there are several methods, such as inhalation, oral, and injections, that are commonly used to deliver drugs. The delivery route is dependent on the drug chemistry and its desired effect and target. Inhalation is a painless method of delivery that is used to administer small particles and proteins, such as insulin, to the lungs to elicit a local or systemic response. It has been long used as a route of delivery for the treatment of asthma and other respiratory ailments. Inhalation delivery has several drawbacks because drugs have to be designed to avoid disrupting breathing. Another disadvantage is that the patients who have respiratory ailments may not be able to use certain types of inhaled drugs, such as insulin [16]. Oral delivery is usually the most desired method of systemic delivery, due to its ease of administration. However, proteins cannot be delivered orally because they are degraded in the gastrointestinal tract. Drugs that are taken orally have a low bioavailability due to the first pass effect, in which the liver can degrade up to 90-95% of the active drug [17]. Injections are efficient in delivering proteins and vaccines locally and to the systemic circulation. Drugs delivered by injections are able to avoid the first pass effect, thus increasing the bioavailability of the drug and reducing the dosage. Injections are convenient, but are painful and pose a risk of disease transmission due to needle reuse and needle-stick injuries [6].

Another route of drug delivery is the transdermal route, which utilizes the skin's anatomy to deliver drugs both locally and systemically across the skin's surface using transdermal patches or topical ointments. It can be used to overcome some of the difficulties faced by traditional

delivery methods such as pain and the first pass effect. Despite the ease of drug delivery using transdermal patches, the anatomy of the skin only allows low molecular weight (MW< 500 Da) lipophilic molecules, such as estrogen and nicotine, to penetrate intact skin [1]. As a result, at present only 19 drugs or drug combinations have been approved by the FDA to be delivered using transdermal patches [1].

Several novel transdermal delivery technologies such as microneedles, tape stripping, chemical enhancers, electroporation, thermal ablation, and abrasion have been developed to pierce or remove the SC to increase the skin's permeability to water soluble molecules [1, 2]. Microneedles are micron-size needles that can be fabricated out of glass, metals, or polymers that pierce the superficial dermis [1, 4-6, 18, 19]. Therapeutics that are administered using microneedles can be delivered as a bolus or in a slower sustained release [4, 5]. Microneedles also cause less pain than traditional hypodermic needles due to the shallow depth of insertion [6]. Tape stripping involves the use of adhesives, such as tape or glue, to remove SC to increase the skin's permeability. It is widely used for permeability studies, but the procedure is time consuming and some anatomical locations require a large amount of stripping for SC removal [20]. Chemical enhancers create channels in the SC by disrupting the lipid structure [21]. Enhancers increase the skin's permeability, but strong enhancers can cause skin irritation or damage. Ablation utilizes energy generated by lasers or resistive heating to remove SC. Ablation can remove small or large areas of SC depending on the drug that is being delivered. The procedure is quick and relatively painless since it is limited to the SC. However, laser equipment can be expensive and trained personnel is required for the procedure to avoid severely damaging the skin [20]. Ablative devices that use resistive heating are portable and safer and easier to use than lasers [11]. Abrasion uses coarse paper or pressurized particles to remove the SC [8, 11, 13,

22]. Abrasion can be coupled with a patch or can be carried out using commercially available instruments such as the case of MDA [23]. Abrasion is quick, painless, and can completely remove the SC. The disadvantage of using abrasion is that it may be difficult to get reproducible results due to the heterogeneity in SC thickness and professional MDA equipment requires trained technicians. The research of this thesis will examine the use of abrasion, more specifically MDA, as a method for drug delivery and we seek to increase its reliability and simplicity of use.

The benefits of the new transdermal delivery technologies is that they can bypass the first pass effect, which results in higher bioavailability, fewer side effects, and lower drug doses. They also can reduce or eliminate pain associated with drug delivery by selectively piercing or altering the SC, which is not innervated. These technologies can be designed to administer single doses or release a constant dose over a specific period of time. Compared to traditional methods of drug delivery, transdermal drug delivery has the potential to increase patient compliance due to the ease of administration and the absence of needles. The drawback to the novel methods is that the devices have to be able to compete with current technologies, which despite the disadvantages have already been proven to effectively deliver drugs. The newer technologies must also be able to deliver therapeutic drug doses.

Skin Anatomy/Barrier Properties

The skin is the body's largest organ and serves as a protective barrier to the external environment and protects against water loss. The skin, shown in Figure 1, is divided into three layers: epidermis, dermis, and the subcutaneous fat layer. The epidermis is the outermost layer and is further divided into the SC and viable epidermis (VE). The SC is the outermost layer of

the epidermis and is 15-20 μm thick. It is composed of dead flattened corneocytes that are surrounded by a lipid extracellular matrix. The cells are derived from terminally differentiated keratinocytes from the VE and are arranged in a brick and mortar structure [17, 24]. The corneocytes undergo desquamation, the process of naturally shedding from the SC every two weeks [21]. Due to the SC structure, only low molecular weight (<500 Da) lipophilic compounds can diffuse across intact SC.

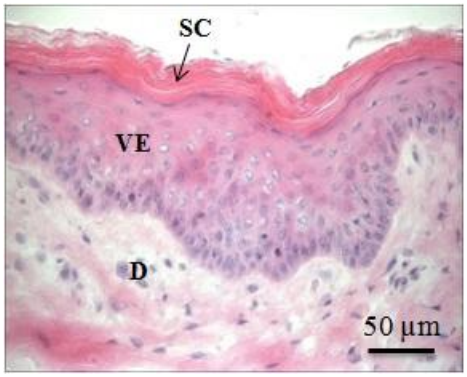

Figure 1. A picture of intact porcine skin. The skin layers are labeled: SC=stratum corneum, VE=viable epidermis, and D=dermis.

The VE is located beneath the SC and the thickness ranges from 50 to 200 μm depending on the anatomical location [21, 24]. The VE provides structural support and contains many cell types such as melanocytes, which give the skin its pigmentation, and immune cells that protect the body during injury [24]. Unlike the SC which contains only 20% water, the VE is 70% water and is more permeable to water soluble compounds [21, 24]. The VE is mainly composed of proliferating epithelial cells that will eventually undergo the process of cornification to become terminally differentiated keratinocytes that will become SC. The kerotinocytes originate from proliferating cells in the basal lamina, the epithelial cell layer that separates the VE from the

dermis. Since the VE is not vascularized, the basal lamina receives nutrients and oxygen via diffusion from the dermal capillaries. As the kerotinocytes migrate away from the basal lamina and move toward the skin's surface, they undergo the process of cornification. During cornification, the organelles disappear and the intracellular space becomes filled with keratin [24]. The cells flatten out and eventually become the SC. The cells will eventually undergo desquamation and shed from the SC and will be replaced with underlying keratinocytes. It takes four weeks for cells to migrate from the basal layer to the skin's surface [24].

The dermis is 2 to 4 mm thick and contains nerves, blood vessels, and the skin appendages, such as hair follicles and sweat glands. The dermis is composed of mainly Type I collagen and elastin and provides structural support for the skin [25]. The dermis also provides the nutrients and oxygen to the epidermal cells. The dermis contains dermal dendritic cells that protect the skin from pathogens during injury [11, 26]. Beneath the dermis is the subcutaneous layer. It is primary composed of adipocytes and it functions to provide warmth to the body and structural support [24].

Microdermabrasion

As mentioned in the transdermal drug delivery section, abrasion can be used as a method of disrupting SC to increase the skin's permeability to water soluble drugs and compounds. The focus of the research presented in this thesis will be to examine the use of microdermabrasion as a transdermal drug delivery method. Microdermabrasion (MDA) is an FDA-approved cosmetic procedure that was developed in 1985 to reduce the appearance of large pores, fine lines, wrinkles, tattoos, and scars [14, 27]. MDA works by removing SC with abrasive particles, such as alumina or sodium chloride, under vacuum. Removing SC induces an inflammatory response

that results in increased collagen remodeling and proliferation which produces the positive cosmetic results seen after MDA, such as noticeably firmer skin [28]. The MDA machine works by placing the handpiece on the skin and occluding the opening of the plastic tip with the skin. A schematic of the MDA machine is shown in Figure 2. The crystals flow from the machine into the handpiece inlet port to impel and abrade the skin. While the crystals are flowing to the skin, used crystals and skin debris are shunted back through the outlet port to the machine and collected in a waste container. The closed-loop system prevents cross contamination among patients. The procedure is painless, short, and requires no down time for recovery. Typically, MDA is performed at spas or in a cosmetic surgeons' office as an outpatient procedure by doctors or technicians.

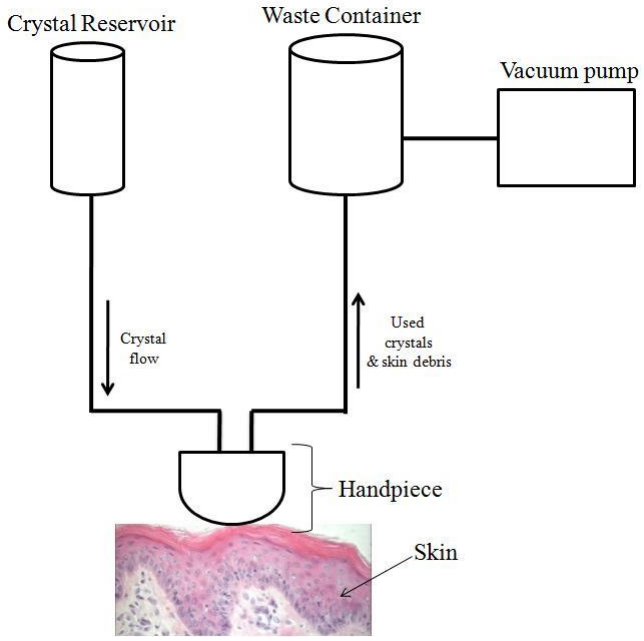

Figure 2. MDA machine schematic. Crystals flow from the reservoir and impel the skin, then the used crystal and skin debris flow back into the machine into the waste container.

Until recently, MDA has been used only for cosmetic purposes. Recently more studies have been conducted on using MDA for drug delivery. One such study that demonstrated the use of MDA for drug delivery was published in 2004 by Lee, et al. Their study used MDA to deliver vitamin C (MW 176 Da), a very low molecular weight hydrophilic molecule, to nude mice skin after MDA [8]. Although they were able to deliver 15 times more vitamin C in abraded skin than the unabraded control sample, the study did not completely remove the SC. They also delivered vitamin C to tape stripped skin, where the SC was completely removed, and they were able to deliver 157 times more vitamin C than the unabraded control [8]. Other studies that did not completely remove the SC have been successful in delivering other very low molecular weight hydrophilic drugs such as 5-aminolevulinic acid (MW 168 Da) and 5-fluorouracil (MW 130 Da), which are both used to treat local skin ailments [7, 13]. The studies conducted by Lee the others were limited to low molecular weight compounds. These studies did not address delivery of larger molecules (MW>500 Da), which we hypothesize requires full removal of SC.

Skin abrasion has been shown to be successful for delivering vaccines to elicit an immune response. In a study conducted by Gill et al., that formed the preliminary data for this thesis, it was demonstrated that MDA can be used to selectively and completely remove the SC in humans and monkeys for drug delivery. Modified Vaccina Ankara (MVA), a vaccine, was delivered to abraded monkey skin that had complete SC removal and a measurable antibody response was obtained [12]. Due to its large size, MVA cannot penetrate intact skin, so this study demonstrated the importance of completely removing the SC for macromolecule and vaccine delivery. Another study developed a portable disposable skin abrasion device that delivered vaccines and adjuvants, such as cholera toxin and heat-labile E. coli enterotoxin, for traveler's diarrhea [29, 30]. The device was also used to deliver adjuvants for vaccine dose sparing to

reduce the amount of vaccine that was needed to elicit an immune response [23, 29, 30]. The abrasion device consisted of abrasive paper that disrupted the SC to increase the skin's permeability to the molecules. Vaccines were delivered to skin that was only abraded with the device, while adjuvants were delivered to skin that was treated with an intramuscular injection of a vaccine. Using the device, an increase in IgG antibodies were reported in mice, guinea pigs, and humans that were administered vaccines or adjuvants [23, 29, 30].

Studies have also delivered hydrophobic drugs, such as estradiol and clobetasol, using MDA [13, 15]. Estadiol and clobetasol can both diffuse across intact skin due to their small size and lipophilicity (MW<500 Da). The estradiol study demonstrated a higher penetration depth of estradiol in abraded hairless mice skin than the unabraded control [15]. However, the clobetasol study showed higher molecule penetration in unabraded porcine skin as opposed to abraded skin [13]. The conflict in the results may be due to the difference in the compounds molecular weights and the animal models they used. These studies suggest that hydrophobic compounds may be less suitable for delivery using MDA, however there are many hydrophobic substances that can transverse intact skin and are used in current transdermal therapies.

Most previous studies only partially removed SC and demonstrated increased flux of low molecular weight compounds across skin. Our preliminary studies demonstrated complete and selective removal of SC, which was associated with increased skin permeability to particulate viral vaccine. In this thesis we sought to establish a more detailed relationship between MDA conditions and SC removal and to determine its effects on skin permeability to macromolecules.

Skin Mechanical Properties

The skin is a nonlinear viscoelastic heterogeneous composite material and each layer has its own unique mechanical properties [31, 32]. The SC is a stiff layer that has a breaking strength of 6 to 2000 MPa, depending on the level of hydration and the testing method used for measurement [33]. The modulus of the SC helps it to withstand daily interactions with the outside environment. The VE and dermis are less rigid than the SC. The VE is mostly composed of epithelial cells and differentiating keratinocytes. The dermis is composed of collagen and elastin, which gives the skin its elastic nature that allows it to return to its original state after applied tensile stress [24]. The SC and dermis are more commonly studied in mechanical tests than the VE. Studies that measure the skin's mechanical properties usually use suction, indentation, or tensile tests to determine the modulus and breaking strength of the skin layers.

The mechanical properties of the skin are important in maintaining the skin's integrity. An imbalance in the mechanical properties, especially the SC, results in barrier pathologies that put the body at risk of infections and dehydration. Novel technologies that aim to target the SC either by piercing or removal must consider the mechanical properties. The technologies must be able to exert forces that are larger than the breaking strength of SC for penetration or removal. For MDA, understanding the mechanical properties of the skin will explain why certain abrasion conditions are able to remove SC more effectively than others. It will also explain the rapid destruction of VE after the SC is removed if the procedure is not properly controlled.

Vaccine Delivery and Immunity

Vaccines are commonly inactivated, live, or attenuated pathogens that are administered to impart immunity against future infections. Vaccines have successfully led to the eradiation of

polio in developed countries and small pox throughout the world [34, 35]. Currently, most vaccines are delivered either by subcutaneous or intramuscular injections, which are relatively convenient, inexpensive, and have been proven to elicit an effective immune response. However, needles are painful, carry the risk of needle-stick injuries, and have a high disposal cost [11]. Newer delivery methods are being researched to target the VE to decrease vaccine dosage, increase the vaccine immunogenicity, and reduce or eliminate needle use.

The VE, located beneath the SC, is populated with many immune cells such as Langerhans cells and the dermis contains dermal dendritic cells and macrophages that act as the first line of defense to fight pathogens in breached skin [11, 26]. Delivery to the VE targets the Langerhans cells, the largest population of epidermal immune cells. Langerhans cells are antigen-presenting dendritic cells that function to activate T cells during microbial invasion. When the skin is breached, the antigen binds to the Langerhans cell and is internalized and processed into a single strand oligonucleotide. The oligonucleotide is then presented to T cells through major histocompatibility complex class II interactions on the cell surface. This antigen presentation activates T cells to initiate an immune response to the pathogen [26]. The abundance, location, and T cell activation action of the Langerhans cells make the epidermis possibly a better target for vaccine delivery than traditional methods.

Some of the newer epidermal and dermal vaccine delivery methods include abrasion, intradermal injections, and jet injections [11]. Abrasion systems use micron-sized projections or abrasive paper to abrade the SC to allow topical vaccine delivery [23, 36]. The vaccine can either be administered in the form of a liquid or patch. One vaccine that has been delivered by abrasion is influenza [23, 36]. Some abrasion vaccine formulations also contain adjuvants, compounds that enhance the immune response. This increased immune response leads to a decrease in the

amount of vaccine needed for immunity [23, 36]. The advantage to using abrasion is that it is fast and results in minor skin irritation and pain and uses smaller doses of vaccine [36]. The drawback is that the SC must be effectively disrupted to allow the vaccine to cross the skin surface.

Intradermal injections use needles to penetrate into the dermis for vaccine delivery [11]. The needles can either be hypodermic needles or micron-size needles [19, 37]. Vaccines that are delivered using intradermal injections are smallpox, tuberculosis, BCG, and sometimes rabies. The advantage to using skin vaccination is that it can use smaller doses of vaccine and it may elicit a more robust immune response than traditional delivery methods. The disadvantage is that targeting the skin is difficult and may require special training [11].

Jet injectors use pressurized liquids or powders to administer vaccines to the skin [10, 11, 38, 39]. The liquid creates micron-sized channels that allow the entry of the pressurized vaccine into the skin. Vaccines such as smallpox, measles, polio, meningitis, and yellow fever have been delivered using jet injection systems. Jet injectors are quick and the resulting vaccination has an immune response that is equal to or better than traditional injections. The disadvantage to using jet injector systems is that they can be painful and there is a risk of disease transmission among patients due to blood splatter contamination [11].

Along with targeting the skin, mucosal points of entry into the body have also been targeted for vaccine delivery to take advantage of the large number of immune cells present in mucosal tissue. One mucosal delivery method is inhalation, which is used to deliver vaccines to the nasal passages and lungs [40]. Products such as FluMist^{TM}, which was approved by the FDA in 2003, have been developed to delivery influenza using inhalation [11]. The nasal passages are populated with immune cells and are a common entry way for airborne pathogens. The

advantage to using inhalation delivery is that it can result in a stronger immune reaction as compared to common injections. The drawbacks are that it may be difficult to deliver a consistent dose, the vaccine may affect the cranial nerves, and virus can be possibly transmitted to others by spraying the drug [11].

Skin Resealing after Injury

The skin's main function is to protect the body from the external environment and when it is breached due to injury, its ability to restore the barrier is important to protect the body from pathogens and water loss. The rate of skin recovery is determined by the depth and severity of the wound. Superficial wounds, which reach into the superficial dermis (200 μm deep), exhibit rapid healing and do not result in the formation of a scar [41, 42]. Injuries that occur deep in the dermis and subcutaneous fat layer often result the formation of a scar and require a longer time for barrier recovery [41]. To heal properly, deep wounds often require closing either by sutures or bandages to reduce the gap in the area of tissue damage [42].

After injury, the skin heals in three phases: inflammation, reepithelialization, and tissue remodeling [43]. The inflammation phase occurs within a few minutes after injury and involve the activation of neutrophils and the release of cytokines and growth factors [43]. The cytokines and growth factors stimulate fibroblast proliferation and also attract monocytes that circulate in the blood to the site of injury to fight pathogens that may have entered the skin [43]. These cells release chemicals in the inflammation phase initiate the healing process.

Reepithialization or tissue formation occurs within hours or can take up to one week after injury [41, 43]. During reepithialization the stem cells in the basement membrane proliferate to repair the damaged area and cells from appendages migrate to the injury site [43]. Organisms

that have a higher density of appendages, such as rodents, exhibit a more rapid healing response to injury [44]. If the wound is deep (extending deep into the dermis) granular tissue will form during the reepithialization phase. The granular tissue is composed of macrophages, fibroblast, and connective tissue. The fibroblasts produce collagen that will repair and replace the damaged tissue. Neovascularization also occurs to form new blood vessels [43].

The final step of healing is tissue remodeling and it occurs two to four weeks after injury. Wound contraction occurs during this phase to close the wound. Excess connective tissue that was formed during the reepithialization phase is degraded by matrix metollaproteinases (MMP) to remodel the tissue back to its natural form and function [43]. Depending on the depth and severity of the wound, a scar may remain after the final phase of healing [41].

The rate of wound healing can be affected by the type of dressing that is applied to the wound. Wound covers are grouped into three categories: occlusive, semi-occlusive, and non-occlusive. Occlusive covers prevent oxygen from diffusing into the wound and also prevent the wound from losing moisture. In a study conducted on humans and pigs, occlusive dressings were shown to accelerate the rate of reepithialization and prevent the formation of eschars (scabs) [45]. However, occlusion can also delay the formation functional SC after injury [46]. Semi-occlusive coverings allow oxygen to diffuse into the site and wound retains its moisture. In a study conducted by Visscher et al. it was found that semi-occlusive membranes promoted better healing than occlusive and non-occlusive membranes for tape stripped skin [47]. Non-occluded wounds remain open to the environment. Oxygen can penetrate the injury site and the wound dries out. Non-occlusive wounds tend to form eschars during the healing process [45].

CHAPTER 3

MATERIAL AND METHODS

Controlled Pore Formation in Stratum Corneum Using Microdermabrasion

Microdermabrasion Procedure

Microdermabrasion experiments were conducted on excised adult feeder porcine (2-9 month old, average weight 32 kg) dorsal skin (Pel-freeze Biologicals, Rogers, AR) using a Gold Series MegaPeel microdermabrasion machine (DermaMed USA, Lenni, PA) with the gold handpiece assembly. Pig skin was obtained with approval from the Georgia Tech Institutional Animal Care and Use Committee (IACUC). The skin was stored at -70 °C prior to use. Before the experiments were conducted, subcutaneous fat was removed from the skin using a scalpel (Fisher Scientific, Fair Lawn, NJ) and the hair was carefully removed using surgical prep razors (Medex Supply, Monsey, NY) without damaging the skin.

A picture of a microdermabrasion machine tip and the alumina crystals are shown in Figure 3A and B, respectively. The experiments were carried out using two different abrasion modes: static and dynamic. For the static mode, the machine handpiece remained stationary on the skin for 6 s. For the dynamic mode, it was moved along the skin for 10 passes at a rate of 1 pass/s. The dynamic mode experiments were carried out by first isolating the area of abrasion with a rectangular foam adhesive (Avery Dennison, Painesville, OH) having inner dimensions measuring 41 mm long and 15 mm wide and sliding the probe back and forth within this area. For both abrasion modes, the effect of crystal flow rate and suction pressure were examined. The crystal flow rate was varied from the minimum value (corresponding to a setting of 9 turns of the

crystal flow rate knob on the microdermabrasion machine) to the maximum value (corresponding to a setting of 0 turns of the crystal flow rate knob). As discussed in the Appendix, we determined this range of crystal flow rates to span $8.9x10^2$ to $2.2x10^5$ particles/s or <0.01 to 0.80 g/s of particles. The suction pressure was also varied from -30 kPa to -60 kPa. All experiments were carried out in triplicate.

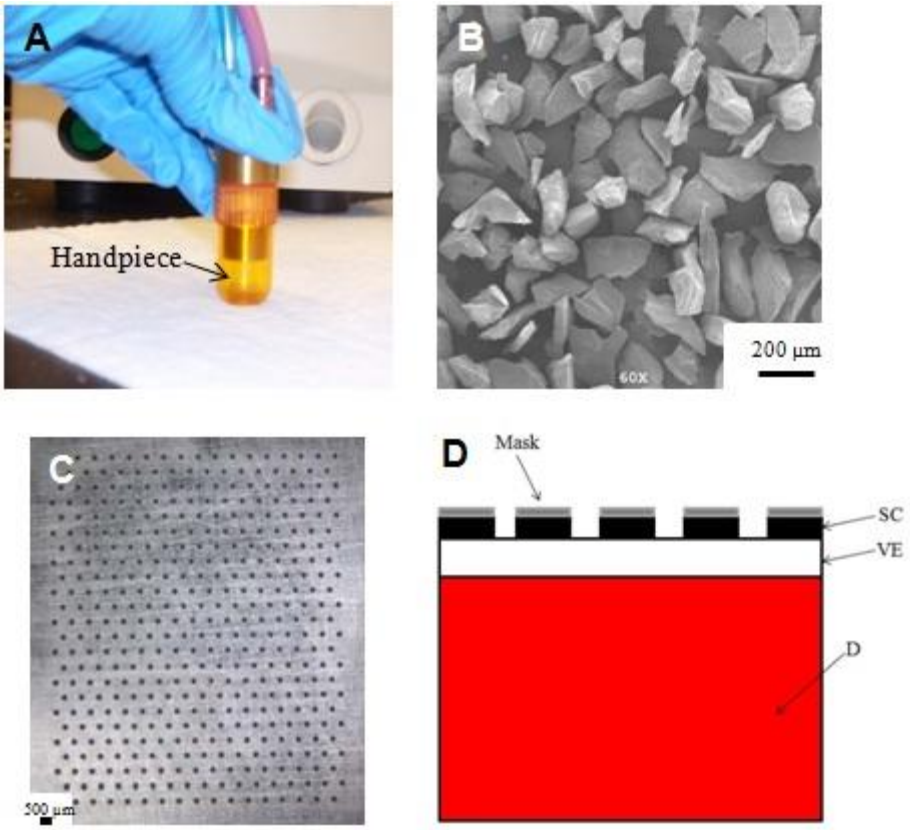

Figure 3. Microdermabrasion device and mask. (A) Microdermabrasion machine handpiece and (B) the alumina abrasion crystals (~100 µm in diameter). (C) Stainless steel mask with 408 holes (125 µm diameter). (D) Schematic diagram of the skin after abrasion with the mask, where the stratum corneum is selectively removed and the underlying layers are intact. SC = stratum corneum, VE = viable epidermis, and D = dermis.

We also studied the effect of time on depth of skin abrasion as a function of the crystal flow rate and pressure for the static and dynamic abrasion modes using porcine skin. For the

static mode, the crystal flow rate was fixed at 4 turns and the time points studied were 3, 20, and 45 s at suction pressures of -30, -40, and -50 kPa. For the dynamic mode, the flow rate was set to 4.5 turns and the suction pressures examined were -25 and -45 kPa for 1, 10, and 50 passes. All experiments were carried out in triplicate.

At the conclusion of each experiment, an 8 mm skin biopsy was taken with a biopsy punch (Miltex Inc, York, PA) and embedded in Optimal Cutting Temperature (OCT) compound (Sakura Finetek, Torrance, CA) and frozen in dry ice for histological analysis. The skin was sectioned using a Leica 3050S cryostat (Leica Microsystems, Wetzlar, Germany) at a thickness of 10 µm, stained with routine hematoxylin and eosin (H&E), and imaged using a Nikon 600E microscope (Nikon, Tokyo, Japan) and Qcapture software (Q Imaging, Pleasanton, CA).

Abrasion Depth Quantification

The depth of abrasion was quantified by assigning values to indicate the degree of stratum corneum removal. For the experiments in which the time was held constant, 0 indicated stratum corneum not removed, 0.5 represented partial stratum corneum removal, and 1 for complete stratum corneum removal. For the experiments in which the time was varied, 0 was assigned for stratum corneum not removed, 0.5 for partial stratum corneum removal, 1 for complete stratum corneum removal, and 1.5 for viable epidermis removal. For each condition 10 histological sections from 3 replicate experiments were examined and scored. Average scores are reported in the figures.

Microdermabrasion Using a Skin Mask

To control the area of abrasion, two masks with an array of holes (125 μm or 250 μm diameter) were designed using AutoCAD software (Autodesk, San Rafael, CA) and fabricated out of stainless steel (75 μm thickness, Trinity Brand Industries, Countryside, IL). The pattern was cut into the metal using an infrared laser (Resonetics Maestro, Nashua, NH) and the masks were manually cleaned with detergent (Contrex, Decon Labs, King of Prussia, PA) to de-grease the surface and remove slag and oxides deposited during laser cutting, which was followed by thorough rinsing in running deionized (DI) water. To deburr and clean edges, the masks were electropolished in SS Electropolish solution (E972, ESMA, South Holland, IL). The process was carried out in an electropolisher (model no. E399-100, ESMA, South Holland, IL) using 6 V for 15 min. After electropolishing, the masks were cleaned by dipping alternately three times in de-ionized water and 25% nitric acid (Fisher Scientific, Fair Lawn, NJ) for 30 s each. This was followed by another washing step in hot running water and a final wash in running de-ionized water. Due to the electropolishing process, the thickness of the masks was reduced to 50 μm. Masks were dried using compressed nitrogen.

For the microdermabrasion experiments, the mask was adhered to the center of a rectangular foam adhesive (Avery Dennison, Painesville, OH) and attached to the skin. A picture of the mask and a schematic of the skin after abrasion are shown in Figure 3C and D, respectively. In experiments using the mask, excised porcine cadaver skin was abraded at a pressure of -50 kPa at the maximum crystal flow rate (0 turns) for 30, 45, 60, 90, and 120 s to determine the optimal removal setting. The site of abrasion was revealed by staining with green dye (McCormick & Co, Hunt Valley, MD). After the experiment, the area of abrasion was

excised and frozen for histological examination using the same protocol as mentioned in the previous section.

Statistical Analysis

Statistical analysis was carried out using Minitab software (Minitab Inc., State College, PA). A two-way ANOVA was used for statistical evaluations. The p value was set to 0.05.

Transdermal Delivery of Macromolecules Using Microdermabrasion

Abrasion Protocol

All the microdermabrasion experiments without the use of the mask were conducted on excised full thickness adult feeder porcine dorsal skin (2-9 month old, average weight 31.8 kg, Pel-freeze Biologicals, Rogers, AR) using a Gold Series MegaPeel MDA machine (DermaMed USA, Lenni, PA) with the gold handpiece assembly. The subcutaneous fat was removed with a scalpel (Fisher Scientific, Fair Lawn, NJ), although a thin layers of the subcutaneous tissue remained adherent, and the hair was shaved with surgical prep razors (Medex Supply, Monsey, NY) prior to the experiment. The abrasion area was bounded by a window cut out of a piece of rectangular adhesive foam (L=41 mm and W=15 mm) applied to the skin and the microdermabrasion handpiece was moved along the skin within the window in the adhesive foam at a constant speed of 1 pass/s at suction pressures of -25, -45, and -50 kPa for 10 or 50 passes at a crystal flow rate of 0.35 g/s (4.5 turns of the crystal flow rate knob).

Sulforhodamine Delivery

Sulforhodamine B (SR, Invitrogen, Carlsbad, CA), a fluorescent molecule, was used as the low molecular weight hydrophilic drug model. The molecular weight is 558 g/mol. Each delivery experiment was conducted by first generating a standard curve by measuring the fluorescence of different SR dilutions that ranged from 10^{-6} to 10^{-9} M with a spectrofluorimeter (Photon Technology International, Birmingham, NJ). The area under the emission curve for each concentration was calculated by Felix Fluorescence Analysis Software (Photon Technology International, Birmingham, NJ). The solution concentrations and the area under the emission curves were plotted for the standard curve.

The delivery experiments was carried out by abrading the skin at two vacuum pressures, -25 and -45 kPa, for 10 and 50 passes each. The crystal flow rate was set to a crystal flow rate of 0.36 g/s (4.5 turns of the crystal flow rate knob). After abrasion, the treated skin and an untreated control were placed in horizontal diffusion cells (PermeGear, Bethlehem, Pa) with a water jacket set to 37 °C. Three milliliters of 10^{-3} M SR and phosphate buffered saline (PBS, Sigma-Aldrich, St. Louis, MO) were added to the donor and receiver chambers, respectively. The skin was exposed for 1, 6, or 24 h. The concentration of SR was quantified by emptying the receiving chamber solution every hour and measuring the fluorescence with the spectrofluorimeter. Fresh PBS was added to the receiving chamber at each sampling point. The 24 h experiments were split into two 12 h experiments that measured SR diffusion from hours 1 to 12 and 13 to 24. The 1 to 12 h experiment was conducted by sampling the receiving chamber solution for the first 12 h. For the 13 to 24 h experiment, the receiving chambers were not sampled for the first 12 h. At hour 12, the receiving chambers were emptied, washed three times with PBS, and filled with fresh PBS. The receiving chambers were then sampled from 13 to 24 h. Three replicates for each time point were carried out. At the conclusion of the experiments, the skin was embedded in Optimal Cutting Temperature compound (Sakura Finetek, Torrance, CA) and frozen in dry ice for histological analysis. Shown in Appendix C is the experimental setup for the in vitro drug delivery experiments.

Bovine Serum Albumin Delivery

Texas Red-labeled bovine serum albumin (BSA, Invitrogen, Carlsbad, CA), a fluorescent labeled protein, was used as a model compound for protein delivery. BSA has a molecular weight of 66 kDa. The porcine skin was abraded at a pressure of -50 kPa for 50 passes at half of

the maximum crystal flow rate to remove the stratum corneum. The penetration was studied in the same manner as SR, except the skin was placed in vertical Franz cell diffusion chambers (PermeGear, Bethlehem, Pa). The Franz cells permitted the use of a smaller donor solution volume. The Franz cells were placed in a heating blocking (PermeGear, Bethlehem, Pa) that was set to 37 °C. One hundred microliters of 10^{-5} M BSA and 5 mL of PBS were added to the donor and receiver chambers, respectively. The skin was exposed to BSA for 1, 6, and 24 hours. The flux was not measured since it was determined in separate experiment that BSA did not penetrate the entire skin thickness in 24 hours. At the completion of the experiment the skin was frozen, sectioned, and imaged to assess the molecule penetration depth.

Inactivated Influenza Vaccine Delivery

The model vaccine used for delivery was inactivated influenza virus (MW $3.0x10^6$ Da). Influenza virus was conjugated to R18 (octadecyl rhodamine B chloride) for fluorescent imaging. To conjugate R18 to the virus, 10 µL R18 was mixed with 200 µL (3 mg/ml) of inactivated virus. The solution was incubated for 1 hr at room temperature, then ultracentrifuged at 28000 rpm for 1 hr to remove unbound R18. After centrifugation, 1 mL 20% sucrose, 9 mL PBS (without Ca, Mg), and 1 mL inactivated virus formulation (200 µL R-18 stained inactivated virus, 0.7 mL PBS, and 0.1 mL fetal bovine serum) were mixed. The supernatant was removed and 200 µL of PBS was added to resuspend the solution overnight at 4 ^oC. The abrasion settings and the diffusion experiments for influenza was conducted using the same abrasion and delivery protocol as the BSA experiment. Histology was used to assess the penetration depth. Due to its large molecule weight, the flux of virus was not measured.

Mask Delivery Study

Excised split thickness human cadaver skin (National Disease Research Interchange, Philadelphia, PA) that was dermatomed to a thickness of 200 to 600 μm was used to deliver sulforhodamine B (SR) and insulin using microdermabrasion. The skin was abraded through a polymer mask to reduce the area of abrasion. The masks were fabricated out of 70 μm thick polyethylene terephthalate (McMaster Carr, Aurora, OH) and the holes (125 μm diameter) were laser cut with a Hermes LS500XL CO_2 laser (Gravograph, Duluth, GA). One pass of the laser was used and the power and speed were set to 15% and 10%, respectively.

The mask was adhered to the skin using tape (Fisher Scientific, Fair Lawn, NJ) and the skin was abraded using the conditions -30 kPa at a crystal flow rate of 0.23 g/s (5 turns of the crystal flow rate knob) for 20 s and -50 kPa at a crystal flow rate of 0.95 g/s (0 turns of the crystal flow rate knob) for 60 s to remove the stratum corneum and viable epidermis, respectively. Three replicates of each condition were used for the experiment. Three positive and negative controls were also used for both experiments. The negative controls were not abraded and were exposed to the drug. The positive controls were abraded, but were only exposed to PBS. The microdermabrasion tip was moved to multiple sites on the mask to maximize the area of abrasion. After abrasion, the pores were revealed with green dye (McCormick & Co, Hunt Valley, MD) and photographed using an Olympus SZX12 stereoscope (Olympus, Tokyo, Japan), Leica DC 300 camera (Leica Microsystems, Wetzlar, Germany), and Adobe Photoshop software (Adobe Systems, San Jose, CA). The skin was placed in Franz cell diffusion chambers and the chambers were housed in a heating block set to 37 °C. At the conclusion of both delivery experiments, the area of abrasion was re-revealed using green dye and the skin was snap frozen in dry ice for histological analysis. The skin was sectioned at a 10 μm thickness with a Microm

cryostat (Thermo Fisher, Walldorf, Germany). The sections were photographed to measure the molecule penetration depth with a Nikon E600 microscope (Nikon, Tokyo, Japan) and Qcapture camera and software (Q Imaging, Pleasanton, CA). The slides were stained with routine H&E in a Leica autostainer (Leica Microsystems, Wetzlar, Germany).

For the SR delivery experiments, 200 µL of 10^{-3} M SR and 5 mL of PBS were added to the donor and receiver chambers, respectively. The donor chamber was covered with parafilm (Pechiney Plastic Packaging, Chicago, IL) to reduce evaporation. The receiver chamber was at each time point. The SR concentration in the receiving chamber was measured, using fluorescence, in the same manner as the SR experiments in the previous section.

To measure insulin diffusion, 100 µL of a U500 Humalog-R (Eli Lilly, Indianapolis, IN) mixture was added to the donor chamber. The Humalog mixture consisted of 80 µL of U500 and 20 µL of FITC-labeled bovine insulin (Sigma-Aldrich, St. Louis). The bovine insulin was used to visualize insulin diffusion during the histological analysis. The receiving chamber contained 5 mL of PBS mixed with 0.01 M sodium azide (Sigma-Aldrich, St. Louis, MO), a preservative. The donor chamber was covered with parafilm and the donor solution was replaced at each sampling time due to the instability of U500 insulin. The receiving chamber was sampled every 6 hours for 54 hours in the same manner as the SR experiments. The concentration of the FITC-labeled bovine insulin was measured using fluorescence using the same protocol as the SR experiments. The total insulin concentration in the receiving chamber solution was additionally quantified using a rat insulin enzyme-linked immunoassay (ELISA) kit (Alpco Diagnostics, Salem, NH), which had cross-reactivity with the Humalog insulin used in this study. The assay was carried out according to the manufacturer's protocol.

Transdermal Insulin Delivery Using Microdermabrasion

Microdermabrasion Protocol

The The skin was microdermabraded using a Gold Series MegaPeel machine (DermaMed USA, Lenni, PA), with the gold handpiece assembly, through a polyethylene terephthalate polymer mask to control and reduce the area of abrasion. The mask, shown in Figure 4, was an array of 408 holes (125 μm in diameter) with a center to center spacing of 500 μm. The masks were fabricated out of 70 μm thick polyethylene terephthalate (McMaster Carr, Aurora, OH) and the holes were laser cut with a Hermes LS500XL CO_2 laser (Gravograph, Duluth, GA). Prior to abrasion, the skin was gently cleaned with alcohol swabs (Becton and Dickinson, Franklin Lakes, NJ) and allowed to air dry. The mask was adhered to the skin with tape (Fisher Scientific, Fair Lawn, NJ) and the area of abrasion was maximized by moving the microdermabrasion tip to different sites on the mask. The skin was abraded at a suction pressure of -30 kPa for 30 s at a crystal flow rate of 0.19 g/s (6 turns of the crystal flow rate knob) to remove the stratum corneum. The viable epidermis was removed using a suction pressure of -50 kPa for 60 s at a crystal flow of 0.95 g/s (0 turns of the crystal flow rate knob). After abrasion, green dye (McCormick & Co, Hunt Valley, MD) was applied to the skin for 20 s and wiped cleaned with alcohol swabs to reveal the holes.

Figure 4. The polymer mask used for the insulin delivery study. The 408 holes (125 μm diameter) were drilled into the mask using a CO2 laser. The mask was adhered to the skin with tape and the microdermabrasion tip was placed on it, at multiple sites, to maximize the area of abrasion.

Diabetes Induction Protocol

Rapid acting U100 Humalog-R insulin (Eli Lilly, Indianapolis, IN) was delivered to 39 six weeks old diabetic hairless rats (CD Strain, Charles River Laboratories, Wilmington, MA). Prior to the experiment, the rats were allowed unrestricted access to food and water. The animal protocol was approved by the Georgia Institute of Technology Institutional Animal Care and Use Committee. To induce diabetes, the rats were weighed to determine the streptozocin (Sigma-Aldrich, St. Louis, MO) dose. They were anesthetized with isoflurane and the blood glucose was measured using a NovaMax meter (Nova Biomedical, Bedford, MA) with blood obtained from a tail vein laceration. Two hundred microliters of blood, also from the tail vein, was collected in blood serum tubes (Capiject, Somerset, NJ) for insulin quantification. The rats were injected, in the tail vein, with 300 μL of 80 or 100 mg/kg of streptozocin. Initially 100 mg/kg was used, but the dose was lowered to 80 mg/kg to reduce mortality and severe hyperglycemia. The streptozocin was dissolved in 4 °C citrate buffer (pH 4.5, Sigma-Aldrich, St. Louis, MO) and sterilized by filtering with a 0.2 μm pore syringe filter (Fisher Scientific, Fair Lawn, NJ)

immediately before the injection. Twenty four hours after streptozocin administration the rats were re-weighed to verify that there was no more than a 20% weight loss. The rat was anesthetized with isoflurane and the blood glucose was measured and diabetes was deemed to be induced if the blood glucose exceeded 300 mg/dL. Only rats with <20% weight loss and blood glucose levels higher than 300 mg/dL were used for the study.

Insulin delivery protocol

The rats were divided into four groups: negative control, positive control, stratum corneum abrasion, and viable epidermis abrasion. The negative control group was not abraded and did not receive insulin. The positive control group received a 500 µL subcutaneous injection of 0.1 U of insulin. To prepare the insulin for the injection, 50 µL of U100 Humalog-R was diluted in 25 mL of sterile phosphate buffered saline (Mediatech, Manassas,VA).

After the animals were determined to be diabetic, the rats remained anesthetized and untreated for one hour to make sure the blood glucose levels were stable (i.e., animals with >20% variation were not used). After the stabilization hour, the animals were treated according to their group. A transdermal patch (Altea Therapeutics, Atlanta, GA) filled with 200 µL of a solution containing 80% Humalog-R (100 U/mL) and 20% FITC-labeled bovine insulin (2.5 mg/mL, Sigma-Aldrich, St. Louis, MO) was applied to the site of abrasion in the stratum corneum and viable epidermis removal groups. The bovine insulin allowed visualization of the insulin penetration depth for the histological analysis. The blood glucose was measured every 30 min for the first 2 h and every 2 h for hours 2 to 8. Two hundred microliters of blood was collected at each time point for insulin quantification using enzyme-linked immunoassay (ELISA). The insulin-filled patches were removed at the 4 h time point and the skin was wiped

clean with Kimwipes (Kimberly-Clark, Dallas, TX). The animals remained under anesthesia until they were euthanized with carbon dioxide at the conclusion of the experiment. Animals were euthanized during the experiment if their blood glucose exceeded 475 mg/dL or fell below 45 mg/dL.

Serum Insulin Determination

The rat blood was allowed to clot at room temperature for two hours after collection. The blood was centrifuged (Eppendorf AG, Hamburg, Germany) at 1200 g for 10 min. After centrifugation, the serum was removed and stored at -70 °C. The concentration of Humalog and the endogenous rat insulin in the serum was quantified using a rat insulin ELISA kit (Alpco Diagnostics, Salem, NH) that detected both Humalog and rat insulin. The rat insulin kit was used because ELISA insulin kits that detected Humalog also cross reacted with endogenous rat insulin. Human insulin kits were not used because they cannot detect Humalog since the amino acid structure of native insulin and synthetic insulin differ. The assay was carried out according to the manufacturer's protocol.

Data Analysis

The area under the curve for the blood glucose and serum insulin data was determined with NCSS software (NCSS LLC, Kaysville, UT). The statistical analysis was performed using Minitab software (Minitab Inc., State College, PA). A one-way ANOVA was conducted on the data and a p value less than 0.05 was considered significant.

Skin Repair Kinetics after Stratum Corneum Removal Using Microdermabrasion in Hairless Guinea Pigs

Skin Abrasion Protocol

Sixteen hairless guinea pigs (Charles River Laboratories, Wilmington, MA) were divided equally into four groups that corresponded to the skin healing time points. Two additional guinea pigs were used for a sham experiment. The animal protocols were approved by the Georgia Institute of Technology Institutional Animal Care and Use Committee. Prior to the experiment, the animals were given free access to food and water. The dorsal skin was prepared for abrasion by thoroughly cleaning with alcohol swabs (Becton and Dickinson, Franklin Lakes, NJ) and allowing it to air dry. The abrasion area was marked using a rectangular foam adhesive (Avery Dennison, Painesville, OH) that had a length of 41 mm and a width of 15 mm. Each guinea pig was abraded in two sites on the back on opposite sides of the spinal column that were not in contact with each other. The guinea pigs were abraded using a DermaMed Gold Series microdermabrasion machine (DermaMed USA, Lenni, PA) with the gold tip assembly. The skin was abraded at a suction pressure of -40 kPa, at half of maximum crystal flow, by moving the microdermabrasion tip back and forth along the abrasion area for 10 passes (1 pass/s). After abrasion, one site was occluded with a non-gel electrode (Thought Technology, Montreal, Canada) and Blenderm Tape (3M, St. Paul, MN). The area was further secured with Tegaderm (3M, St. Paul, MN) and a Coban elastic bandage (3M, St. Paul, MN) to prevent the animal from disturbing the site. The other abraded site remained uncovered. An additional site on the back was used for the negative control and was not abraded or occluded. For the sham experiments,

microdermabrasion was performed without crystals or pressure for 10 passes (1 pass/sec) on the two guinea pigs after euthanasia.

Electrical Resistance Measurements

Electrical resistance was used to monitor the stratum corneum barrier recovery after microdermabrasion treatment at 0, 4, 12, and 24 hours after abrasion. The four animal groups corresponded to the skin healing monitoring time points. The guinea pigs were lightly sedated with isoflurane and the baseline skin impedance for every group, except for sham, was measured using a resistance reader (EIM-105 Prep-Check, 30 Hz, modified with a 200 kΩ resistor in parallel; General Devices, Ridgefield, NJ, USA) one and two hours prior to the experiment and three minutes before abrasion [48]. A gelled reference electrode (Lead-Lok Biomedical Innovations, Sandpoint, ID) was placed on the upper back near the base of the skull. A non-gel electrode (Thought Technology, Plattsburg, NY) was used to measure the resistance of the negative control and two abrasion sites. The non-gel electrodes were adhered to a thin foam adhesive (Avery Dennison, Painesville, OH) that isolated the measurement site and prevented the electrode's adhesive from damaging the skin. The resistance was measured 4, 12, and 24 hours after abrasion. Each group included all the measurements prior to the designed endpoint. For example, the 24 hour group included resistance readings at 4, 12, and 24 hours after abrasion. The actual value of the skin resistance was determined by subtracting the meter's inline 200 kΩ resistor from the measured value and multiplying the values by the electrode contact area. All statistical tests were performed by Minitab software (Minitab Inc, State College, PA). A P value of less than 0.05 was considered significant. A two way ANOVA and a Student's t-test was used for all the statistical evaluations.

Dye Penetration Test

All the animals were sacrificed using pentobarbital at the designated endpoint. The animals' time group indicated the time of euthanasia; for example the zero hour group animals were euthanized immediately after abrasion. After euthanasia, 100 µL of 10^{-2} M sulforhodamine B (Invitrogen, Carlsbad, CA) was applied to the abrasion sites, using a cotton swab, for 15 min to determine if the stratum corneum was reformed and mature. Sulforhodamine is a hydrophilic molecule that will not penetrate intact skin. After the incubation, the sulforhodamine B was removed by gently cleaning the skin with deionized water and Kimwipes (Kimberly-Clark, Neenah, WI) and the skin was excised for histological analysis.

All tissue samples were embedded in Optimal Cutting Temperature compound (Sakura Finetek, Torrance, CA), and snap frozen in dry ice for histological analysis. The skin was sectioned using a Leica 3050S cryostat (Leica Microsystems, Wetzlar, Germany) at a thickness of 10 µm. The sulforhodamine B fluorescence was photographed before the sides were stained with routine hematoxylin and eosin (H&E). All the slides were imaged using a Nikon 600E microscope (Nikon, Tokyo, Japan) and Qcapture software (Q Imaging, Pleasanton, CA).

CHAPTER 4

CONTROLLED PORE FORMATION IN STRATUM CORNEUM USING MICRODERMABRASION

Microdermabrasion has been shown to increase skin permeability for transdermal drug delivery by damaging or removing skin's outer layer, stratum corneum. However, relationships between microdermabrasion parameters and effects on the stratum corneum barrier have not been developed. In this study, we determined the effect of microdermabrasion crystal flow rate, time, and suction pressure applied in both static and dynamic modes on the extent of stratum corneum removal from excised porcine skin. In addition to controlling the depth of tissue removal by microdermabrasion parameters, we also controlled the area of tissue removal by applying a metal mask patterned with 125- or 250-μm holes to selectively expose small spots of tissue to microdermabrasion. We found that the extent of stratum corneum removal depended strongly on the crystal flow rate and exposure time and only weakly on pressure or static/dynamic mode operation. Masking the skin was effective to localize stratum corneum removal to exposed sites. Overall, this study demonstrates that optimized microdermabrasion in combination with a mask can be used to selectively remove stratum corneum with three-dimensional control, which is important to translating this technique into a novel method of transdermal drug delivery.

Introduction

Transdermal drug delivery involves the administration of drugs, usually from transdermal patches or topical formulations, across the skin's surface and typically into the systemic circulation [1, 49]. This is a convenient and desirable route of delivery because skin offers a large area for delivery, therapeutics can be administered in a consistent dose that avoids the first

pass effect of the liver, and needle-free delivery avoids pain and the dangers associated with hypodermic injection. Despite the ease of drug delivery using transdermal patches and ointments, the anatomy of skin only allows small amounts of low molecular weight, lipophilic molecules, such as estrogen and nicotine, to penetrate intact skin at therapeutic levels. This is because the main barrier to transdermal transport is the stratum corneum, which is the outer 10-15 μm layer of skin. The stratum corneum is composed of nonviable corneocytes that are surrounded by a lipid extracellular matrix. The viable epidermal and dermal layers beneath the stratum corneum typically offer much less resistance to drug transport.

To overcome the stratum corneum barrier and increase skin's permeability to hydrophilic and macromolecular compounds, the stratum corneum is often pierced for injection or removed by stripping, ablation, or abrasion [50, 51]. Devices that pierce the stratum corneum involve the use of hypodermic needles, microneedles, or jet injectors [52, 53]. These methods lend themselves to bolus delivery and are typically either invasive, painful or both. Stratum corneum removal can be done by tape stripping, but the procedure is time consuming and requires expert technique [15] Ablation utilizes energy generated by lasers or heating elements to remove the stratum corneum [51]. Abrasion uses sandpaper or pressurized particles, such as microdermabrasion, to remove the stratum corneum [7, 8, 12, 13, 15, 54]. The advantage to using abrasion is that it is quick and painless, and that microdermabrasion is already approved by the FDA for other applications. However, current microdermabrasion equipment requires detailed characterization to determine conditions that selectively remove stratum corneum for transdermal drug delivery. Because it is the rate-limiting barrier, removal of stratum corneum by microdermabrasion can dramatically increase skin permeability, even to large molecules including proteins and vaccines [12].

Microdermabrasion is an FDA-approved cosmetic procedure that was developed in the 1980's to reduce the appearance of large pores, fine lines, wrinkles, tattoos, and superficial scars [14]. Microdermabrasion damages the stratum corneum by bombarding it with abrasive particles, such as alumina or sodium chloride, under vacuum [55]. Damaging stratum corneum induces an inflammatory response that results in increased collagen remodeling and proliferation, which produces the positive cosmetic results seen after microdermabrasion treatment, such as noticeably firmer skin [56].

The microdermabrasion machine works by placing a handpiece on the skin, which occludes the opening of the plastic tip to create a vacuum. Upon tip occlusion, the crystals flow from the machine into the inlet port and abrade the skin. At the same time, the skin debris and used crystals are shunted back through the outlet port to the machine and collected in a waste container. This closed-loop system prevents cross-contamination between patients and exposure of medical personnel. Typically, patients undergo several sessions of microdermabrasion, depending on the severity of the skin condition, to improve the skin's appearance [28, 56]. The procedure is noninvasive, painless, and short, and requires no down time for recovery. Typically, microdermabrasion is performed at spas or by cosmetic surgeons or dermatologists.

Several studies have shown that microdermabrasion can be used to increase transdermal delivery of low molecular weight compounds such as vitamin C (176 Da), 5-aminolaevulinic acid (130 Da), 5-Fluorouracil (467 Da), lidocaine (234 Da) and estradiol (272 Da) [7, 8, 13, 15, 39]. We also showed in a previous study that microdermabrasion can be used to completely remove the stratum corneum in humans and monkeys and demonstrated increased skin permeability to fluorescein (332 Da) and a model viral vaccine (Modified Vaccina Ankara) [12].

Microdermabrasion can also be used in conjunction with a mask to control the area of abrasion and deliver drugs to the skin[39].

Building off these previous findings, this study sought to develop a microdermabrasion method that offers three-dimensional control over stratum corneum removal, which should provide improved control over transdermal drug delivery. Control over depth of abrasion, and the ability to completely remove stratum corneum without damaging deeper tissue, was pursued through a detailed analysis of the effects of microdermabrasion crystal flow rate, time, suction pressure, and handpiece movement. To control the area of abrasion, we designed a mask to cover the skin and allow microdermabrasion to occur only through small holes in the mask, thereby localizing tissue removal to specific locations. In this way, we could control the size of holes made in the skin by microdermabrasion in all three dimensions.

Results

Control Over Depth of Microdermabrasion by Optimization of Operating Parameters

To control depth of microdermabrasion, this study sought to understand how the primary microdermabrasion operating parameters of crystal flow rate, suction pressure, time, and handpiece movement affected stratum corneum removal.

Static Mode

For the static mode, the microdermabrasion handpiece was held stationary against the skin for 6 s at the specified conditions. The skin was abraded at suction pressures of -30, -40, -50, and -60 kPa at 1, 4, and 9 turns of the crystal flow rate knob. A setting of 1 turn of the crystal flow rate knob corresponded to a flow rate of ~$2x10^5$ particles/s or ~0.7 g/s at an average

velocity of ~1.5 m/s. A setting of 4 turns corresponded to a flow rate of ~$1x10^5$ particles/s or ~0.3 g/s at an average velocity of ~2 m/s. The flow rate was too low for accurate quantification at a setting of 1 turn, but the average velocity was found to be ~3 m/s. See the Appendix for more information about these measurements and calculations.

For reference, Figure 5 shows an intact piece of skin without microdermabrasion treatment. The full thickness of red-stained stratum corneum is present, the blue-stained nuclei of the viable epidermis are seen below, and the pink-stained dermis is deeper still.

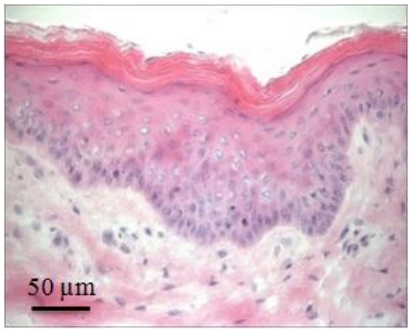

Figure 5. Histological section of intact porcine cadaver skin stained with H&E. The stratum corneum appears on top with a red stain. Viable epidermis is immediately below with characteristic blue staining of epidermal cell nuclei. The pink-stained dermis is below that.

Figure 6 and Figure 7 show the results of the static mode experiments. Figure 6 presents histological images of representative skin sections after microdermabrasion and Figure 7 quantifies these data by scoring the extent of stratum corneum removal and averaging among replicates. Overall, as the crystal flow rate increased, the degree of stratum corneum removed increased for all pressures (Figure 7, two-way ANOVA, $P < 0.05$). Pressure did not significantly affect stratum corneum removal (Figure 7, two-way ANOVA, $P > 0.05$). As shown in the left column of Figure 6, microdermabrasion at the most aggressive crystal flow rate (1 turn) completely removed the stratum corneum from skin abraded at pressures of -50 and -60 kPa and

partially removed at pressures of -30 and -40 kPa. Partial stratum corneum removal is indicated by bits of stratum corneum still adherent to the skin surface. The viable epidermis remained intact under these conditions, except at -60 kPa, which had small focal areas of deeper tissue removal.

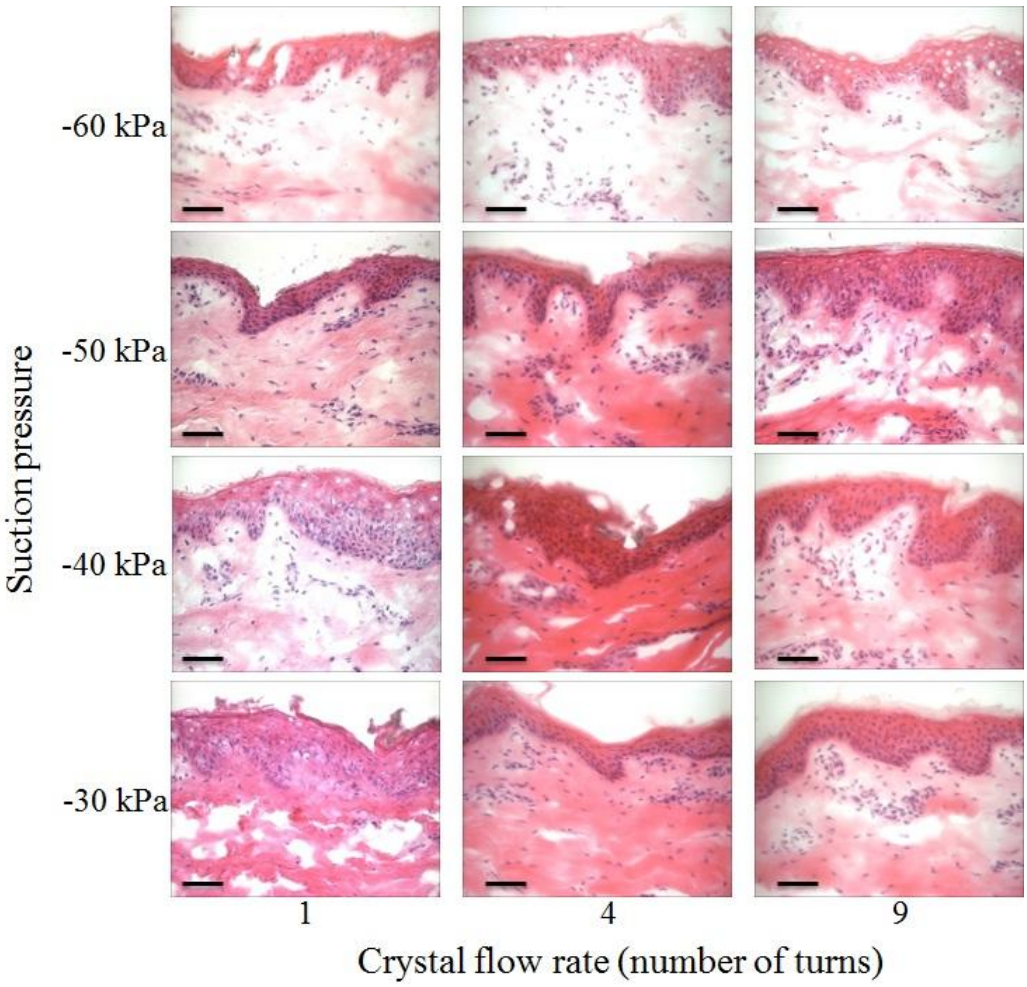

Figure 6. Skin abraded using static mode microdermabrasion at -30, -40, -50, and -60 kPa suction pressure for 1, 4, and 9 turns of the crystal flow rate knob. Crystal flow rate scales inversely with the number of knob turns, such that 1 turn corresponds to the largest crystal flow rate (see Appendix for more information). Representative H&E-stained sections of porcine cadaver skin are shown. Scale bar = 50 μm.

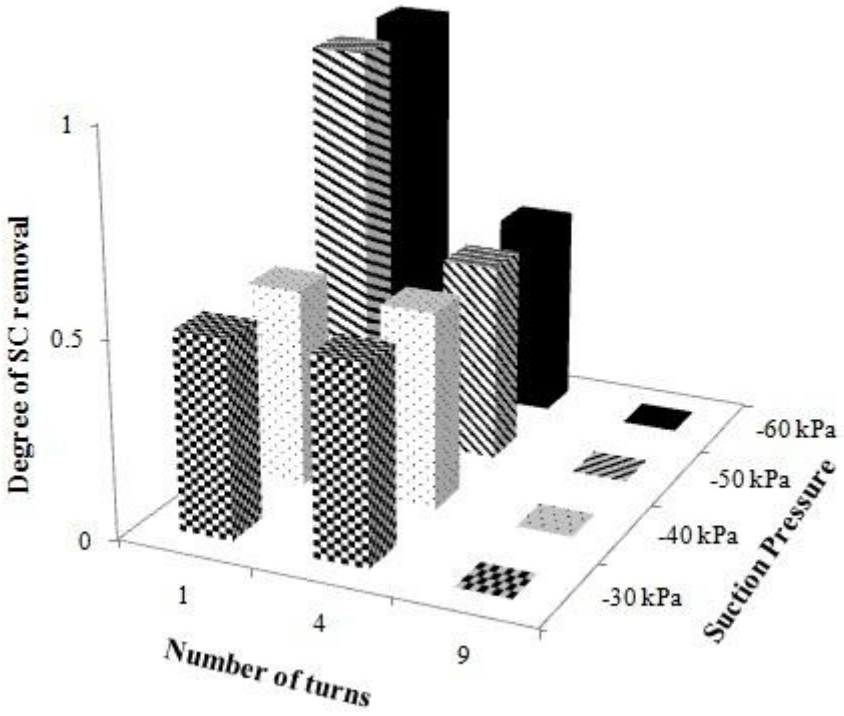

Figure 7. Degree of stratum corneum removal during static mode microdermabrasion at -30, -40, -50, and -60 kPa suction pressure at 1, 4, and 9 turns of the crystal flow rate knob. Complete stratum corneum removal = 1, partial stratum corneum removal = 0.5, and stratum corneum not removed = 0. Data represent the average of three replicate measurements. No error bars are shown because all three measurements at each condition gave identical results.

The intermediate crystal flow rate (4 turns) resulted in partial stratum corneum removal at all suction pressures (Figure 6, center column). For all suction pressures at the lowest crystal flow rate (9 turns), the stratum corneum remained intact (Figure 6, right column). At 9 turns, the greatest contribution to possible tissue removal appeared to be suction pressure, because there is very little crystal flow.

We also sought to evaluate the effect of time on the amount of stratum corneum removal. For the static mode, the skin was abraded at suction pressures of -30, -40, and -50 kPa for 3, 20, and 45 s at 4 turns of the crystal flow rate knob. The histological results for the static mode are

shown in Figure 8. Quantification of the amount of stratum corneum removed is presented in Figure 9. For all pressures, at 3s, the stratum corneum remained intact (Figure 8 left column). However, at 20 and 45 s stratum corneum and viable epidermis were removed at all pressures tested ((Figure 8 center and right columns). Overall, time had a significant effect on tissue removal (Figure 9, two-way ANOVA, $P < 0.05$), but the effects of pressure were not significant (Figure 9, two-way ANOVA, $P > 0.05$). These results demonstrate the importance of exposure time on the depth of abrasion, in addition to the important role of crystal flow rate demonstrated above.

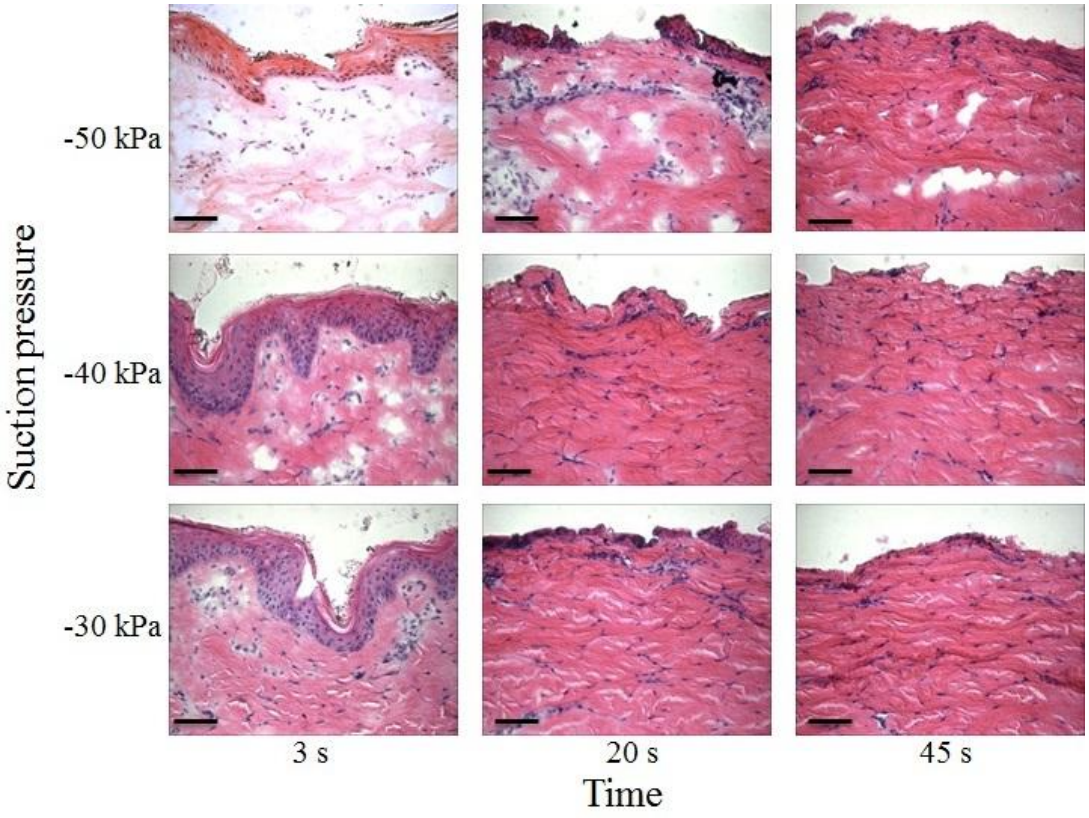

Figure 8. Skin abraded using the static mode at -30, -40, and -50 kPa suction pressure at 4 turns of the crystal flow knob applied for 3, 20, and 45 s. Representative H&E-stained sections of porcine cadaver skin are shown. Scale bar = 50 µm.

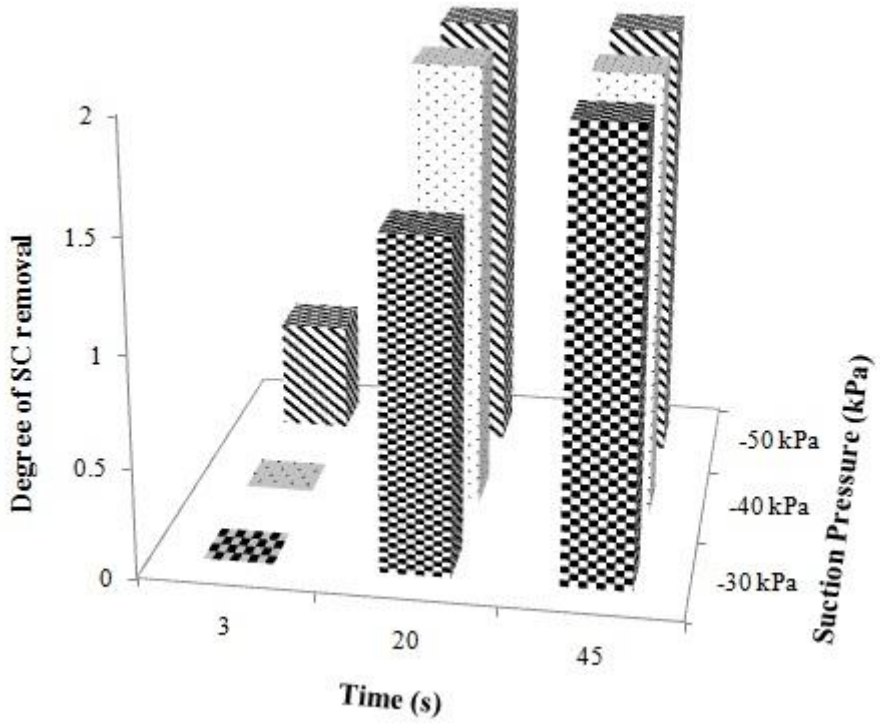

Figure 9. Degree of stratum corneum removal during static mode microdermabrasion at -30, 40, and -50 kPa suction pressure at 4 turns of the crystal flow knob applied for 3, 20, and 45 s. Viable epidermis removal=1.5, complete stratum corneum removal = 1, partial stratum corneum removal = 0.5, and stratum corneum not removed = 0. Data represent the average of three replicate measurements. Error bars are not shown to simplify the presentation.

Dynamic Mode

For the dynamic mode experiments, the skin was abraded at the same crystal flow rates and suction pressures as the static mode, but the microdermabrasion handpiece was moved across the skin for 10 passes at a rate of 1 pass/s. Figure 10 presents histological images of representative skin sections after microdermabrasion and Figure 11 quantifies these data. Similar to the static mode, increasing the crystal flow rate significantly increased the amount of stratum corneum removal (Figure 11, two-way ANOVA, $P < 0.05$), whereas suction pressure did not have a significant effect (Figure 11, two-way ANOVA, $P > 0.05$). At the most aggressive crystal flow rate (1 turn), the stratum corneum was completely removed for all pressures and the viable

epidermis remained intact (Figure 10, left column). At 4 turns of the crystal flow rate knob, the stratum corneum was partially removed for all pressures (Figure 10, center column). At 9 turns, the stratum corneum remained intact on the skin (Figure 10, right column).

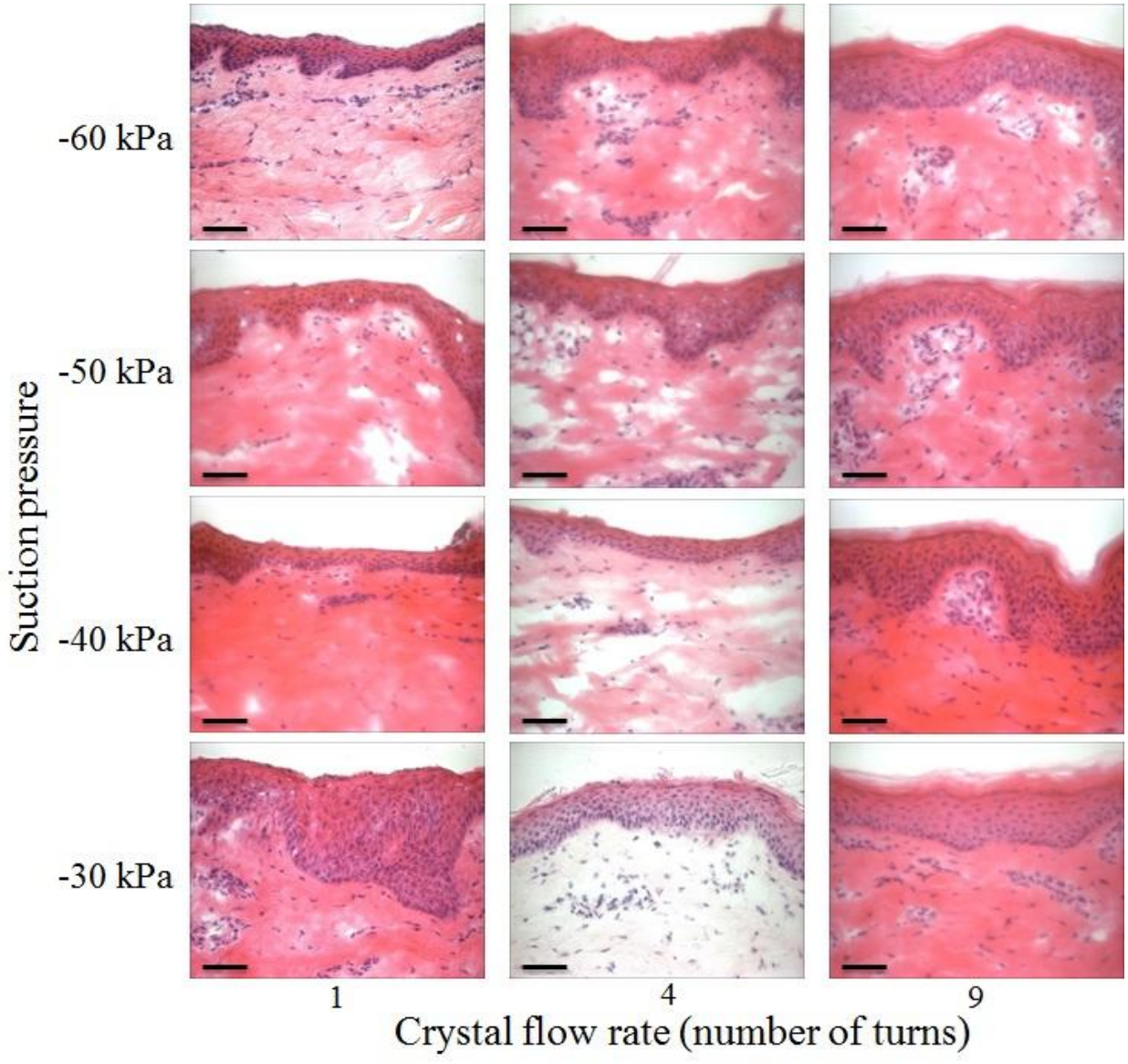

Figure 10. Skin abraded using dynamic mode microdermabrasion at -30, -40, -50, and -60 kPa suction pressure for 1, 4, and 9 turns of the crystal flow rate knob. Crystal flow rate scales inversely with the number of knob turns, such that 1 turn corresponds to the largest crystal flow rate (see Appendix B for more information). Representative H&E-stained sections of porcine cadaver skin are shown. Scale bar = 50 µm.

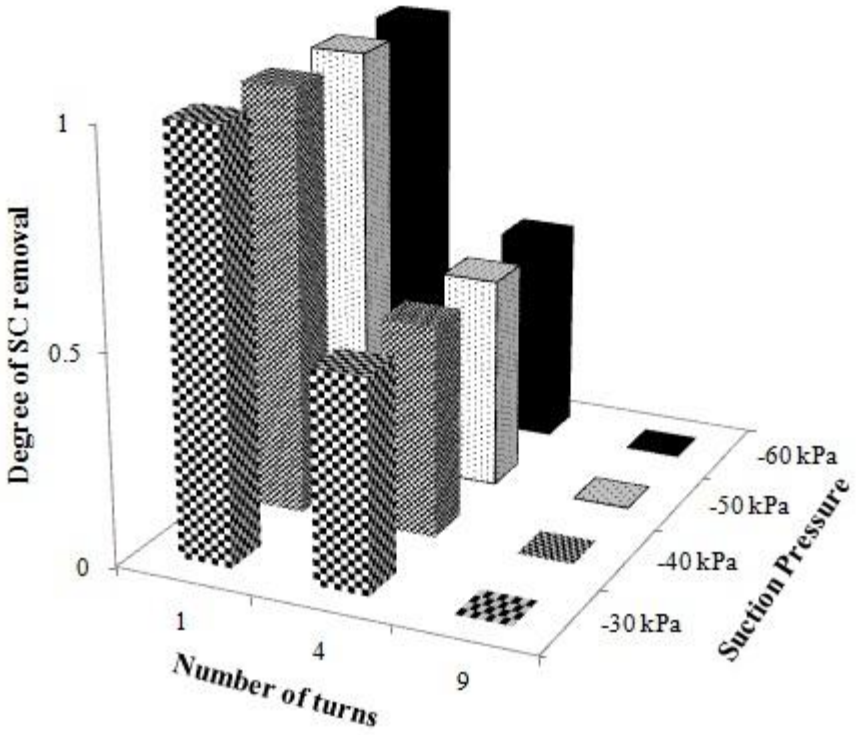

Figure 11. Degree of stratum corneum removal during dynamic mode microdermabrasion at -30, 40, -50, and -60 kPa suction pressure at 1, 4, and 9 turns of the crystal flow rate knob. Complete stratum corneum removal = 1, partial stratum corneum removal = 0.5, and stratum corneum not removed = 0. Data represent the average of three replicate measurements. No error bars are shown because all three measurements at each condition gave identical results.

For the dynamic mode time experiments, the number of passes was set at 1, 10 or 50 passes, which was performed using suction pressures of -25 and -45 kPa at 4.5 turns. The histological images of skin and quantitative analysis of the degree of stratum corneum removal is shown in Figure 12 and Figure 13, respectively. For both pressures at 1 pass, the stratum corneum remained intact (Figure 12 right column). At the 10 passes, the skin treated at -25 kPa had partial stratum corneum removal and skin abraded at -45 kPa had complete stratum corneum removal (Figure 12 middle column). At 50 passes, both samples had complete stratum corneum

removal (Figure 12 left column). For all times and pressures the viable epidermis remained intact. Through quantitative analysis of these experiments, however, neither time (Figure 13, two-way ANOVA, $P = 0.07$) nor pressure (Figure 13, two-way ANOVA, $P > 0.05$) was found to have a statistically significant effect. This lack of statistical significance is possibly due to the small sample size, because only two pressures were examined.

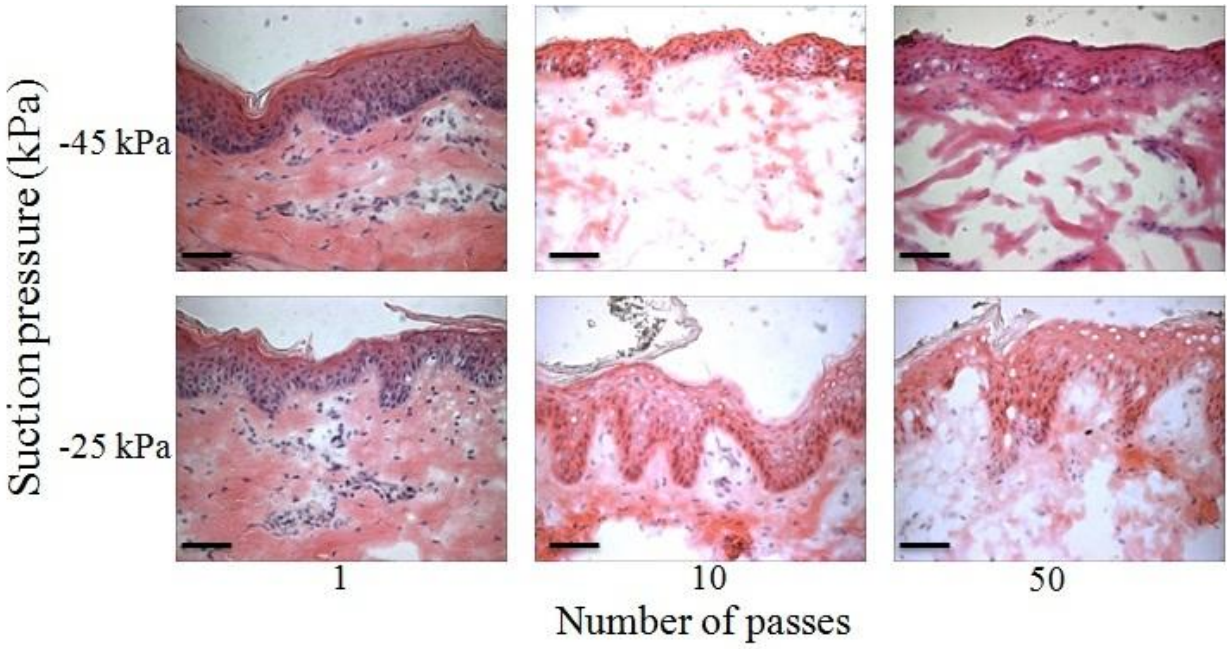

Figure 12. Skin abraded using the dynamic mode microdermabrasion at -25 and -45 kPa suction pressure at 4.5 turns of the crystal flow rate knob applied for 1, 10, and 50 passes. Representative H&E-stained sections of porcine cadaver skin are shown. Scale bar = 50 µm.

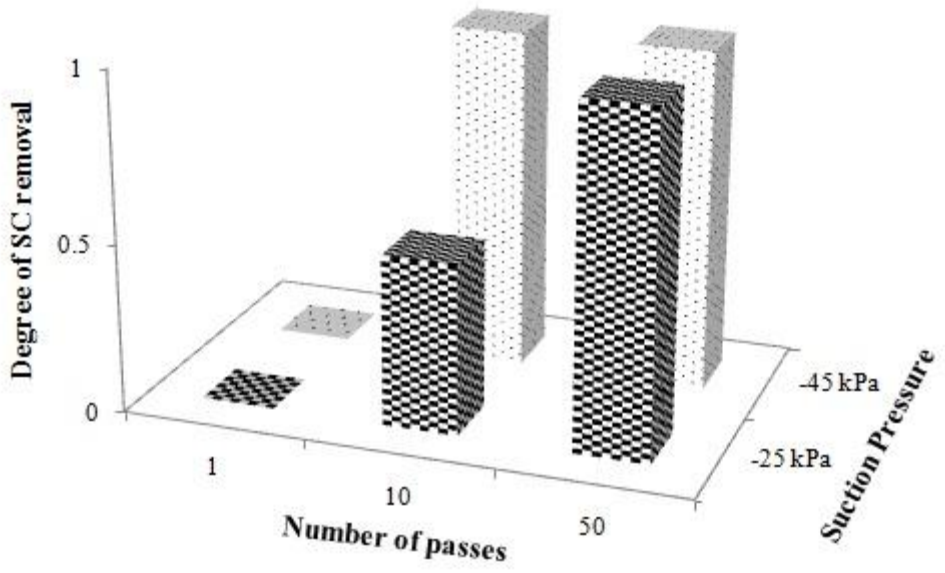

Figure 13. Degree of stratum corneum removal during dynamic mode microdermabrasion at -25 and -45 kPa suction pressure at 4.5 turns of the crystal flow rate knob applied for 1, 10, and 50 turns. Complete stratum corneum removal = 1, partial stratum corneum removal = 0.5, and stratum corneum not removed = 0. Data represent the average of three replicate measurements. Error bars are not shown to simplify the presentati**on.**

Control over Area of Microdermabrasion by Using a Mask

We have shown above that optimization of microdermabrasion parameters can control the depth of stratum corneum removal. Next, we wanted to control the area of removal and thereby achieve three-dimensional control over pore formation. To accomplish this, we designed a mask to partially cover the skin's surface and, in that way, only expose selected spots on the skin to microdermabrasion (Figure 3C).

Mask Design

In the experiments to optimize microdermabrasion conditions presented above, a single, large area of skin (i.e., many cm^2) was abraded. Abrading such a large area may be cosmetically

unacceptable, take too long to heal, and present increased risk of infection. For that reason, we now introduce the use of a mask to make an array of microscopically small pores. While we wanted the holes in the mask to be as small as possible, they also needed to be large enough to permit the microdermabrasion crystals to flow through and contact the skin. Larger holes also reduced the chances of occlusion due to particle clogging. Because the particles have a diameter of about 100 μm, we selected a hole size of 125 μm. Center-to-center spacing between the holes was set at 500 μm.

Mask thickness was also a concern, because a thicker mask would increase the distance between the skin and the crystal flow from the machine, making particle entry into the hole to contact the skin more difficult. However, a thinner mask might be excessively damaged during the abrasion process (i.e., the crystals not only abrade the skin, but also abrade the mask). Given these constraints, we selected a mask thickness of 50 μm. Made out of stainless steel, this mask provided sufficient durability, but was also sufficiently flexible to conform to the skin surface.

Lastly, we found that the presence of hairs was an important factor because hairs impeded good contact between the mask and the skin. Moreover, the hairs themselves served as masks that blocked microdermabrasion crystals from contacting the skin. This may not be as great a concern for use in humans. However, the very thick hairs present on the porcine skin used in this study needed to be shaved for good results.

Microdermabrasion Using a Mask

The effect of the mask during microdermabrasion was assessed using the static abrasion mode at a suction pressure of -50 kPa for 30, 45, 60, 90, and 120 s at the maximum crystal flow rate (0 turns). For all times, complete removal of stratum corneum was observed and the viable

epidermis remained intact, as shown in Figure 14. We used these relatively aggressive microdermabrasion conditions because of the expectation that the presence of the mask would (i) reduce the effectiveness of microdermabrasion and (ii) provide a possible self-limiting effect due to the inability of microdermabrasion crystals to penetrate deeply through the narrow holes in the mask.

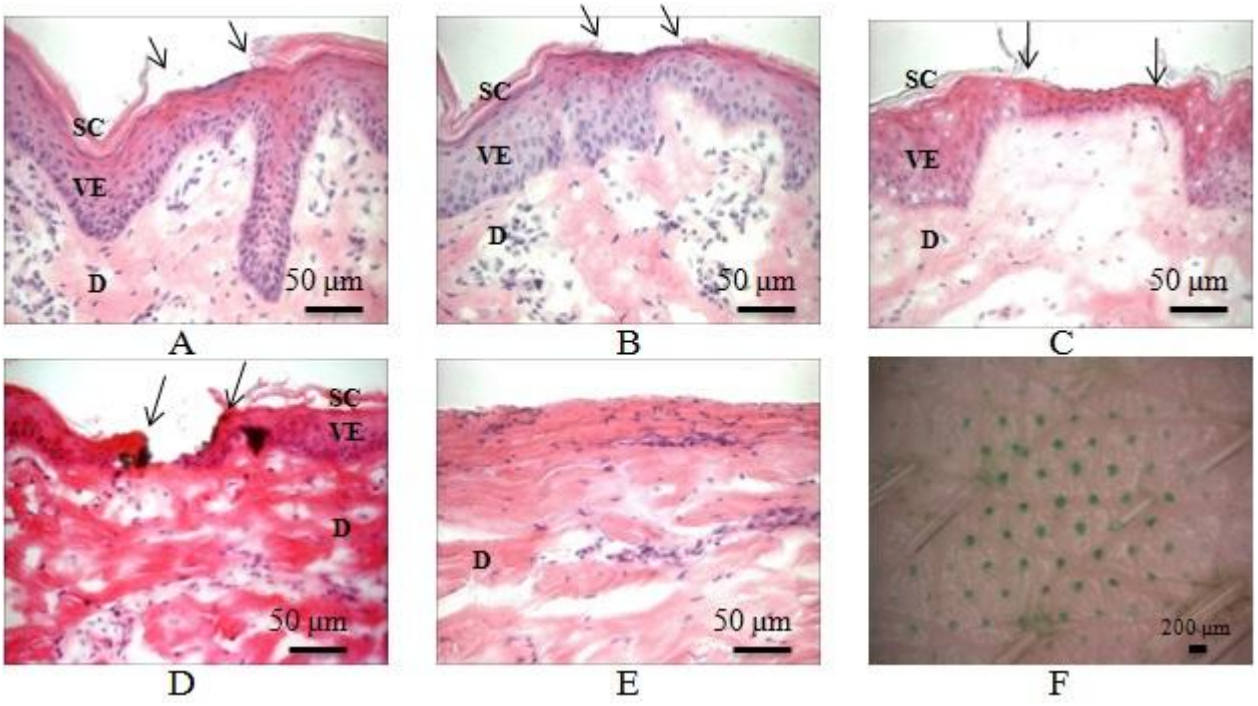

Figure 14. Skin abraded using a mask containing 125 µm-diameter holes at -50 kPa suction pressure and the maximum crystal flow rate (0 turns) for 45 s (A), 60 s (B) and 90 s (C). (D) Skin abraded using a mask containing 250 µm-diameter holes at -50 kPa suction pressure at the maximum crystal flow rate for 30 s. The arrows point to sites of SC removal. (E) Skin abraded at the same condition as (A) without the mask; both the SC and VE were removed. (F) Skin abraded at the same condition as (B) imaged en face at lower magnification to show the holes stained with green dye. SC = stratum corneum, VE = viable epidermis, and D = dermis.

Histological examination presented in Figure 14A– Figure 14C shows representative pores formed in the skin. Their depth spans the full thickness of the stratum corneum, but without damaging viable epidermis. The average width of the pores was 87 ± 22 µm, based on

measurement of 10 pores from 3 different skin samples. This pore size is somewhat smaller than the mask hole size probably because microdermabrasion crystals, which abrade the skin by impacting it primarily at an angle, have difficulty abrading skin along the edges of the mask hole.

Figure 14F shows a lower-magnification, en face view of the skin surface after microdermabrasion at the same conditions used in Figure 14B. Staining with a green dye shows pore formation in the skin following the pattern of the mask (Figure 3C). Closer examination of the pores shows that the green-stained spots have an average diameter of 118 ± 39 μm, based on measurement of 10 pores from 3 different skin samples. Some of the pore diameters were larger than the mask hole diameter and the pore size shown by histology, possibly due to lateral diffusion of dye within the skin.

In Figure 14D, microdermabrasion was carried out using a mask with 250 μm diameter holes. This larger mask hole size led to removal of stratum corneum as well as much of the viable epidermis. This shows that mask hole size not only affects the area of tissue removal but also affects the depth of tissue removal. In Figure 14E, skin was microdermabraded at the same condition as the skin in Figure 14A, but without any mask. In this case, not only was the area of skin abrasion large, but the full epidermis was removed. This further shows that the mask not only limits the area of abrasion, but also influences the depth. The observation that microdermabrasion with the 125-μm mask was independent of exposure time over the range of 30–120 s studied here further suggests a self-limiting feature enabled by the mask. We hypothesize that microdermabrasion crystals are only able to penetrate to a limited depth into the mask holes and this limits how much tissue they can remove. Moreover, we observed the holes to become clogged with microdermabrasion particles over time. This may close off holes and

thereby stop further skin abrasion after a period of time. More work is needed to fully understand this self-limiting feature.

Discussion

This study showed for the first time that controlled microdermabrasion using optimized operating parameters in combination with a mask enabled three-dimensional control of tissue removal that selectively and completely removed small spots of stratum corneum without removing the viable epidermis. Selective removal of stratum corneum is important because damage to the viable epidermis causes trauma to living tissue that could be painful, take longer to heal, and generate cosmetically undesirable appearance. Complete removal of stratum corneum is important because this is needed to eliminate the primary barrier to drug delivery.

We studied the effect of crystal flow rate, suction pressure, exposure time, and handpiece movement on stratum corneum removal and found that crystal flow rate and exposure time had the greatest impact on stratum corneum removal. Over the range of conditions studied, suction pressure had no significant effect. Both static and dynamic handpiece movements were effective. We believe that the crystal flow rate was important because the crystals shear and tear the stratum corneum and, therefore, the number of times crystals impact the skin should correlate with the degree of tissue removal [14]. The exposure time was also an important parameter for similar reasons; increased exposure time increased the number of crystal-skin impacts. The suction pressure, in contrast, had no significant effect on the crystal flow rate or velocity (see Appendix) and, correspondingly, no significant effect on tissue removal. We believe that the suction pressure serves to help remove skin debris and crystals from the skin surface and into the

refuse canister of the microdermabrasion machine. In this way, suction is important to proper function of the microdermabrasion method, but it does not control the tissue removal process.

The importance of crystals in microdermabrasion has been shown in a previous study in which inclusion of crystals increased the expression of proteins needed for dermal remodeling, which is the primary purpose of conventional cosmetic microdermabrasion, as compared to suction pressure alone [57]. However, suction pressure alone (i.e., without crystals) has been shown to remove stratum corneum at pressures of -20 to -40 kPa when the skin was exposed for 24 s [33]. Although similar suction pressures were applied in this study for up to similar periods of time ($\leq$ 45 s static mode and $\leq$ 50 s dynamic mode), no stratum corneum removal was observed without significant crystal flow. While the different exposure times may play a role, the fact that our study used pig skin in vitro and the study that removed stratum corneum with suction alone used human skin in vivo may also be relevant. Consistent with this expectation, a previous study with human skin in vivo found that static mode microdermabrasion at conditions that removed stratum corneum also caused microblisters (i.e., localized separation of epidermis from the underlying dermis) [12] but this was not observed in the present study using pig skin in vitro. This suggests that human skin in vivo may be more susceptible to suction-induced damage than pig skin in vitro.

Both handpiece abrasion modes resulted in selective stratum corneum removal, however the dynamic mode appears to offer advantages (in addition to the lack of microblisters found previously [12]. For example, stratum corneum removal in the static experiments was not as uniform as in the dynamic experiments and the area of tissue removal is limited to that of the microdermabrasion tip (0.4 cm^2). The dynamic mode enabled a larger area of removal (3 cm^2 in

this study) and the results were more consistent. Additionally, the dynamic mode is typically used in the clinical setting for cosmetic microdermabrasion.

Use of a mask in combination with microdermabrasion limited both the area and depth of tissue removal. As discussed above, generating an array of small pores using a mask may be preferable from a safety, cosmetic and patient preference perspective compared to removing stratum corneum from large, continuous areas of skin. By selecting mask hole diameters not much larger than the size of the crystal particles, the mask further served to limit the depth of tissue remove, such that 125 μm holes provided a self-limiting feature that achieved selective removal of stratum corneum independent of exposure time and using aggressive microdermabrasion operating parameters. In this way, the use of a mask was critically important, and arguably more important than the microdermabrasion operating parameters, to enable three-dimensional control over pore formation on the micron scale localized to the stratum corneum.

The pores generated in this study were on the order of 10 μm deep and 100 μm wide. The width of these pores is similar to those created by thermal ablation and piercing with microneedles [50, 51, 53], both of which have been well tolerated in numerous human studies and both of which enable delivery of a broad range of compounds, including large hydrophilic molecules and vaccines. This suggests that the holes made by microdermabrasion should likewise be well tolerated and effective for drug delivery. However, the pores made in the present study are much less deep that those made by thermal ablation or using microneedles, which may make them still better tolerated by patients.

Comparing more broadly to other methods of transdermal drug delivery, there are several additional expected advantages to using microdermabrasion to increase skin permeability. First, microdermabrasion is a well-established clinical technique used routinely for cosmetic

applications that is safe, minimally invasive, requires no down time, and does not leave scars [13]. Competing methods that disrupt stratum corneum structure on the molecular scale, such as chemical enhancers, ultrasound, and iontophoresis, are generally limited to delivering low molecular weight molecules and small macromolecules, because the stratum corneum is left largely intact [1, 49]. Methods that pierce the stratum corneum, such as microneedles, jet injectors, and hypodermic needles, can cause pain, require regulated disposal, and may require professional help for administration. Other methods that completely remove the stratum corneum, such as tape stripping and laser ablation, are generally regarded as impractical for widespread use due to cost and reproducibility [7, 15]. In contrast to these other methods, microdermabrasion has the advantage of being quick, painless, reproducible and able to generate micron-scale pores that selectively breach the stratum corneum barrier layer.

CHAPTER 5

TRANSDERMAL DELIVERY OF MACROMOLECULES USING MICRODERMABRASION

Microdermabrasion is a non-invasive skin resurfacing technique that removes the stratum corneum with pressurized abrasive particles. This study examined the use of microdermabrasion as a skin permeability method to deliver hydrophilic molecules, proteins, and vaccines. Excised full thickness porcine skin was abraded with two conditions that resulted in partial and complete removal of stratum corneum. The skin was exposed to sulforhodamine B, Texas Red bovine albumin, and inactivated influenza A vaccine for 1, 6, and 24 hours. The flux of the sulforhodamine B was measured and the value for the skin with complete stratum corneum removal at 24 hours was 147 times higher than the negative control. Split thickness human skin was also abraded through a polymer mask to remove the stratum corneum and viable epidermis for delivery of sulforhodamine B and U500 Humalog insulin. The penetration of sulforhodamine B and insulin in the skin with the viable epidermis removed was eight times higher than the skin with stratum corneum removal. The abrasion depth and the drug molecular weight were the most important factors that determined the diffusion rate and penetration depth of the molecule. This study demonstrates that microdermabrasion can be used to increase the skin's permeability to water soluble molecule larger than 500 Da.

Introduction

Transdermal drug delivery is a highly favored route of drug administration due to the skin's large surface area and ease of administration [1]. The advantages are that it avoids drug

degradation due to the first pass effect of the liver, does not involve the use of needles, and does not cause pain. Despite the advantages, the skin serves as a barrier that protects the body from the external environment and prevents water loss. This barrier function also prevents most hydrophilic and large molecular weight drugs (MW>500 Da) from penetrating intact skin. The main barrier to transdermal drug delivery is the stratum corneum, the top layer of skin. The stratum corneum is composed of dead flattened keratinocytes that are surrounded by a lipid extracellular matrix [24]. Some compounds that are lipophilic and have a molecular weight less than 500 Da can penetrate intact stratum corneum at useful rates. As a result, only 19 drugs have been approved by FDA for delivery in transdermal patches [1].

Several transdermal techniques have been developed to pierce or remove the stratum corneum to increase the penetration of hydrophilic drugs and proteins to the skin. Such techniques include microneedles, chemical enhancers, tape stripping, thermal ablation, and abrasion. Microneedles are micron-size needles that pierce through the stratum corneum to deliver drugs and vaccines [1, 19, 53, 58-60]. Due to their shallow penetration depth, they cause less pain than traditional hypodermic needles [6, 60]. Chemical enhancers alter the lipid structure of stratum corneum to increase drug delivery [1, 61]. Tape stripping, thermal ablation, and abrasion remove the stratum corneum with adhesives, heat, or abrasive particles, respectively [9, 13, 50, 53]. This study focuses on the use of abrasion, specifically microdermabrasion, as a method of increasing the permeability of water soluble molecules across skin.

Microdermabrasion is a non-invasive FDA-approved cosmetic technique that reduces the appearance of superficial scars and wrinkles [15, 27, 57]. The procedure removes the stratum corneum by bombarding it with abrasive particles under vacuum [14, 56]. Although it was originally designed for cosmetic use, several published studies that have used microdermabrasion

to deliver low molecular weight molecules such as vitamin C (MW 176 Da), 5-aminolevulinic acid (MW 168 Da), and 5-fluorouracil (MW 130 Da) to the skin [7, 8, 13]. In those studies the abrasion resulted in partial stratum corneum removal. In another study conducted by Gill et al. microdermabrasion was used to completely remove the stratum corneum and Modified Vaccina Ankara, a vaccine, was delivered to rhesus macaques monkeys [12]. The vaccine generated a measurable antibody response in the monkeys. This study delivered large hydrophilic molecules (MW>500 Da) and proteins to skin after controlled microdermabrasion that completely and selectively removed the stratum corneum or viable epidermis to examine the barrier properties of both layers. This study uses microdermabrasion, with and without a mask, to remove the stratum corneum to increase the skin's permeability to hydrophilic drugs.

Results

Skin Abrasion

Shown in Figure 15 is intact skin (picture A), skin abraded without a mask with the stratum corneum removed (picture B), and skin abraded with a mask with stratum corneum (picture C) and viable epidermis removal (picture D). The intact skin (picture A) has all the layers present. The stratum corneum, the top layer, is stained pink and the viable epidermis, located directly beneath the stratum corneum, has blue staining indicating the nuclei of the cells. The dermis, the third layer, is stained pink and has areas of nuclei staining. Shown in picture B is skin that was abraded without a mask. The stratum corneum was removed and the viable epidermis remained intact. The skin shown in pictures C and D was abraded through a mask and the stratum corneum and viable epidermis were removed, respectively. The arrows point to the site of abrasion.

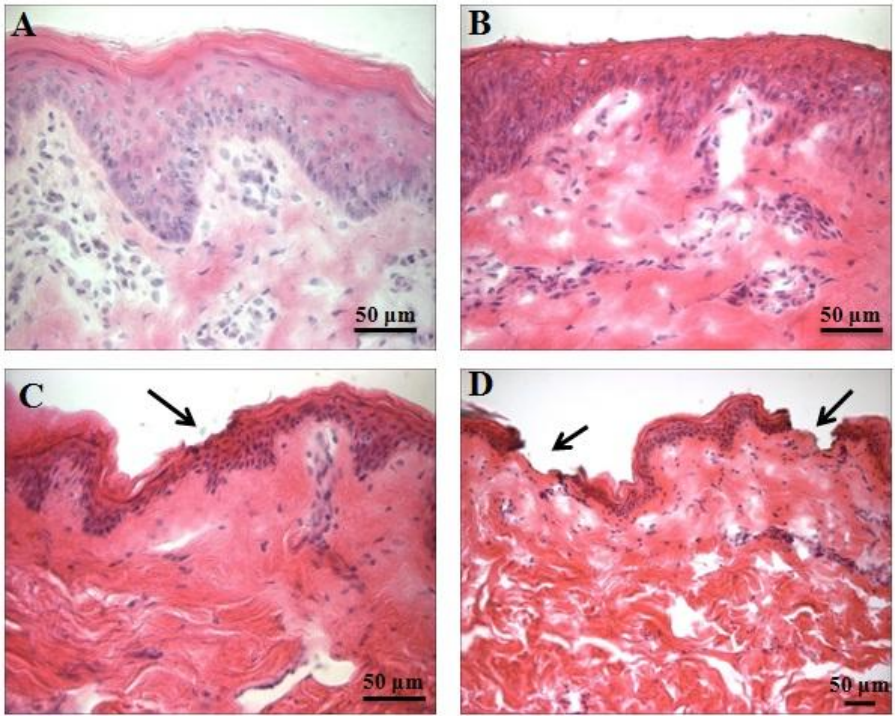

Figure 15. Shown in the picture is intact skin (A) and skin treated with microdermabrasion, without a mask, with the stratum corneum removal (B). Skin abraded through a mask with the stratum corneum removed (C) and viable epidermis removed (D). The arrows point to the site of skin removal.

Sulforhodamine B Delivery

The fluorescent images from the full thickness skin SR diffusion experiments that were abraded using the condition -45 kPa for 50 passes are shown in Figure 16. The pictures were taken at the same exposure time and gain to compare the depth and intensity of the SR at each time point. The SR penetration through non-abraded skin was low, as expected. In contrast, the SR penetration through abraded skin was significantly larger and increased throughout the experiment. The skin that was exposed for 1 h had a detectable amount of SR into the superficial dermis, while the 6 and 24 h exposed skin had SR penetration within the dermis.

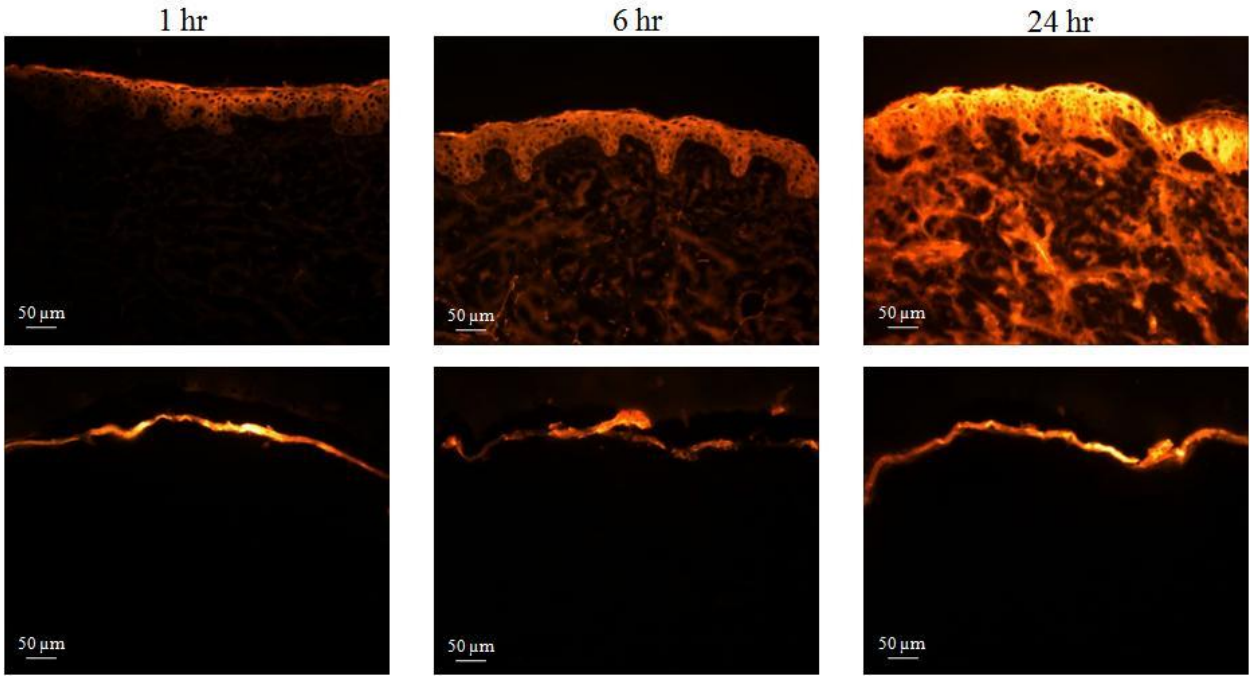

Figure 16. SR delivery into skin treated with microdermabrasion (P=-45 kPa for 50 passes). The top row is abraded skin and the bottom row is control, unabraded skin, for each time point.

The cumulative SR penetration data for the 24 hour experiments are shown in Figure 17. The SR penetration in the negative control skin was low, as expected. That result was confirmed by the histology shown in Figure 2. In contrast, the sulforhodamine B penetration through abraded skin was significantly larger and increased throughout the experiment. The milder settings, 10 passes, resulted in partial SC removal and had lower sulforhodamine B penetration than the 50 passes. All the samples had a 12 hr time lag for delivery and steady state was reached after the 17th hour. At 24 hr, the skin abraded at -45 kPa for 50 passes had five times more SR delivery than -25 kPa for 50 passes. At 24 hours the penetration of the most aggressive setting (-45 kPa for 50 passes) was 140 times more than negative control. These results are consistent with our expectation that microdermabrasion under conditions that remove stratum corneum can dramatically increase skin permeability to hydrophilic molecules.

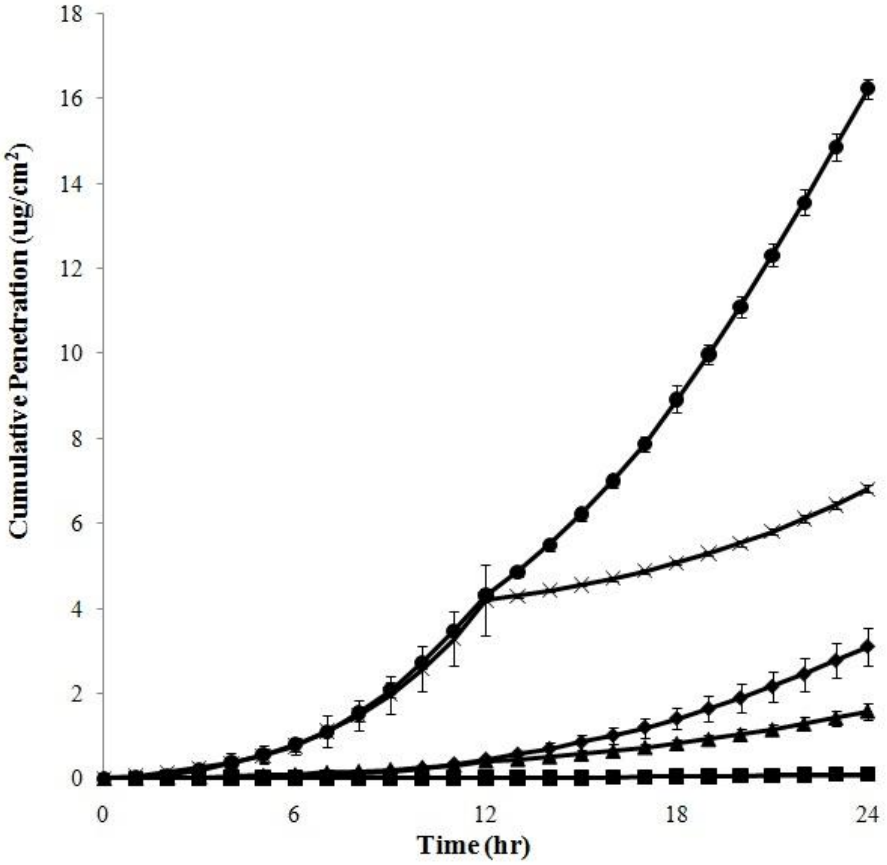

Figure 17. The cumulative penetration of sulforhodamine B in abraded skin over 24 hours. The control skin (■) had the lowest penetration. The skin abraded at -25 kPa (▲) and -50 kPa (♦) with 10 passes both had a lower penetration of sulforhodamine than the same pressures at 50 passes. The sulforhodamine B penetration in the -25 kPa with 50 passes (x) and -50 kP with 50 passes (●) had similar penetration values up to 12 hr, but the -50 kPa penetration greatly increased and exceed the -25 kPa sample from hours 13 to 24. Each line represents three replicates.

Bovine Serum Albumin Delivery

The fluorescent pictures for the abraded and the control skin that were exposed to Texas Red bovine serum albumin for 1, 6, and 24 hours are shown in Figure 18. All the pictures were taken at the same exposure time and gain. The pictures on the top and bottom row are the abraded skin and negative controls, respectively. Texas Red bovine serum albumin did not diffuse the negative control skin. In the abraded skin, the molecule was mainly localized in the

viable epidermis as indicated by the layer's fluorescence intensity. In the skin exposed for one hour, the molecule penetrated the viable epidermis and superficial dermis. Texas Red bovine serum albumin diffused into the viable epidermis and dermis in the 6 and 24 hour exposed skin; however, it did not diffuse into the entire thickness of the dermis. There was no difference in the Texas Red bovine serum albumin intensity in the 6 and 24 hours experiments as compared to the sulforhodamine B experiments. The flux was not measured because preliminary diffusion experiments showed that Texas Red bovine serum albumin did not diffuse across the dermis.

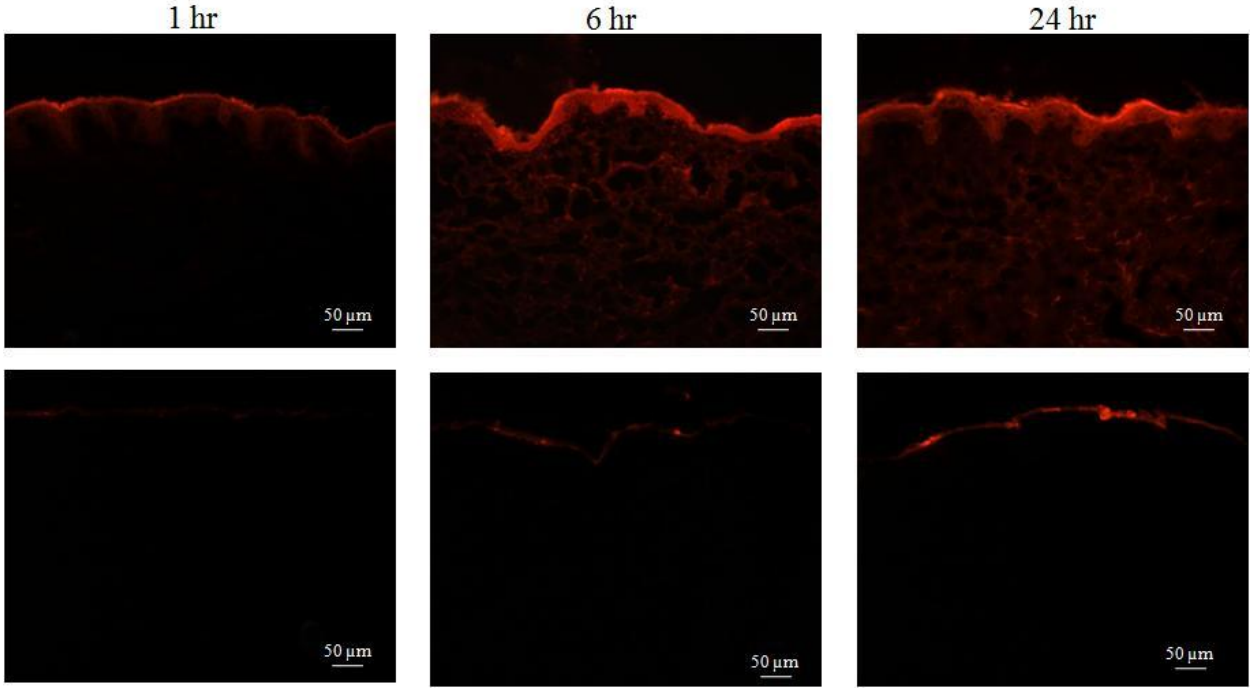

Figure 18. BSA delivery into abraded skin exposed for 1, 6, and 24 hours. The skin that was treated with microdermabrasion is shown on the top row and the control skin on the bottom row.

Inactivated Influenza Delivery

The histology pictures for the inactivated influenza A vaccine are shown in (Figure 19). The vaccine penetrated the 24 hr sample, but not the negative control, 1, or 6 hr sample. The

virus particles were larger than sulforhodamine B and Texas Red bovine serum albumin and diffused slowly into the skin. The flux and penetration of the influenza virus was not quantified since it did not diffuse across the dermis.

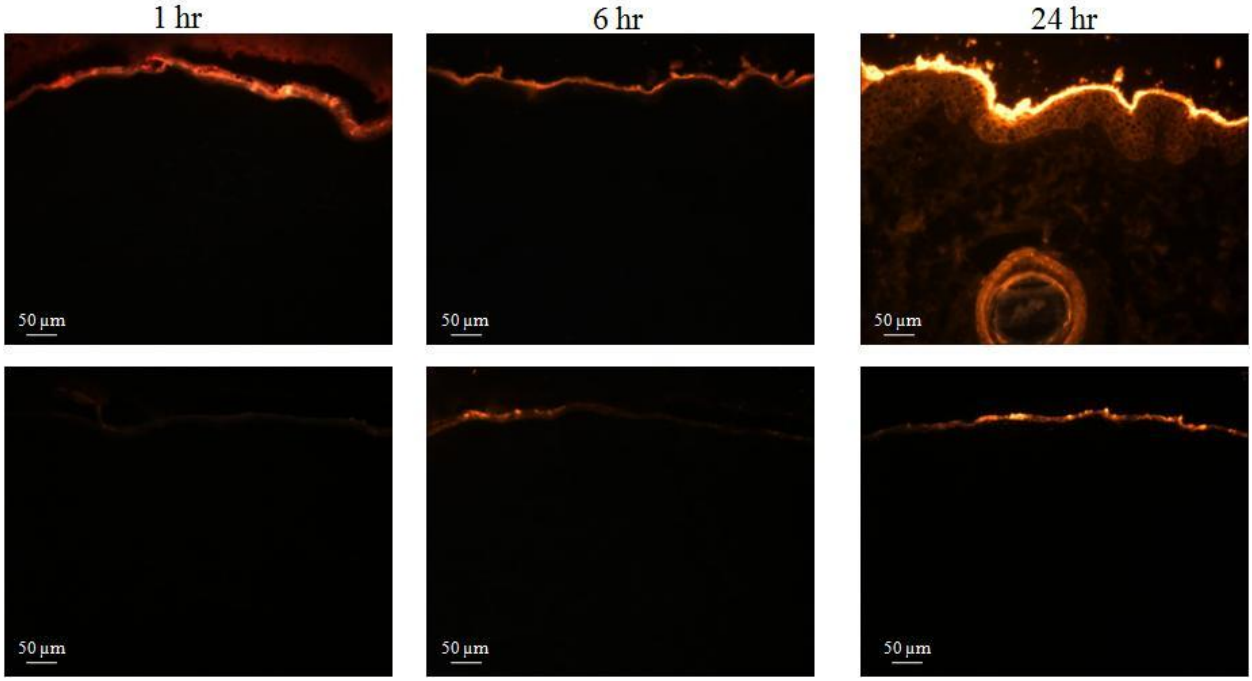

Figure 19. Delivery of R18-labeled inactivated influenza A virus to abraded skin for 1, 6, and 24 hr. The top row is the abraded skin, while the bottom row is the negative control for the time points.

Mask Delivery

The histological results from the split thickness sulforhodamine B experiment are shown in Figure 20. Shown on the top row is the skin after abrasion. The area of abrasion was revealed using green dye. Picture A and B is the skin that has stratum corneum and viable epidermis removal, respectively. Lateral diffusion of the dye can be seen in the viable epidermis photograph, indicating a deeper abrasion than the skin with stratum corneum removal. The sulforhodamine B penetration is shown the skin with stratum corneum removal (picture C) and

viable epidermis removal (picture D). The pictures were taken at the same exposure time and the viable epidermis removal picture had a higher concentration of sulforhodamine B as indicated by the dye intensity. The bottom row is the H&E stained pictures of the skin after sectioning. The arrows point to the area of abrasion.

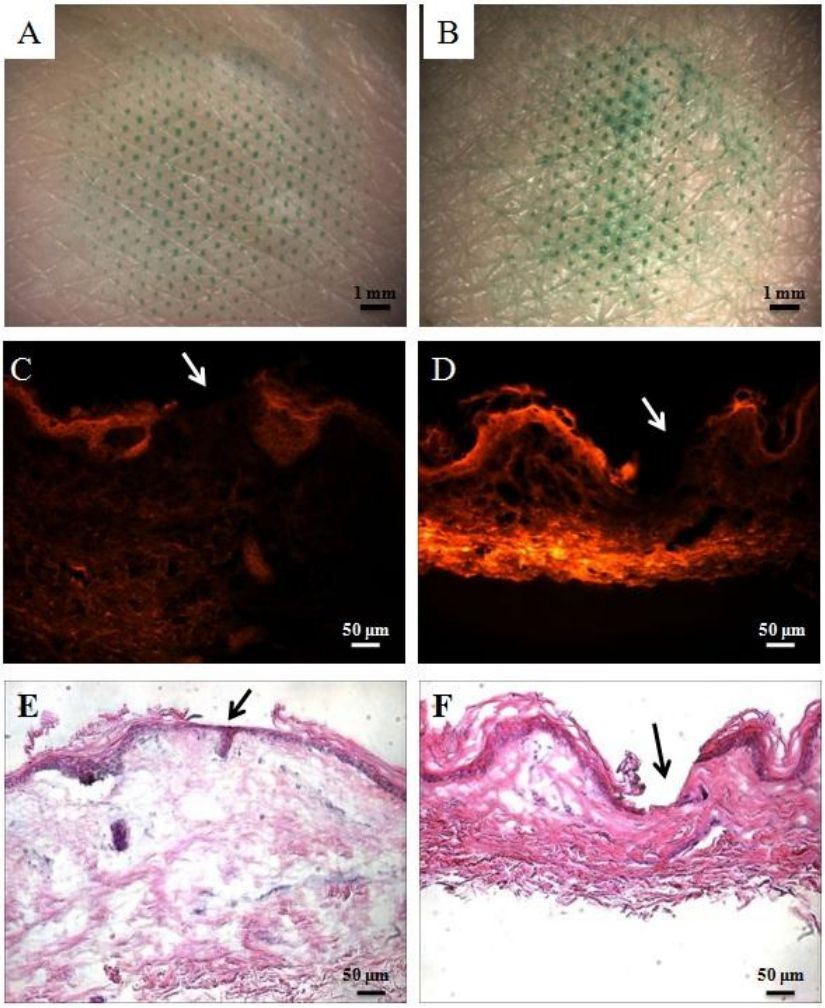

Figure 20. Human split thickness skin that was abraded through a mask to remove the stratum corneum (A) and viable epidermis (B). The area of abrasion was revealed with green dye. The skin with the stratum corneum (C) and viable epidermis (D) removed was exposed to sulforhodamine B for 12 hr. Pictures E and F are the H&E stained pictures for skin with stratum corneum and viable epidermis removal, respectively. The arrows point to the area of abrasion.

The cumulative penetration results for sulforhodamine B delivery to split thickness skin with stratum corneum and viable epidermis removal after masked abrasion are shown in Figure 21. Sulforhodamine B did not penetrate the intact negative control skin. Removing the viable epidermis significantly increased the flux and penetration of the molecule in the skin in comparison to removing only stratum corneum. The skin with viable epidermis removal had a seven times higher penetration than the stratum corneum removal group. Both samples reached steady state within four hours.

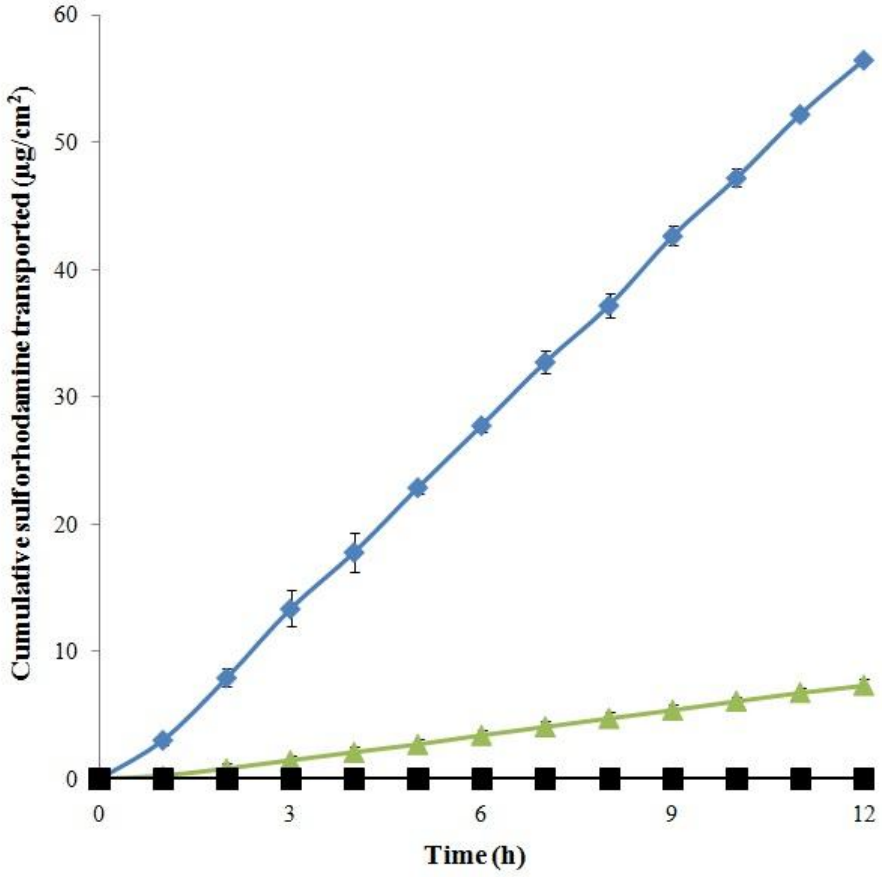

Figure 21. Sulforhodamine delivery in split thickness abraded skin, through a polymer mask, for 12 hours. Sulforhodamine did not penetrate the negative control skin (■). The penetration in the skin with viable epidermis (VE) removal (♦) was seven times higher than the stratum corneum (SC) removal (▲) group at 24 hours.

An insulin solution consisting of 80 % U500 Humalog and 20 % FITC-labeled bovine insulin was delivered to skin with SC and VE removal after abrasion using a mask. The histology pictures for the insulin delivery experiments are shown in Figure 22. The top row is the fluorescent images of the FITC-labeled bovine insulin penetration in the skin and shown on the bottom row is the H&E pictures of the skin. The arrows are pointing to the site of stratum corneum removal (C) and viable epidermis removal (D). Since the skin was exposed to the donor chamber for 54 hrs the affect of over-hydration is present in the H&E pictures.

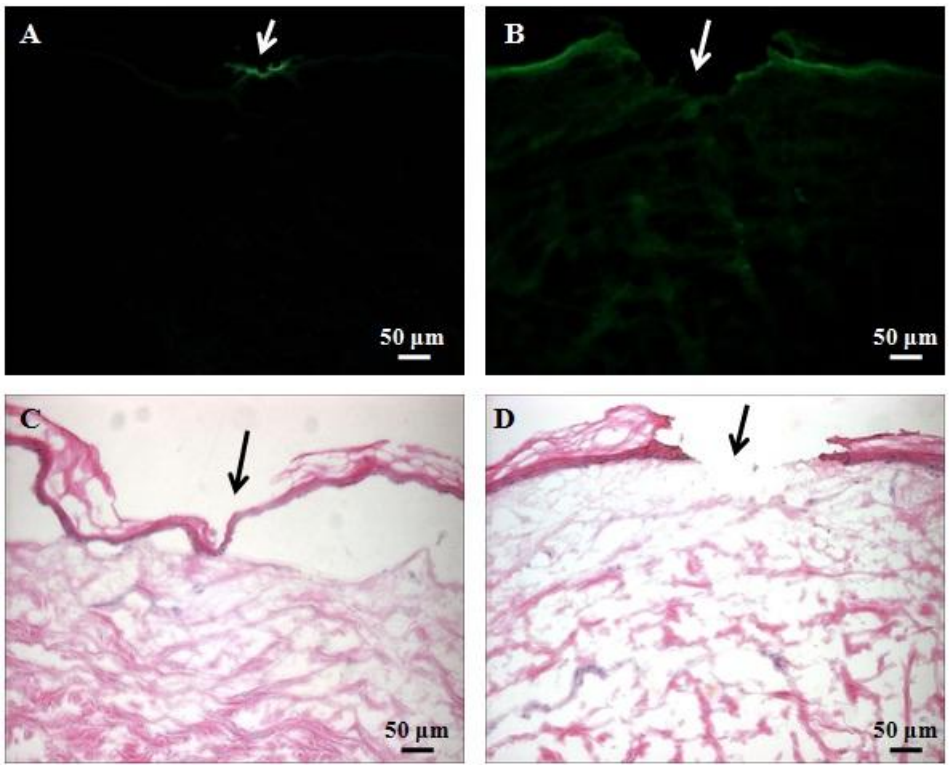

Figure 22. Skin abraded and exposed to U500 and FITC-insulin bovine insulin for 54 hours. Pictures A and C is the skin with stratum corneum removal, while pictures B and D is the skin with viable epidermis removal. The arrows point to the area of abrasion.

The penetration of the FITC-labeled bovine insulin was measured using florescence and is shown in Figure 23. The insulin penetration in the VE removal skin was 17 times higher than

the skin with SC removal at the end of the experiment. The insulin did not penetrate the negative control. The skin with the stratum corneum removed had a lower FITC-insulin penetration than the skin with viable epidermis removal. The insulin penetration in the viable epidermis removal skin was 17 times higher than the skin with stratum corneum removal at the conclusion of the experiment.

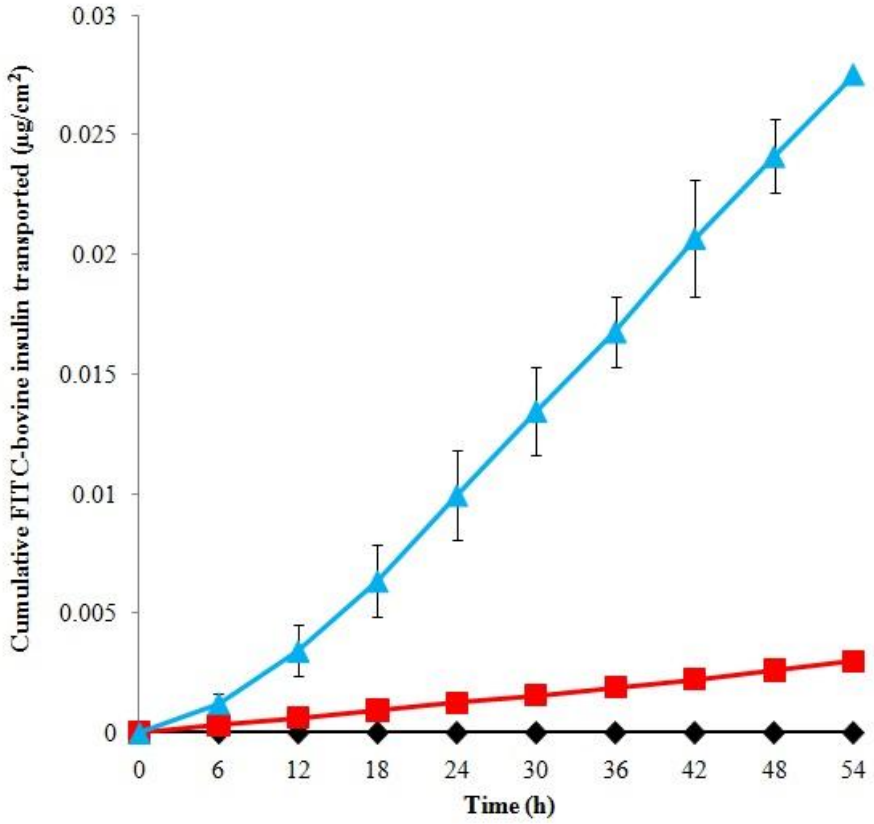

Figure 23. The cumulative penetration of FITC-labeled bovine insulin that was delivered to split thickness human skin that was abraded through a mask. The FITC did not penetrate the negative control skin (♦). The penetration of the FITC-labeled bovine insulin in the viable epidermis group (▲) was higher than the stratum corneum group (■). At the conclusion of experiment, the penetration of the skin that had viable epidermis removal was 17 times higher than the skin with the stratum corneum removed. Each line represents three replicates.

The amount of insulin that was delivered was determined using ELISA and results are shown in Figure 24. The concentration of insulin delivered in the skin that with viable epidermis removal was almost ten times higher than the stratum corneum removal group. Both removal groups were significantly higher than the negative control. The ELISA information confirms the fluorescence measurements in showing that the removing the viable epidermis increases the amount of insulin that can be delivered.

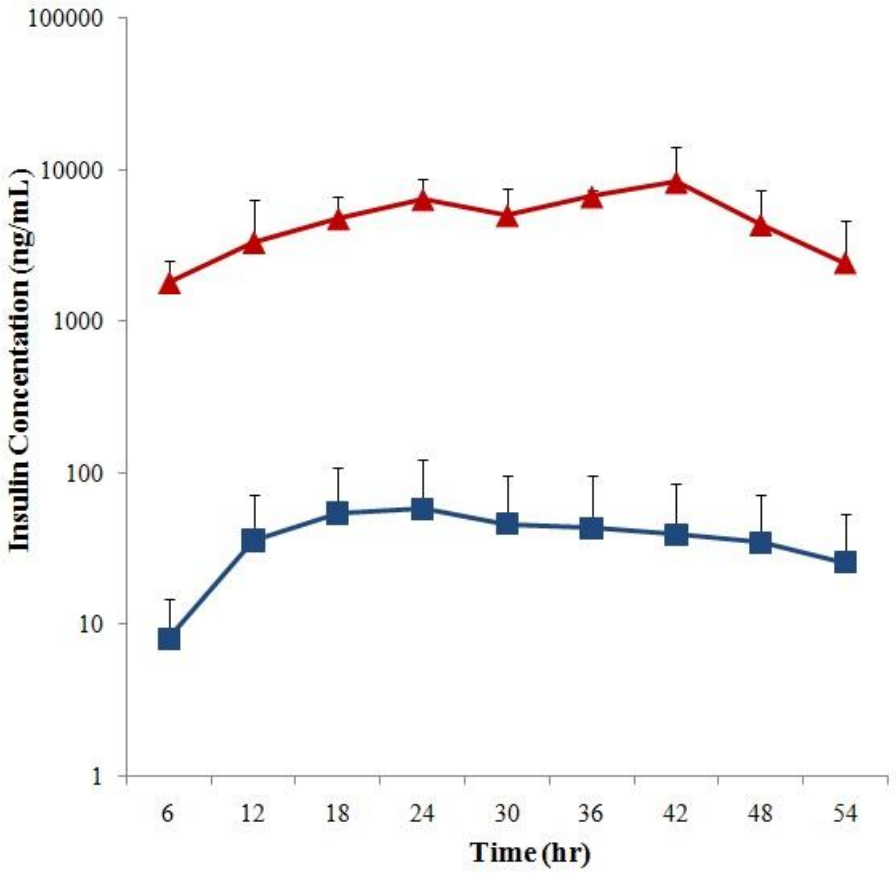

Figure 24. Shown in the graph are the ELISA results for the insulin delivery experiment. The stratum corneum removal (■) concentration ranged from 10 to 58 ng/mL and the viable epidermis group (▲) concentration ranged from 1800 to 8000 ng/mL.

Discussion

By using microdermabrasion to remove the stratum corneum, we were able to demonstrate that hydrophilic molecules and proteins with a molecular weight larger than 500 Da can be delivered for transdermal drug delivery. We also showed that the viable epidermis serves as an important barrier for molecule transport. For the sulforhodamine B study in full thickness skin, without a mask, sulforhodamine B penetrated the entire dermis within six hours for the samples in which the stratum corneum was completely abraded (-45 kPa for 50 passes). In the case of the settings with 10 passes, where the SC was partially removed, sulforhodamine B penetrated the skin but the penetration and flux were significantly lower than the samples with complete sulforhodamine B removal. These results show that partially removing the sulforhodamine B increases the skin's permeability, but maximum drug delivery is achieved when the sulforhodamine B is completely removed.

Due to the molecular weight of Texas Red bovine serum, all the sulforhodamine B was removed during the delivery experiments. The skin was abraded without the use of a mask. Texas Red bovine serum penetrated the abraded skin, but did not diffuse into the untreated control skin. There also was a significant time lag in the rate of diffusion and the fluorescence intensity did not change between the 6 and 24 hour sample. Compared to sulforhodamine B, Texas Red bovine serum was mostly localized in the viable epidermis. This is likely due to the basal lamina, located between the viable epidermis and dermis, which serves as a barrier to compounds larger than 40 kDa [62]. This barrier dramatically slowed down the diffusion of Texas Red bovine serum and resulted in it penetrating the dermis only in the 6 and 24 hour experiments. Also due its large molecular weight, Texas Red bovine serum did completely diffuse across the entire dermis, but it reached the site of the systemic circulation

(epidermis/dermis junction). Proteins that are delivered using microdermabrasion may be beneficial for treating skin diseases in the viable epidermis and superficial dermis.

The influenza delivery results were similar to Texas Red bovine serum. The penetration of the vaccine occurred between 6 and 24 hours. The delivery time was due to the large molecular weight of the virus. Also the virus was inactivated, so the delivery relied primarily on diffusion. Vaccine delivery was examined because studies have found that delivering vaccines to the epidermis can illicit a greater immune response than traditional routes [63]. This is due to the large number of dendritic and Langerhan's cells that are found in the viable epidermis and dermis. These cells are first line of defense in protecting the body against infection when the skin is breached [63]. Many vaccines for tuberculosis and small pox are delivered into the viable epidermis and dermis [11].

Using a mask in conjunction with abrading the skin allowed better three dimensional control of the abrasion site. The mask experiments were carried out in split thickness skin because it was determined in preliminary experiments that the concentration of the molecules could not be measured. Removing the viable epidermis resulted in ten fold increase the penetration of sulforhodamine B and insulin. Decreasing the skin thickness also significantly decreased the delivery lag time. Compared to the full thickness skin the split thickness skin was three times higher than the full thickness skin. This is due to the fact that all of the subcutaneous fat was not completely removed from the dermis and this created an additional barrier. Also, there was a large variability in the skin thickness, the full thickness skin was 3.5 mm and the split thickness skin was 500 μm.

The delivery of the drugs relied primarily on diffusion. The lower molecular weight drug was able to diffusion faster than the protein and vaccine. The depth of abrasion was an important

parameter that determined the penetration of drugs. Although we showed that you can deliver a range of compounds using microdermabrasion, other factors such as dose and application time should be considered for administering drugs using microdermabrasion. Large molecular weight drugs are probably impractical to deliver due to the long diffusion time. Future experiments will be conducted to determine the efficacy of proteins that are administered using microdermabrasion to determine if a therapeutic amount can be delivered to the systemic circulation.

CHAPTER 6

TRANSDERMAL INSULIN DELIVERY USING MICRODERMABRASION

Diabetes mellitus is a metabolic disorder that is characterized by the lack of insulin production or insulin resistance. Traditionally diabetes is treated by administering insulin with a subcutaneous injection or by an insulin pump. This study investigates the use of microdermabrasion, a non-invasive cosmetic skin resurfacing technique, as a method to administer insulin to diabetic rats. Thirty-nine rats were injected with streptozocin to induce diabetes. The rats were abraded through a polymer mask to control the area of abrasion with conditions that removed the stratum corneum and viable epidermis. After abrasion, an insulin-filled patch was placed on the area of abrasion and insulin was delivered for four hours and the blood glucose was monitored for eight hours. The maximum blood glucose decrease for the rats with stratum corneum removal was 48 mg/dL at 6 h after abrasion. However, removing the viable epidermis resulted in a maximum blood decrease of 147 mg/dL at 4 h after abrasion. The peak concentration of insulin that was detected in the blood serum of the stratum corneum and viable epidermis removal groups was 0.51 and 1 ng/mL ($1.77x10^{-8}$ and $2.31x10^{-8}$ U/mL), respectively. The depth of abrasion was the most significant factor on the rate of insulin delivery. Microdermabrasion can be used as a transdermal drug method for administering insulin and can significantly lower the blood glucose levels.

Introduction

Diabetes mellitus is a metabolic disorder that is characterized by the lack of insulin production (Type I) or insulin resistance (Type II) [64, 65]. Insulin is a protein that is produced by the beta cells in the pancreas and it functions to allow cells to transport glucose from the

blood. People who suffer from Type I diabetes, also known as juvenile diabetes, do not produce insulin due to autoimmune destruction of the beta cells [65]. Type I patients are insulin dependant and require frequent daily insulin injections to regulate blood glucose levels. Type II diabetes, also known as adult onset diabetes, is caused by insulin resistance and is often attributed to obesity [64, 66]. Typically, patients can avoid becoming insulin dependant by taking medication and making lifestyle changes [64]. In 2010, it was estimated that were 150 million people in the world who suffer from diabetes [64].

Traditionally diabetes is treating by measuring the blood glucose and administering insulin with a subcutaneous injection or an insulin pump. The insulin pump is a delivery device that is programmed by the user to administer the proper insulin dose through a catheter implanted in the skin. Although these delivery routes are the most common and effective methods of delivering insulin, there are several drawbacks to using syringes and pumps. Needle-phobia, pain, regulated waste disposal, cost, and needle stick injuries are disadvantages to traditional diabetes treatment. These disadvantages have lead to the discovery of less invasive methods for treating diabetes to the reduce use of hypodermic needles.

Several new delivery methods and devices, such as inhalation and microneedles, have been designed to treat diabetes and resolve the issues associated with using hypodermic needles. Inhalable insulin formulations are designed to eliminate injections and deliver insulin into the bloodstream through the lung mucosa. One such pharmaceutical product is Exubera®, which was approved by the FDA in 2006. However, due to its side effects it was later withdrawn from the market [67]. Microneedles are micro-size needles that can be used to deliver insulin either in conjunction with a patch or by infusion [18, 58]. One published study used solid microneedle in conjunction with a insulin reservoir to successfully lower the blood glucose in

diabetic rats [58]. Another study used hollow microneedle to infuse insulin to diabetic human subjects [60]. The study lowered the patients' blood glucose and it also reported that the subjects did not report pain, which would increase patient compliance.

Another method of administering insulin is microdermabrasion, a superficial cosmetic resurfacing technique that removes the skin's layers by bombarding them with pressurized particles [14, 15]. Traditionally, microdermabrasion is used to lessen the appearance of fine lines, wrinkles, and scars [15, 56]. In recent years, microdermabrasion has been used as a method of disrupting the stratum corneum for transdermal drug delivery [1, 7, 8, 12, 13]. This study investigated the use of microdermabrasion, in conjunction with a polymer mask, as a method of delivering insulin to diabetic rats.

Results

We wanted to determine if microdermabrasion can deliver a therapeutic dose of insulin and if the depth of abrasion had an affect on the rate of insulin delivery. The cumulative blood glucose change for all the groups are shown in Figure 25. Only the animals that survived the entire experiment and met the diabetes induction criteria were used for the blood glucose and insulin quantification analysis. The negative control group maintained high blood glucose values throughout the experiment. The positive control animals were used to estimate the amount of insulin that was delivered using microdermabrasion. The positive control animals received a bolus injection of 0.1 U of insulin and exhibited a 63 ± 24 point decrease in blood glucose levels within 30 min of administration. However, the blood glucose returned to hyperglycemic levels (i.e.,>250 mg/dL) after 4 h. By the conclusion (i.e.,after 8 h) of the experiment, the subcutaneous group's blood glucose levels had returned to their initial values.

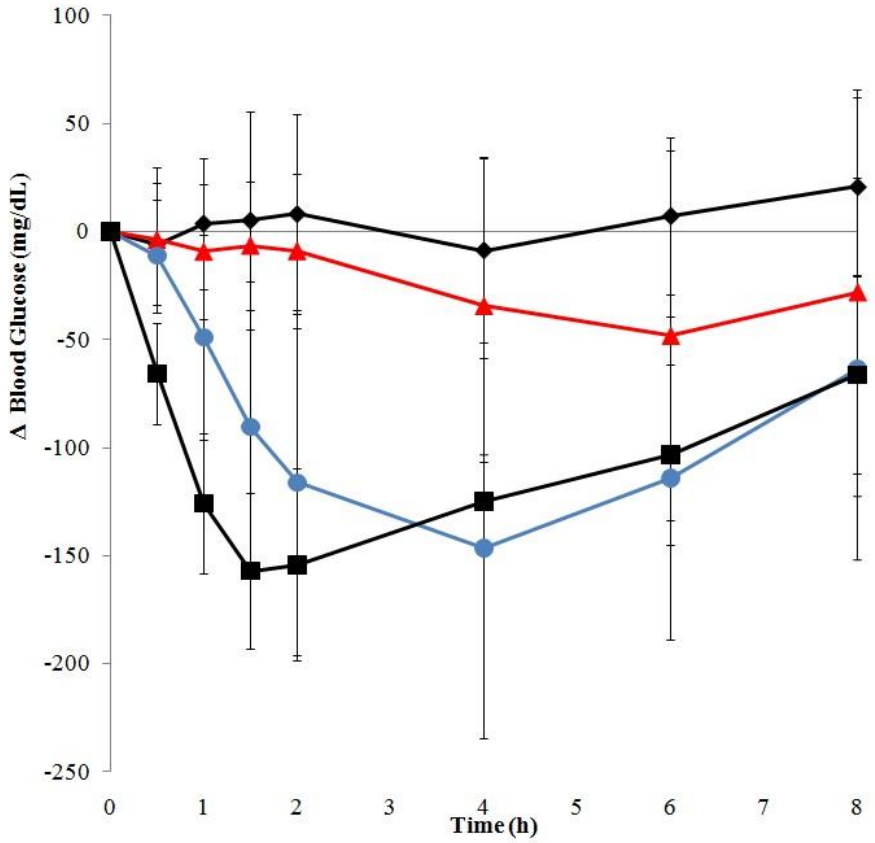

Figure 25. The cumulative change in the blood glucose levels for all the experimental groups are shown in the graph. The negative control rats (♦) were not abraded or given insulin. The rats that were injected with 0.1 U of Humalog (■). The stratum corneum (▲) and viable epidermis (●) abrasion groups were administered 200 µL of a solution containing 80% U100 Humalog and 20% FITC-labeled bovine insulin, via a transdermal patch, at the abrasion site. The standard deviation for all the groups ranged from 18 to 94 mg/dL.

Shown in Table 1 is the time to the lowest blood glucose value (t_{max}, glucose) and maximum blood glucose reduction ($C_{max,}$ glucose), and area under the curve (AUC) for the blood glucose versus time graph for all the animals that were administered insulin. The positive control achieved a peak blood glucose reduction of 157 mg/dL after 1.5 hr and then gradually returned to baseline values over the remaining 6.5 h. The total area under the curve of the blood glucose curve was 889. The stratum corneum removal group maximum blood glucose reduction of 48.2

after 6 h and then gradually returned to baseline values over the remaining 2 h. The total area under the curve of the blood glucose curve for the stratum corneum group was 215. The viable epidermis removal group maximum blood glucose of 146 after 4 h and the blood glucose gradually increased over the remaining 4 h. The total area under the curve of the blood glucose curve for the viable epidermis group was 805. Removing viable epidermis resulted in a shorter delivery lag time and a greater blood glucose decrease than the stratum corneum removal group. The negative control rats maintained stable hypoglycemic blood glucose values throughout the experiment. The maximum blood glucose decrease for the negative control was 9 mg/dL after 4 h.

Table 1. The time to the maximum blood glucose reading (t_{max}), maximum blood glucose decrease (C_{max}) and the area under the blood glucose curves shown in Figure 25 are shown in the table.

Group	**(t_{max}, glucose) hr**	**(C_{max}, glucose) mg/dL**	**Area under curve ($AUC_{glucose}$)**
Positive control (0.1 U insulin)	1.5	157	889
Stratum corneum removal	6	48.2	215
Viable epidermis removal	4	146	805

The standard deviation for the blood glucose graph ranged from 18 to 93 mg/dL. The large deviation was probably due to large variability in the blood glucose values and the animals' response to the insulin. The animals were given the same dose of streptozocin and there was a large variability in the blood glucose. There was no way to predict the resulting effect of streptozocin exposure. The rats also responded differently to the Humalog. Rats with high blood glucose (>400 mg/dL) responded slower to the insulin, including those that were administered the bolus injection, compared to the rats with lower blood glucose values (<400 mg/dL). These results caused a large standard deviation for some of the groups.

The streptozocin administration protocol resulted in 100% induction of diabetes in all the rats. However, the blood glucose was highly variable among the rats and ranged from 313 to 450 mg/dL. The initial the blood glucose values before streptozocin exposure ranged from 113 to 165 mg/dL. The animals were under terminal anesthesia for the entire experiment and this may have also contributed to hyperglycemic blood glucose levels. The high blood glucose levels and prolonged anesthesia led to the death of four rats. In a two cases, the blood glucose exceeded 475 mg/dL and animals were euthanized.

The total concentration of insulin that was delivered was quantified by ELISA and the results are shown in (Figure 26). The delivered concentration was determined by subtracting the insulin concentration at 0 h, before insulin administration, from all the time points. Shown in Table 2 is the time to the highest serum insulin value (t_{max}, insulin) and maximum insulin concentration (C_{max}, insulin), and area under the curve (AUC) of the insulin concentration versus time graph for all the animals that were administered insulin. The measured insulin concentration is the sum of the endogenous rat insulin and the delivered Humalog-R. The positive control maximum serum insulin concentration of 0.37 ng/mL ($1.4x10^{-8}$ U/mL) peaked at 30 min and the insulin concentration decreased for the remainder of the experiment. The area under the curve for serum insulin levels for the positive control was 0.45. The stratum corneum removal group maximum serum insulin concentration of 0.18 ng/mL ($6.7x10^{-9}$ U/mL) peaked at 4 h and declined for the remainder of the experiment. The area under the curve was 0.69. The viable epidermis group maximum serum insulin concentration of 0.74 ng/mL ($2.8x10^{-8}$ U/mL) peaked at 2 h. The area under the curve was 2.62. The negative control rats were untreated and maintained low serum insulin levels. This result correlated with the negative control's hyperglycemic blood glucose behavior throughout the experiment. Using one way ANOVA, it

was determined that the positive control group was significantly different ($p<0.05$) than the negative control and the stratum corneum groups, but not the viable epidermis group ($p>0.05$). The stratum corneum group serum insulin levels was significantly different than all the other groups ($p<0.05$). The viable epidermis group was significantly different that the negative control and stratum corneum group ($p<0.05$), but not positive control group ($p>0.05$).

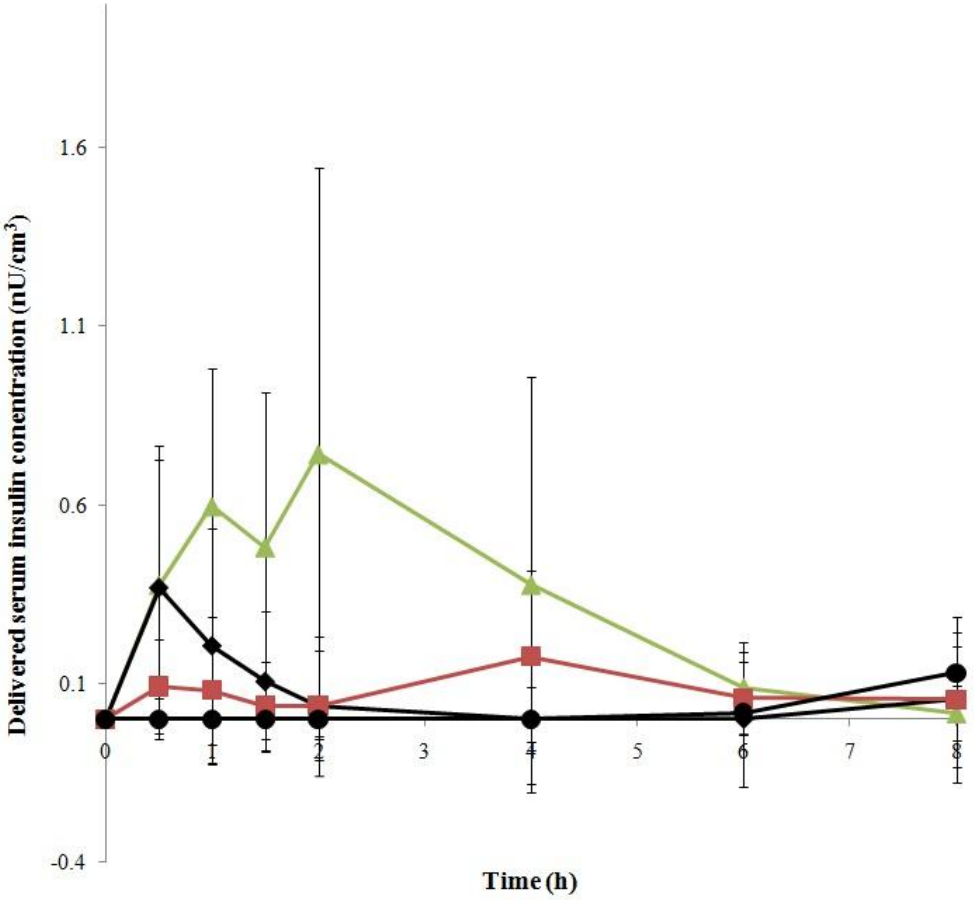

Figure 26. Shown in the graph is the serum insulin concentration that was determined by ELISA. The negative control (●) rats had the lowest insulin levels. The positive control (♦) insulin levels peaked at 30 min and declined for the remainder of the experiment. The stratum corneum group (■) insulin levels peaked at hour 4, but were lower than the viable epidermis and positive control groups. The viable epidermis group (▲) had the highest insulin level from hours 1 to 6. The standard deviation for the groups ranged from 0.08 to 0.75 ng/mL.

Table 2. The time to the maximum insulin concentration (t_{max}), maximum insulin concentration (C_{max}) and the area under the insulin concentration curves shown in Figure 26 are shown in the table.

Group	**(t_{max}, insulin) hr**	**(C_{max}, insulin) ng/mL**	**Area under curve ($AUC_{insulin}$)**
Positive control (0.1 U insulin)	0.5	0.37	0.45
Stratum corneum removal	4	0.18	0.69
Viable epidermis removal	2	0.74	2.62

We wanted to visualize the depth of the insulin penetration in the abraded skin. FITC-labeled bovine insulin was mixed with the Humalog in the transdermal patch and applied to the site of abrasion. The abrasion histology results from the experiment are shown in Figure 27. The pictures on the top row are the gross pictures of the negative control (Figure 27A) and abraded skin (Figure 27B) where the area of abrasion was revealed with green dye. The pictures on the middle row are fluorescence images of the FITC-labeled bovine insulin of the skin after sectioning. The stratum corneum abrasion (Figure 27C) and viable epidermis abrasion (Figure 27D) skin both had penetration of the FITC-labeled bovine insulin. Most of the fluorescence was concentrated near the skin's surface. The penetration of the FITC-insulin was viable epidermis was more extensive than the stratum corneum group. The bottom row consists of the hematoxylin and eosin stained images of stratum corneum group (Figure 27E) and the viable epidermis group (Figure 27F). The stratum corneum, the upper most layer, is stained pink and is removed in Figure 27E. The viable epidermis, located directly beneath the stratum corneum, has blue stained cell nuclei and remained intact. Shown in Figure 27F is skin that had the viable epidermis removed. The pink staining in the viable epidermis is indicative of the skin healing after abrasion.

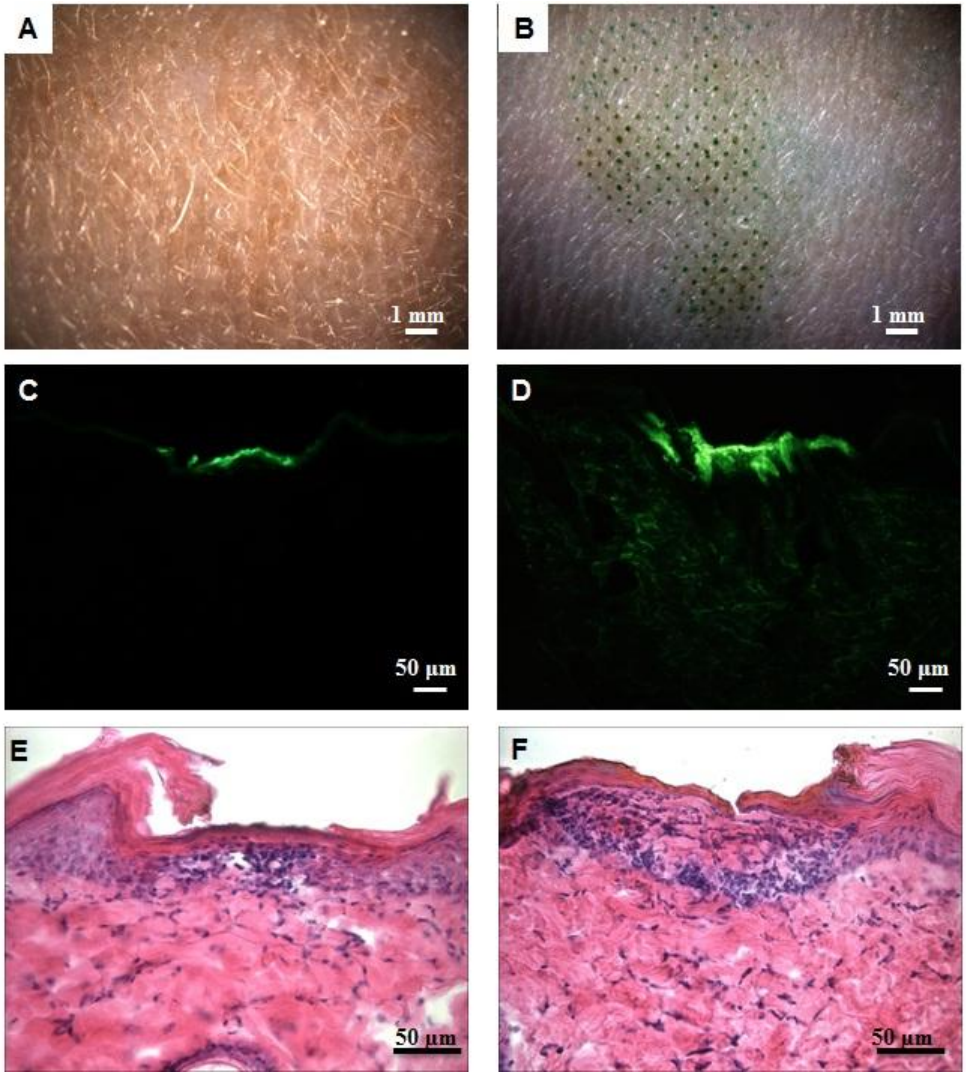

Figure 27. The histology pictures for insulin delivery in hairless rats using microdermabrasion. The control skin (A) was not abraded and the area of abrasion for the microdermabrasion-treated skin (B) was revealed with green dye. The fluorescent images of the diffusion of FITC-labeled bovine insulin in the skin with stratum corneum (C) and viable epidermis removal (D) are shown on the middle row. The H&E stained images for the stratum corneum (E) and viable epidermis abrasion (F) skin are shown on the last row. The extent of the abrasion damage has decreased due to healing.

Discussion

In this study we wanted to determine if microdermabrasion could be used to deliver a therapeutic dose of insulin to significantly decrease the blood glucose in diabetic rats. Removing the stratum corneum resulted in an increased permeability to insulin and a peak blood glucose

decrease of 48 mg/dL at 6 h for the stratum corneum removal group. The abrasion group with viable epidermis removal exhibited a 146 mg/dL peak blood glucose decrease at 4 h after abrasion. Both abrasion groups' blood glucose behavior was significantly different ($p<0.05$) than the untreated control. Based on the results, we showed that microdermabrasion can be used as a method for significantly reducing the blood glucose in diabetic animals.

We also wanted to examine the affect of the depth of abrasion on the rate of insulin transport by removing the stratum corneum and the viable epidermis. Removing only the stratum corneum resulted in a decrease in the rats' blood glucose. The largest decrease in the blood glucose over the duration of the experiment was 48 mg/dL at 6 h. Animals that had severe hypoglycemia (>400 mg/dL) exhibited the smallest decrease in their blood glucose levels. Using a one-way ANOVA ($p=0.05$), it was determined that stratum corneum blood glucose decrease was significantly different than the all the other groups ($p<0.05$). The animals in the stratum corneum group also had a longer insulin diffusion lag time, two hours, as compared to the viable epidermis removal group. The peak insulin value for the stratum corneum group was 0.51 ng/mL ($1.77x10^{-8}$ U/mL) at 4 h and it was lower than the viable epidermis removal group. The serum insulin values for the stratum corneum removal group was significantly different that the negative control and viable epidermis group ($p<0$).

Removing the viable epidermis resulted in the blood glucose decreasing immediately after insulin exposure and that trend continued until the insulin patch was removed at 4 h. Similar to the other rat groups, the viable epidermis abrasion rats had initial blood glucose readings in excess of 300 mg/dL. Removing the viable epidermis reduced the insulin delivery lag time to 30 min and the blood glucose decreased as much as 13 times more than the stratum corneum removal group. The time to reach the maximum decrease in the blood glucose for the

viable epidermis group was 4 h as compared to 6 h for the stratum corneum group. The area under the blood glucose for the viable epidermis was 805, as compared to the stratum corneum group curve area of 215. These results showed that the viable epidermis serves as an important barrier to insulin diffusion. Using a one-way ANOVA ($p=0.05$), it was determined that the viable epidermis blood glucose decrease was significantly different than the negative control and stratum corneum group ($p<0.05$), but was not different than the positive control that received the subcutaneous injection ($p>0.05$). The viable epidermis serum insulin peak concentration was 1.03 ng/mL ($3.58x10^{-8}$ U/mL) at 2 h. The value was twice as much as the stratum corneum group and the concentration peaked 2 h sooner.

Most transdermal drug delivery techniques, such as tape stripping and iontophoresis, are focused on removing, altering, or disrupting the stratum corneum since it serves as an important barrier to the penetration of drugs [1]. The stratum corneum prevents the penetration of water soluble molecules and large molecular weight compounds (>500 g/mol) into the skin. There are few technologies that focus on the viable epidermis for drug delivery. However, the viable epidermis also contributes to the skin's barrier properties and serves as another rate limiting step in the diffusion of molecules. The viable epidermis is composed of viable keratinocytes that undergo the process of cornification to become stratum corneum cells [24]. The viable epidermis is 70% water and similar to the stratum corneum it is not vascularized. At the base of the viable epidermis is basal lamina, which provides the viable epidermis barrier properties.

The basal lamina, located between the epidermis and dermis, serves a semi-permeable membrane between the two skin layers to control cell movement [17]. It is mainly composed of type IV collagen and proteoglycans that provide an anchoring point for epidermal basal cells and controls movement of substances across membrane [26]. It is thought that the basal lamina

restricts the movement of molecules that are larger than 40 kDa [17]. Although insulin has a molecular weight around 4 kDa, the viable epidermis seemed to serve as a barrier and resulted in a higher diffusion of insulin when it was removed.

Since microdermabrasion relies on diffusion to deliver insulin it has the potential to be developed into a method for delivering basal doses of insulin to diabetic patients. The abrasion depth and insulin concentration can be adjusted for the patient's dosage. Microdermabrasion is non-invasive, painless, and does not result in scars. Similar to a transdermal patch, the insulin delivery can be halted by removing the patch. Rather than using a liquid-filled patch, a solid state insulin formulation patch could be developed. The patch can also contain excipients that decrease the rate of skin healing to maximize delivery time. A portable microdermabrasion device can be developed that will allow patients to self administer controlled abrasion and apply the insulin patch without the assistance of medical personnel. Using this technology to administer insulin could result in higher patient compliance since it does require the use of needles and does not cause pain. It will also decrease amount of hazardous sharps waste and its associated cost.

CHAPTER 7

SKIN REPAIR KINETICS AFTER STRATUM CORNEUM REMOVAL USING MICRODERMABRASION IN HAIRLESS GUINEA PIGS

This study examined the kinetics of skin repair after complete removal of the stratum corneum using microdermabrasion in hairless guinea pigs. Microdermabrasion is a minimally invasive cosmetic technique that can be used to remove the stratum corneum. The skin was abraded at two sites using conditions that completely removed the stratum corneum. One site was occluded with an electrode and occlusive tape and the other site remained non-occluded. The rate of barrier recovery was assessed using electrical resistance measurement and histology. The baseline resistance was measured 1 h, 2 h, and 1 min prior to the experiment. The resistance for the experiment was monitored one minute, 4 h, 12 h, and 24 h after abrasion. The resistance for both types of wound coverings decreased after abrasion and the non-occlusive coverings increased throughout the experiment. The occlusive covering skin resistance continued to decrease throughout the experiment and was significantly different than the negative control and non-occluded skin. It was determined that abraded skin was significantly different than the negative control, but there was no difference between the wound coverings. Sulforhodamine B, a water soluble dye was used to determine if the stratum corneum had recovered and if its barrier was functional. At the conclusion of the experiment, the skin was sectioned and stained to visualize the skin's structure. Based on the histology and a dye penetration test, the barrier had reformed and was functional within 12 hours for both coverings. Transdermal drug delivery after microdermabrasion is limited up to 12 hours in guinea pigs; however, humans will probably have a longer delivery time since there are fewer hair follicles, which aid in healing.

Introduction

The skin is a semi-permeable barrier that protects the body from the external environment and prevents water loss. The stratum corneum, the upper 10-15 μm, serves as the skin's primary barrier and is composed of non-viable cornocytes that are surrounded by a lipid extracellular matrix [1]. Due to its structure only low molecular weight (<500 Da) lipophilic molecules can diffuse across intact skin. Water soluble molecules and molecules larger than 500 Da have limited diffusion across intact skin [1]. Due to the stratum corneum selectivity, most pharmaceuticals cannot be administered in a transdermal patch formulation. Several methods such as tape stripping, microneedles, chemical enhancers, electroporation, thermal ablation, and microdermabrasion have been developed to disrupt or remove stratum corneum and increase the skin's permeability to large molecular weight and water soluble molecules for transdermal drug delivery [1, 9, 51, 68]. Transdermal drug delivery is an attractive route of administration due to the ease of applying patches and ointments, the drugs avoid degradation by the liver, and does not require the use of hypodermic needles [1].

One transdermal method that is used to remove the stratum corneum is microdermabrasion. Microdermabrasion is a cosmetic procedure that improves the appearance of superficial skin defects such as fine lines, wrinkles, and scars by abrading the stratum corneum with pressurized particles [13, 14, 28, 55, 57, 69]. The depth of abrasion depends on the severity of the patient's skin, but in a clinical setting the stratum corneum is not usually completely removed [28]. Microdermabrasion was initially designed for cosmetic applications, but it has been used in several studies for delivery of low molecular weight hydrophilic molecules and vaccines [7, 8, 12, 13]. Although previous studies have been successful in completely removing the stratum corneum using microdermabrasion, the recovery of the barrier after complete

removal has yet to be examined. A previous study was conducted to study barrier recovery in humans after microdermabrasion treatment using transepidermal water loss and it was shown that the barrier recovered one day after treatment [54]. It was not indicated if the stratum corneum was completely removed. Other studies examined the recovery of the stratum corneum after complete removal with extensive tape stripping. In one such study, tape stripping was performed on pigs and the stratum corneum recovered within two weeks [70]. The study examined the recovery of the stratum corneum layer using histology, but it did not examine any time points between 30 min and 14 days after stripping, so the actual time of recovery is not known. Other studies have examined stratum corneum barrier recovery after tape stripping skin that was affected by diseases that resulted in impaired stratum corneum function [71]. While those studies provide useful information, there is a need to measure the rate of stratum corneum recovery after complete removal with microdermabrasion for safety and for determining amount of time drugs can be delivered across abraded skin. The goal of this study is to investigate the kinetics of skin resealing after complete removal of stratum corneum using microdermabrasion in hairless guinea pigs. We will also examine the affect wound coverings on the kinetics of stratum corneum recovery.

Skin healing has been extensively studied and characterized in order to understand the response to injury and pathologies that prevent and delay healing. After injury, the skin heals in three phases: inflammation, reepithelialization, and tissue remodeling [43, 72]. The inflammation phase occurs within a few minutes after injury and involves activation of neutrophils and the release of cytokines and growth factors that stimulate fibroblast proliferation and attract circulating monocytes to the injury site [43]. Reepithialization occurs within hours after injury and during the phase the stem cells in the basement membrane proliferate to repair

the damaged area and cells from appendages migrate to the injury site [41, 43]. Organisms that have a high density of appendages, such as rodents, exhibit a more rapid healing response to injury [44, 73]. The final step of healing is tissue remodeling, where collagen is altered to remodel the skin back to its natural form and function. Healing of superficial wounds, such as microdermabrasion, is expected to undergo this healing process, but at a more rapid rate than deep wounds.

The rate of wound healing is affected by severity of the injury and also by the type of dressing that is used. In a study conducted on humans and pigs, occlusive dressings were shown to accelerate the rate of reepithialization and prevent the formation of scabs [45]. However, occlusion can also delay the formation of functional stratum corneum after injury [46]. Non-occlusive wounds tend to form scabs during the healing process [45]. Semi-occlusive coverings have been found to promote healing more effectively than occlusive and non-occlusive membranes in tape stripped skin [47].

Several methods can be used to measure the rate of recovery and functionality of the stratum corneum. One method is histology, which involves sectioning and staining the skin to visualize the layers. Though it can provide useful structural information, it is a destructive technique that requires trained personnel for sectioning and tissue collection, it can be expensive, and is time consuming. Electrical resistance can be used to monitor the skin's integrity non-invasively by measuring the skin impedance [74]. The resistance value of intact skin is higher than when the stratum corneum is breached. The behavior of the skin's impedance can be used to determine the kinetics of recovery. Exposing the skin to hydrophilic dyes is another method of determining the integrity of the stratum corneum. Dyes can be applied to the skin to stain and diffuse into sites where the stratum corneum is compromised. The dye will not stain or penetrate

areas in which the stratum corneum is intact since water soluble molecules do not readily diffuse into stratum corneum. Dye tests are rapid and inexpensive for characterizing the skin surface, but histology is needed to quantify the depth of penetration. This study investigated the effect of wound coverings on recovery and integrity of the stratum corneum after complete removal using microdermabrasion using histology, electrical resistance, and a hydrophilic dye.

Results

Resistance Measurements

We wanted to study the kinetics of stratum corneum recovery after complete removal using microdermabrasion by quantifying skin impedance behavior over the course of the study. The resistance for the abraded skin over the course of the 24 h experiment is shown in Figure 28. The negative control was not treated and maintained a constant resistance value throughout the experiment. The resistance at each time point was not significant (ANOVA, $p>0.05$). The negative control was significantly different than the both types of wound coverings (ANOVA, $P<0.05$) for all time points. The occluded sample resistance remained unchanged for the full 24 h after abrasion and was not significant for all time points (ANOVA, $p>0.05$). At the conclusion of the experiment (24 h), the initial resistance for the occluded covering was less than that the initial pre-abrasion values and the negative control (Student's t-test, $p<0.05$). The non-occluded skin covering increased after abrasion and the resistance was at all time points was significant (ANOVA, $p<0.05$). The non-occluded covering 24 h resistance values was not significantly different than the original pre-abrasion values (Student's t-test, $p>0.05$). The wound coverings were also determined to be significantly different for all time points (ANOVA, $P<0.05$). The

resistance for the sham skin (not pictured) was measured before and after treatment with the microdermabrasion tip. The sham skin resistance decreased after treatment, but were not significant from the negative control (ANOVA, $p>0.05$).

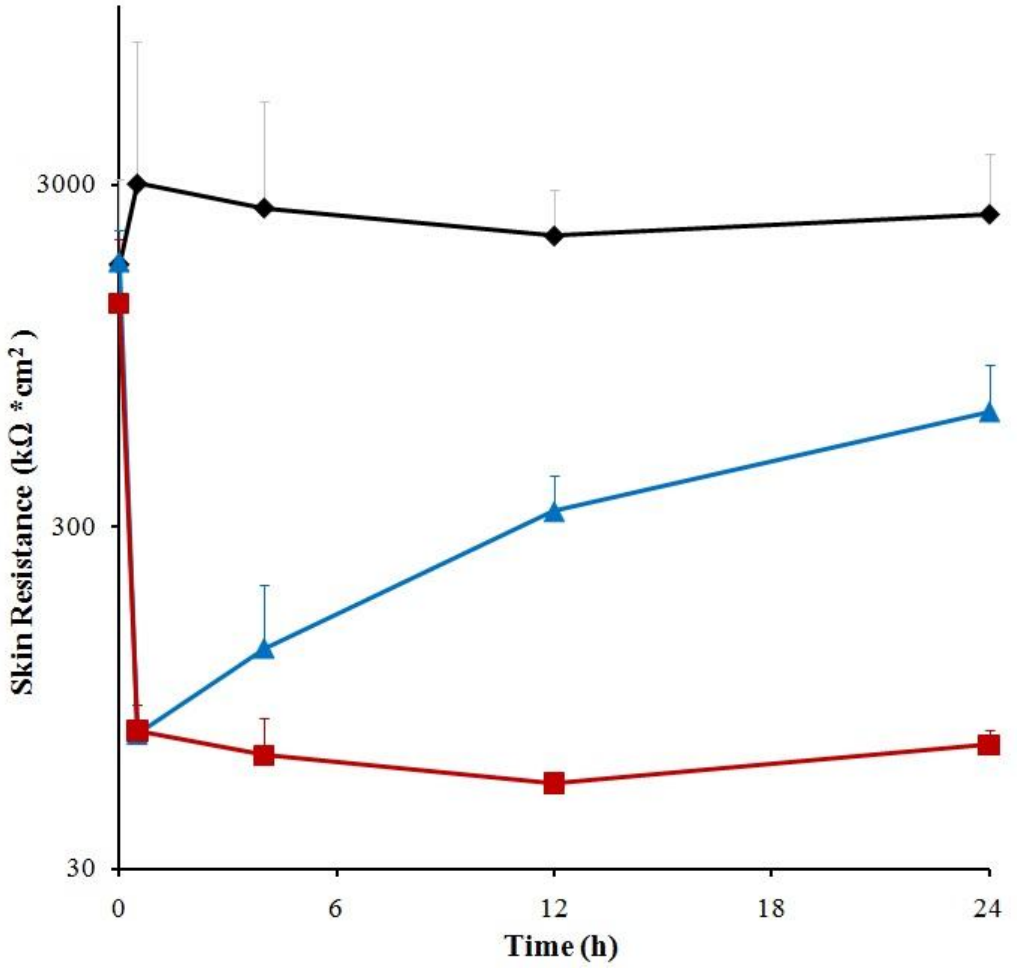

Figure 28. The graph shows the resistance measurements for the skin coverings over 24 h. The negative control (♦) skin maintained high resistance level throughout the experiment. The occluded (■) and non-occluded (▲) skin decreased immediately after abrasion (time>0). The non-occluded sample resistance increased after abrasion. The occluded sample resistance continued to decrease after abrasion and maintained a constant resistance. Neither wound coverings reached their initial pre-abrasion resistance values. Each point is an average of 4 replicates and the error bars were removed to simplify the presentation.

Histological Analysis

Sham experiment

We first wanted to examine the effect of abrading the skin without crystals and pressure on the skin resistance (i.e., sham). Two animals were abraded at two sites for 10 passes (1 pass/s) using the MDA tip. An additional site on each animal was used as a negative control and was not abraded. After treatment, sulforhodamine was applied to the sham and negative control skin to determine if there was penetration of the dye due to breached stratum corneum. Representative histology pictures for the sham skin are shown in Figure 29. The H&E stained sections are shown on the left and the fluorescent pictures that illustrate sulforhodamine B penetration as a result of the breached barrier are shown on the right. The negative control skin was not treated and the skin layers can be seen in Figure 29a1. The stratum corneum is stained pink, the blue-stained nuclei of the viable epidermis are seen below, and the pink-stained dermis is deeper still. The sulforhodamine did not penetrate into the skin (Figure 29a2). The abrasion area did not result in stratum corneum removal (Figure 2b1) or sulforhodamine penetration (Figure 29c1). The sham experiments were performed after euthanasia, so the effect of occlusion or non-occlusion dressings was not examined.

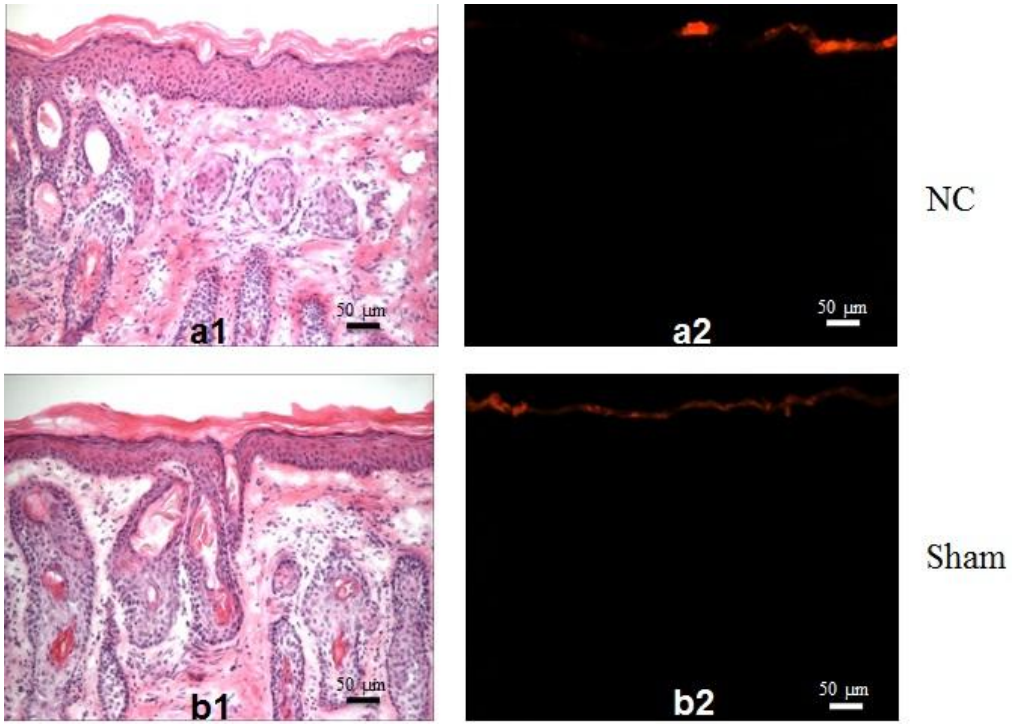

Figure 29. The histology results of the sham experiment are shown above: negative control (NC) and the sham site (Sham). The H&E and fluorescent stained skin are shown on the left and right, respectively. The sham site was abraded for 10 passes (1 pass/s), without crystals or pressure. All the skin layers were intact for both the skin samples.

Occluded Skin

We wanted to further understand the kinetics of skin resealing, after microdermabrasion, by examining the effect of occlusive dressings. The skin was abraded at a suction pressure of -40 kPa for 10 passes and half of the maximum crystal flow rate. After abrasion mild erythema was observed and at the conclusion of the experiment the skin was slightly erythemic. The representative pictures for the skin occluded for 0, 4, 12, and 24 hours are shown in Figure 30. The H&E–stained images are shown on the left and the sulforhodamine B fluorescent pictures are shown on the right. The untreated negative control skin was not abraded, so the stratum corneum remained intact as indicated by the presence of the pink-stained stratum corneum atop the viable epidermis containing blue-stained nuclei in the H&E image (Figure 30a1). The stratum

corneum prevented the sulforhodamine B from penetrating the skin as shown in the fluorescent image (Figure 30a2). The samples immediately after abrasion had complete stratum corneum removal, and indicated by the lack of pink-stained tissue atop the viable epidermis (Figure 30b1) and sulforhodamine B (Figure 30b2) penetrated deeply within the skin. The stratum corneum had not recovered in the four hour skin (Figure 30c1) and sulforhodamine B again penetrated deeply into the skin (Figure 30c2). The four hour skin also exhibited signs of inflammation as indicated by the increased number of blue stained cells, which are believed to be inflammatory cells. The characteristic dermal – epidermal junction was also difficult to see. In the 12 and 24 hour samples, the stratum corneum barrier had recovered as indicated by the return of pink-stained tissue atop the viable epidermis (Figure 30d1 and e1) and the inability of sulforhodamine to penetrate into the skin (Figure 30d2 and e2).

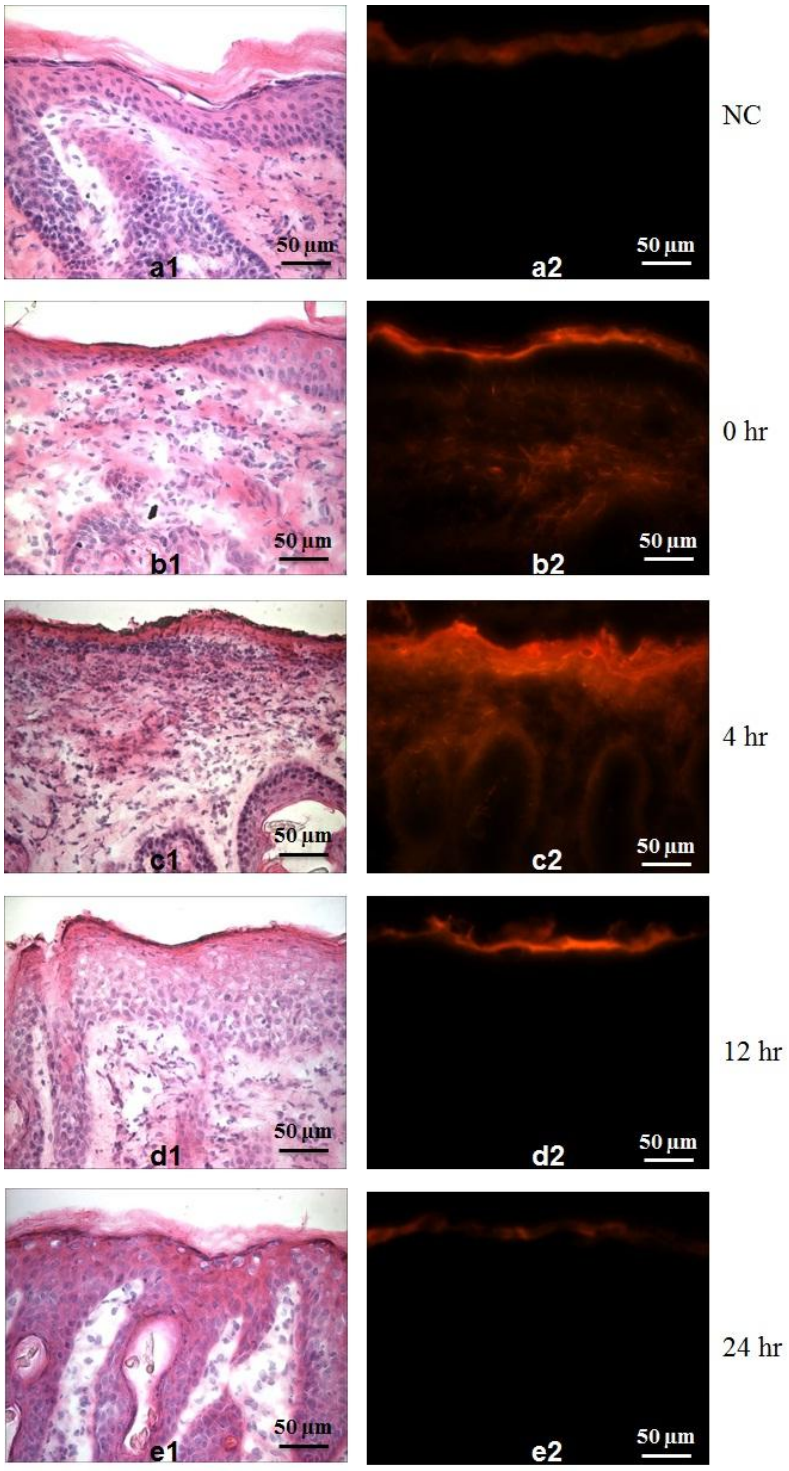

Figure 30. Shown above are the pictures of the occluded experiment skin sections. The pictures on the right are the H&E stained pictures and the left are the sulforhodamine fluorescent pictures. The time points for the pictures is shown on the right.

Non-occluded Skin

We also wanted to observe the kinetics of stratum corneum barrier recovery without occlusion after microdermabrasion. Mild erythema was initially observed, but it resolved within 24 h. The representative pictures for the skin that was abraded and healed without an occlusive covering are shown in Figure 31. Similar to the occluded samples, the H&E pictures are shown on the left and the sulforhodamine B fluorescent pictures are shown on the right. The stratum corneum was intact on the untreated negative control skin (Figure 31a1) and the sulforhodamine B did not diffuse into the skin (Figure 31a2). The stratum corneum was completely removed in the skin samples immediately after abrasion (Figure 31b1) and sulforhodamine B penetrated into the skin (Figure 31b2). The stratum corneum was not present in the four hour skin (Figure 31c1). Similar to the four hour occluded sample, the dermal-epidermal was indistinguishable. Both layers had a large number of blue stained cells, suggesting inflammation. Sulforhodamine diffused deeply into the skin for the four hour group (Figure 31c2). The stratum corneum was present in the 12 and 24 hour groups and was seen in the H&E images (Figure 31d1 and e1) and did not exhibit sulforhodamine B penetration (Figure 31d2 and e2).

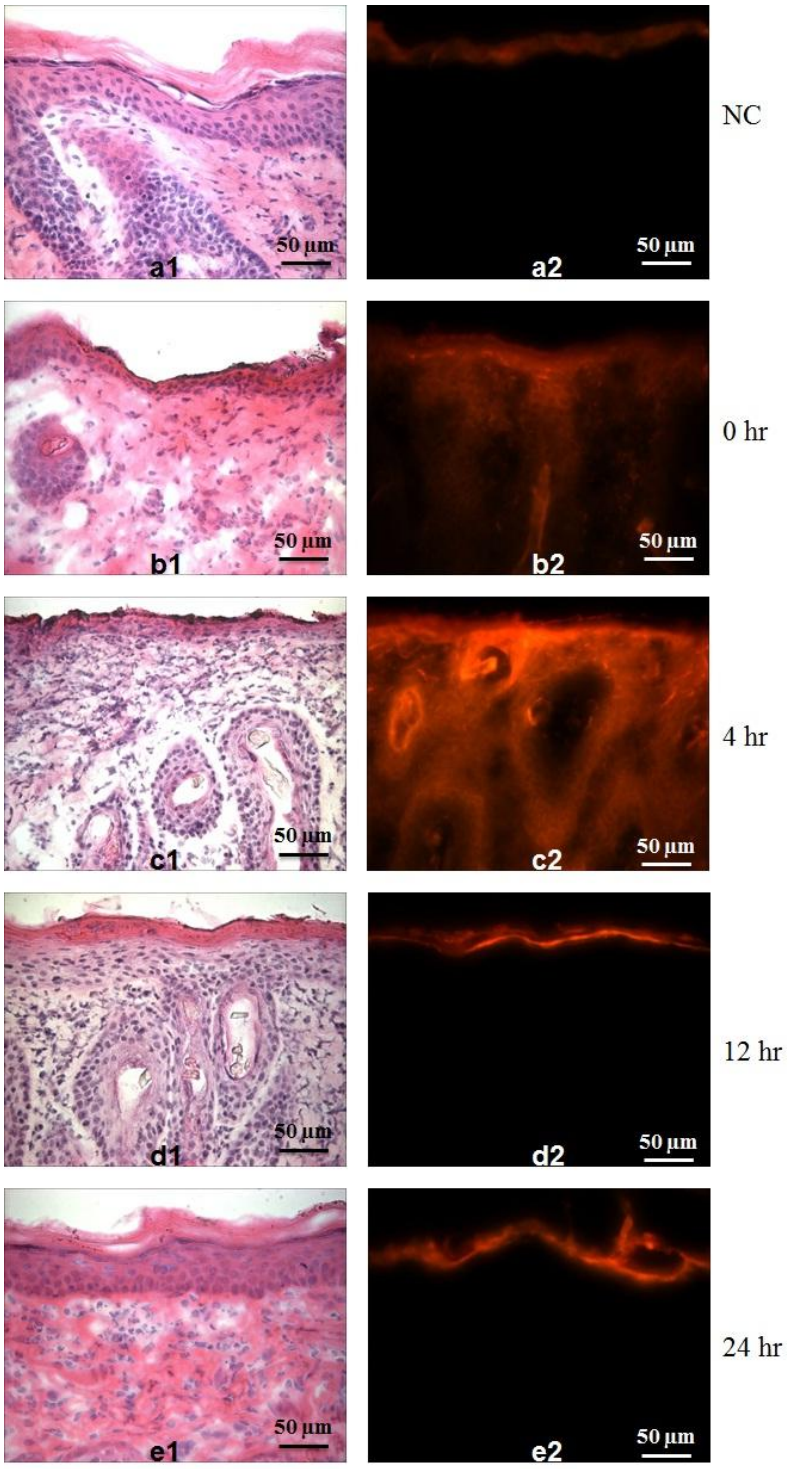

Figure 31. Shown above are the pictures of the non-occluded experiment skin sections. The pictures on the right are the H&E stained pictures and the left are the sulforhodamine fluorescent pictures. The time point for each picture is shown on the right.

Discussion

This study measured the kinetics of the stratum corneum recovery after removal using microdermabrasion. The rate of recovery was studied using skin electrical resistance, histological imaging, and dye penetration. Immediately after abrasion, the electrical measurements for the occluded and non-occluded both wound coverings decreased 1271 ±14 and 1702 ±16 $k\Omega*cm^2$, respectively. The resistance for the occluded skin remained constant during the experiment and the resistance for each time point was not significant (Student's t test, $p>0.05$). The occluded skin resistance was lower than the negative control and non-occluded skin for all time points (ANOVA, $p<0.05$). At 24 h, the final resistance value was significantly different than the initial resistance value, indicating the stratum corneum was not reformed (Student's t test, $p<0.05$). The resistance for the non-occluded skin increased throughout the experiment and all the time points were significantly different (ANOVA, $p<0.05$). The rate of recovery of the stratum corneum recovery in the non-occluded sample and was significantly different than the negative control and the occluded sample for all time points (ANOVA, $p<0.05$). At 24 h, the final resistance value for the occluded skin was not significantly different than the initial resistance value indicating the skin was partially or completely reformed (Student's t test, $p>0.05$).

Based on the resistance data, the non-occluded sample healed at higher rate than the occluded sample. However, these results do not agree with the histology data. Both samples had reformed and functional stratum corneum within 12 hours. One reason for this discrepancy may be due to the collection of interstitial fluid under the occluded skin dressings that may have caused a lower resistance value. The ability of the ions to transverse breached or partially intact stratum corneum more readily than sulforhodamine, because of their low molecular weight, may have also contributed to a higher electrical current and lower resistance values. Another

consideration is that the negative control for the experiment was non-occluded for the duration of the experiment. Comparing the occluded site to an occluded negative control site would have given a better estimate of the change in resistance as a function of time.

Based on the histological results, there was no difference in healing between the two types of wound covering. At four hours after abrasion the viable epidermis and dermis were infiltrated by a large number of cells. This observation was seen in both wound coverings. Those cells were not selectively stained to distinguish between them. The barrier was not reformed and layers of the skin were difficult to distinguish. In both cases, barrier reformed between 4 and 12 hours and was functional based on the results of the dye test. Both types of wound coverings exhibited a large number of cells in the viable epidermis and dermis four hours after abrasion and the response was significantly less noticeable by 12 hours. At 12 and 24 hours the skin layers were reformed and the number of cells in the epidermis had decreased.

Sulforhodamine B, was applied to test the functionality of the recovered stratum corneum because it does not readily penetrate intact skin as shown in the fluorescent picture of the negative control skin. At 4 h, both coverings resistance were significantly different that the negative control (Student's test, $p<0.05$) and the dye diffused into the skin due to the breached barrier. Based on the sulforhodamine B dye penetration test we found that the skin resealed and was functional within 12 h for both wound coverings. The dye penetration data at 12 and 24 h correlates with the electrical resistance data for the non-occluded sample, but not the occluded sample. This is probably due to the accumulation of interstitial fluid that may have decreased the resistance readings in the occluded skin.

While guinea pigs were used for this study because they are easy to house and handle and their skin is an acceptable model for human skin, they may not be the best model for healing.

The rapid stratum corneum recovery that was observed in this study will probably not occur in humans due to the small density of hair follicles and the inability to heal wounds as rapidly as guinea pigs. During the process of healing, cells from the hair follicles migrate to the site of injury to repair the wound [73]. Guinea pigs have a high density of hair follicles which allowed the skin to heal at a faster rate [44, 73]. It has also been shown that rodents can heal centimeter-size skin wounds within 10 days, which cannot be accomplished by a human without medical intervention [44].

Several studies have investigated the recovery of the stratum corneum after disruption with microdermabrasion, chemical treatment, and microneedles. The skin has been shown to heal within between 1 to 2 days following microdermabrasion treatment, with no occlusion, in humans as measured by transepidermal water loss measurements [54, 75]. The microdermabrasion pressure used for the experiment was higher than used for this study, but there was no indication of exposure time and the degree of stratum corneum removal. The stratum corneum recovered more rapidly in this study (12 hours), but this was probably due to the animal model and the small area of stratum corneum removal. Barrier recovery after exposure to chemical peels and acetone was reported after 3 days [54, 76]. The skin was not occluded for the study and was measured using transepidermal water loss measurements. Wounds created from microneedles, which pierce into the superficial dermis, in humans has been shown to heal within 15 min after injury [76]. Although many transdermal methods can result in rapid healing of the skin, but stratum corneum recovery is mostly dependent on the extent of the skin damage and the animal model that is used. The time in which the skin heals also impacts the type of drugs that can be administered for transdermal drug delivery. Small molecular weight drugs can diffuse more readily across breached skin than large proteins. They can be delivered in

systems in which the skin reseals quickly. Larger molecules, such as vaccines and proteins, may require more extensive skin damage, excipients, or coverings that will decrease the rate of healing.

From a safety standpoint the rapid resealing will lower the risk of infections, but it presents a complication for transdermal drug delivery since the time for drug diffusion maybe be short. This study determined that skin healed in guinea pig within 12 h, however we expect the delivery time will be longer in humans. Based on studies that examined skin resealing with occlusion and non-occlusion after microneedle insertion in humans and guinea pigs, it was shown that non-occluded human skin resealed within 2 h and the occluded guinea pig skin resealed after 72 h [77]. Using these studies as a model, we expect the drug delivery time for human skin treated with microdermabrasion to be longer than microneedles since a larger area of skin is removed. Additional studies will have to be conducted to determine the kinetics of stratum corneum recovery of occluded and non-occluded skin in human subjects after microdermabrasion.

Chapter 8: Conclusions

In this thesis microdermabrasion was evaluated as a skin permeability method for transdermal drug delivery. The parameters that resulted in controlled stratum corneum removal were evaluated. The types of drugs that could be delivered to abraded skin and the affect of abrasion depth were examined in vitro and in vivo. To determine the duration of drug and for safety, the rate of stratum corneum removal after abrasion was also studied. Microdermabrasion shows promise as a non-invasive delivery technique that can be used in conjunction with a patch to administer drugs.

This study we sought to determine the parameters that would result in controlled microdermabrasion could selectively remove stratum corneum in a targeted fashion without removing viable epidermis. Crystal flow rate and exposure time were the most important parameters in controlling stratum corneum removal, whereas suction pressure and handpiece movement had lesser effects. Notably, this study introduced the use of a mask to limit tissue removal to an array of micron-scale pores rather than one large region of stratum corneum removal. We found that the mask also influenced the depth of tissue removal; the 125 μm-hole mask limited tissue removal to the stratum corneum in a self-limiting manner independent of exposure time to microdermabrasion. In this way, precise control over pore geometry was achieved such that arrays of pores on the order of 100 μm in diameter and 10 μm in depth (i.e., the thickness of stratum corneum) were demonstrated. Because stratum corneum is the skin's main permeability barrier, controlled microdermabrasion offers a novel approach to increasing rates of transdermal drug delivery. The established clinical safety record and the non-invasive

nature of microdermabrasion suggest that this approach should be safe, painless, cosmetically acceptable and effective to deliver a broad range of pharmaceutical compounds.

After finding parameters that selectively remove stratum corneum, microdermabrasion was used to deliver sulforhodamine, insulin, BSA, and influenza vaccine in vitro. Along with removing stratum corneum, we also removed viable epidermis to determine the affect of the depth of abrasion. Full thickness porcine that was abraded without a mask and split thickness human cadaver skin that was abraded through a mask were exposed to different molecules. Removing the stratum resulted in an increase in the penetration of all the molecules, while removing the viable epidermis resulted in a larger molecule penetration. The molecule diffusion was dependant on the drug's molecular weight and the depth of abrasion. Sulforhodamine diffused through the skin readily, while Texas red bovine serum albumin and influenza did not penetrate the full thickness of the skin. At 12 h for split thickness skin with the viable epidermis, sulforhodamine B penetration was 600 times higher than the insulin penetration. Microdermabrasion shows promise as a transdermal technique that can be used to deliver therapeutics to the skin.

We showed that microdermabrasion can be used to deliver insulin in diabetic rats. The rate of insulin delivery was dependant on by the abrasion depth. Removing stratum corneum resulted in a decrease in the blood glucose, but there was a two hour lag time and largest decrease in the cumulative blood glucose was 46 points. While, removing the viable epidermis resulted in a 30 min time lag and the largest cumulative blood glucose drop was 146 points. The blood glucose behavior for the two groups were significantly different from each other, which demonstrated that removing the viable epidermis was important in delivering insulin. Increasing the abrasion depth increased the penetration of insulin and significantly decreased the lag time

and animal mortality. The viable epidermis is important barrier that is often overlooked for transdermal therapies and by removing it, the amount of drugs that can be delivered into the skin increases greatly.

The skin resealing study examined the rate of barrier recovery and the affect of occlusive and non-occlusive wound coverings on the kinetics of stratum corneum recovery in guinea pigs after microdermabrasion. The barrier, for wound coverings, was determined to be reformed and functional within 12 hours using electrical resistance and histology. Based on statistics, there was no difference between occlusion and non-occlusion on the rate of healing of the stratum corneum removal in hairless guinea pigs. This is possibly due to wound being superficial (15 μm deep), the size of the wound, and the large number of hair follicles. The healing of the skin is important for safety and will determine the range of drugs that can be delivered using microdermabrasion.

Overall, the finding of this thesis show that: (i) controlled microdermabrasion can remove the stratum corneum, the main barrier to drug delivery and (ii) hydrophilic macromolecules can penetrate abraded skin in significantly higher amounts than intact skin and (iii) drug delivered after microdermabrasion in vivo can elicit a therapeutic response and (iv) the depth of abrasion significantly impacts the rate of drug diffusion into the skin and (v) the skin reseals rapidly in guinea pigs after microdermabrasion treatment. Microdermabrasion has the potential to advance the field of transdermal drug delivery and increase the number of therapeutics that can delivered in a topical formulation.

Chapter 9: Recommendations

This thesis work found that controlled microdermabrasion could be used to remove the stratum corneum to increase the skin's permeability to water soluble molecules, proteins, and vaccines. We also found that the depth of abrasion significantly impacted the rate of drug delivery. Removing the viable epidermis reduced the diffusion lag time and up to 13 times more drug was delivered as compared to removing the stratum corneum. Future studies should explore controlled viable epidermis removal with a mask to determine the range of molecules that can be delivered, such as vaccines, and elicit a therapeutic response. The rate of skin healing after removing the viable epidermis should also be studied to make sure there are no adverse effects of removing the layer. The healing study will also determine how long the molecule can be delivered and if occluding the area will decrease the rate of healing.

Since all the studies were conducted on guinea pigs, in vivo studies using humans should be conducted to determine if a therapeutic dose of insulin can be delivered after abrasion. The study can be conducted in conjunction with a skin resealing study to determine the length of time insulin can penetrate the skin. The mask can also be redesigned to allow a larger area of abrasion for insulin delivery.

The safety of repeated abrasions should be investigated. Clinically, the skin is abraded repeatedly over several weeks. However, the stratum corneum or full epidermis is typically not completely removed. Studies should examine the affect of serial abrasion to measure the change in the thickness and mechanical properties of the stratum corneum and viable epidermis and if the settings must be adjusted to remove the layers.

Pain in human subjects should also be investigated for stratum corneum and full epidermis removal. Clinically, microdermabrasion has been shown to not cause pain however, the stratum corneum and full epidermis are not typically removed. A pain study in which the stratum corneum and full epidermis is removed, using the mask, should be conducted. Patients can rank the pain using a pain intensity scale. Subjects can also compare the pain felt during microdermabrasion to that of a hypodermic needle to determine which method they would prefer for drug delivery.

To make the device of use for self administration, a handheld abrasion device that has sensors to control the depth of skin abrasion should be developed. The device should be compact and will rely on the sensors to determine when the stratum corneum or full epidermis has been removed. The sensors can measure the skin's electrical resistance and should turn off and lock the device when the abrasion depth is reach to prevent overabrasion. The device can be coupled with a transdermal patch to deliver the therapeutic. The device can be designed to also work in conjunction with a mask to control the area of abrasion.

Appendix A: Microdermabrasion Device

The schematic of MDA device was described and shown in the Introduction section. A picture of the actual device is shown in Figure 32. Figure 32A shows the front of the device and all the components are labeled. The crystal flow rate and pressure are controlled by the crystal and vacuum knobs, respectively. The crystal flow rate depends on the number of turns of the crystal knob. The flow rate decreases with increasing turns of the knob, which indicates closing of the valve. The pressure ranges from -20 to -60 kPa and the value is displayed on the pressure gauge. The crystals flow from the machine to the handpiece, shown in Figure 32B, through the outlet port and impact the skin. The skin debris and used crystals are suctioned to the waste container in the machine through the inlet port. The gold handpiece assembly shown in Figure 32B is the most aggressive tip that can be used for abrasion and it was used for this thesis. The tip has an open orifice that allows maximum crystal flow. The crystals, waste container, and the plastic handpiece tips were purchased from the manufacturer (DermaMed USA, Lenni, PA). The device was not altered in any manner.

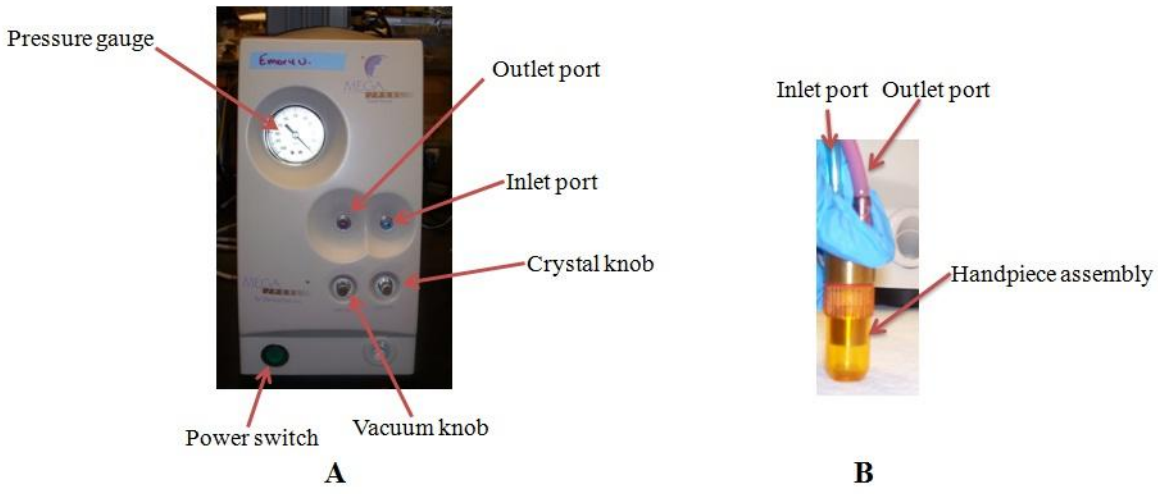

Figure 32. Picture of the MDA device.

Appendix B: Microdermabrasion Device Characterization

Introduction

In this study, we used the DermaMed Goldseries microdermabrasion device. Because the manufacturer provides little information to characterize the device's operating parameters, and not much additional information exists in the literature, we carried out a detailed characterization in order to better understand device performance and interpret our data.

The device has two settings that can be controlled by the operator: "vacuum," which is the suction pressure measured in gauge units of kPa, and "crystal," which is the crystal flow rate measured in relative units ranging from 0 (highest flow rate) to 9 (lowest flow rate) knob turns. We first sought to quantify crystal flow rate in absolute units (i.e., particles per second and mass per second) by directly measuring the mass moving through the machine. We next determined particle velocity as a function of operating conditions using video microscopy.

Materials and methods

The crystal mass flow rate was determined as a function of suction pressure at -30, -40, -50, and -60 kPa and crystal flow rates corresponding to 0, 1, 3, 4, 6, and 9 knob turns for 3 to 60 s. Zero knob turns is the maximum valve opening, whereas at nine turns the valve is almost closed. The absolute crystal flow rate at each turn has not been previously characterized by the manufacturer. Our experiments were carried out by weighing the microdermabrasion device waste container prior to the experiment with a BP 2100 Sartorius balance (Sartorius Group, Goettingen, Germany). The device was then set to a specified pressure and crystal flow rate, and porcine skin was abraded using the static mode. The final weight of the waste container was

measured at the conclusion of the experiment, and the mass of the crystals consumed was determined by subtracting the final canister mass from the initial mass. Measurements at each setting were carried out in triplicate.

To convert mass flow rate into particle flow rate, we used the following equation: $P = M / m$, where P is particle flow rate (particles/s), M is mass flow rate (g/s), and m is the average particle mass, which was determined to be 3 µg per particle. The average particles mass was estimated by counting the number of particles in a 2.2 mg sample of particles by microscopic imaging and averaging the result of three replicate measurements.

The velocity of the particles was measured using a Phantom B4.2 high speed camera (Vision Research, Wayne, NJ). The camera imaged the particles in the handpiece tip at pressures of -30, -40, and -50 kPa and at crystal flow rates corresponding to 0, 3, 6, and 9 turns. Particle velocity was also measured for -60 kPa for 1 and 4 turns. The videos were captured using the Phantom Camera Control software (Vision Research) and analyzed using Image J (National Institutes of Health, Bethesda, MD), QuickTime (Apple, Cupertino, CA), Microsoft Office Picture Manager (Microsoft, Redmond, WA), and Digitizing Tools Software (Hendricks Lab, Chapel Hill, NC) [31]. Each video was recorded for 0.54 s at a capture rate of 10,000 frames/s. Four videos of each setting were recorded and, for each video, 20 particles were tracked over 10 frames to determine the velocity by directly measuring the distance traveled per time increment.

Results

Crystal Mass and Particle Flow Rate

The crystal mass and particle flow rates were determined as a function of crystal flow rate knob turns and as a function of pressure. Figure 33A shows the mass flow rate over time at

crystal knob settings of 1, 3, 6, and 9 turns at a suction pressure of -50 kPa. These data show that (i) mass flow rate did not significantly change with time at all crystal flow rate knob turns (two-way ANOVA, $P \geq 0.05$) and (ii) mass flow rate increased with decreasing crystal flow rate knob turns (two-way ANOVA, $P < 0.05$). In Figure 33B, mass flow rate is shown over time as a function of suction pressure. Over the range of conditions studied, suction pressure did not significantly affect the crystal mass flow rate (two-way ANOVA, $P > 0.05$). Mass flow rate data are also presented as the number of particles per second.

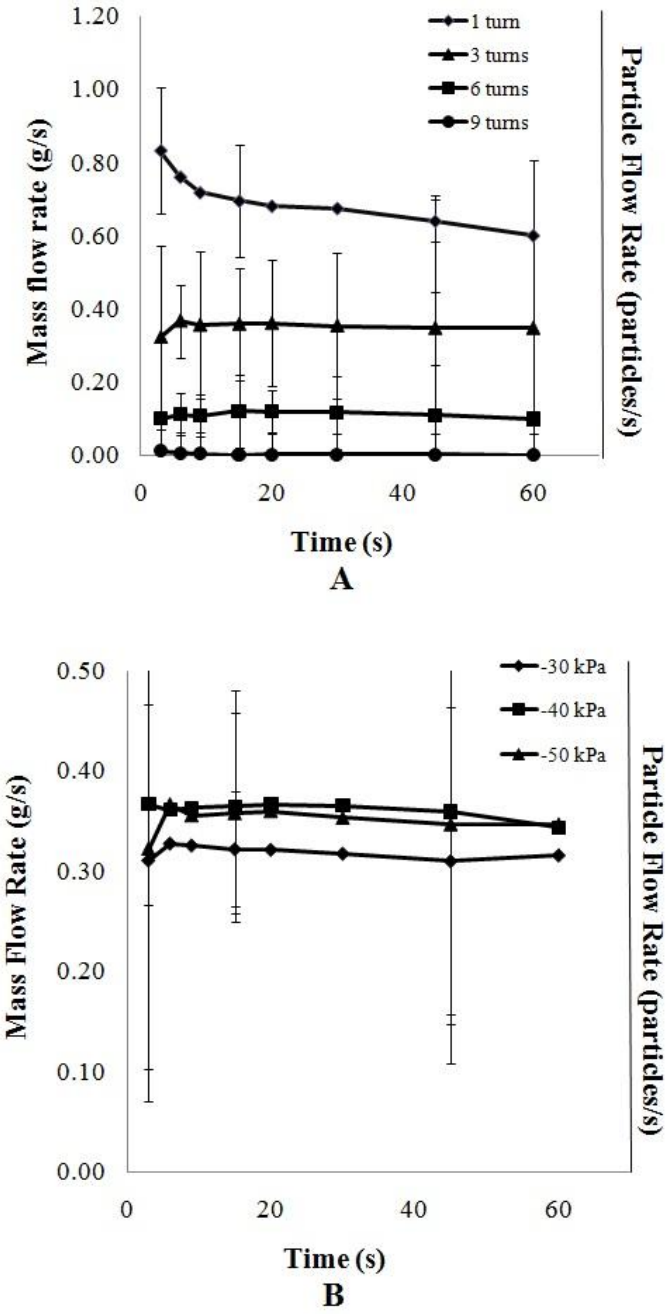

Figure 33. Crystal mass flow rate and particle flow rate shown as a function of time at different crystal knob turns and suction pressures. (A) Mass and particle flow rates at 1, 3, 6, and 9 knob turns at a suction pressure of -50 kPa in the static mode. (B) Mass and particle flow rate at suction pressures of -30, -40, and - 50 kPa at a crystal flow rate at 3 turns in the static mode. Data represent the average of three replicate measurements ± standard deviation**.**

Guided by the observation that crystal flow rate is generally independent of time, we determined mass flow rates over a broader range of suction pressures and crystal flow rates, which is shown in Figure 34. These data further demonstrate that crystal mass flow rate depends on the crystal knob setting (two-way ANOVA, $P < 0.05$) and does not depend on suction pressure (two-way ANOVA, $P > 0.05$). Over the range of conditions used in this study (which generally spans the range of conditions enabled by the microdermabrasion machine), crystal mass flow rates varied up to more than 0.7 g/s and 2×10^6 particles/s.

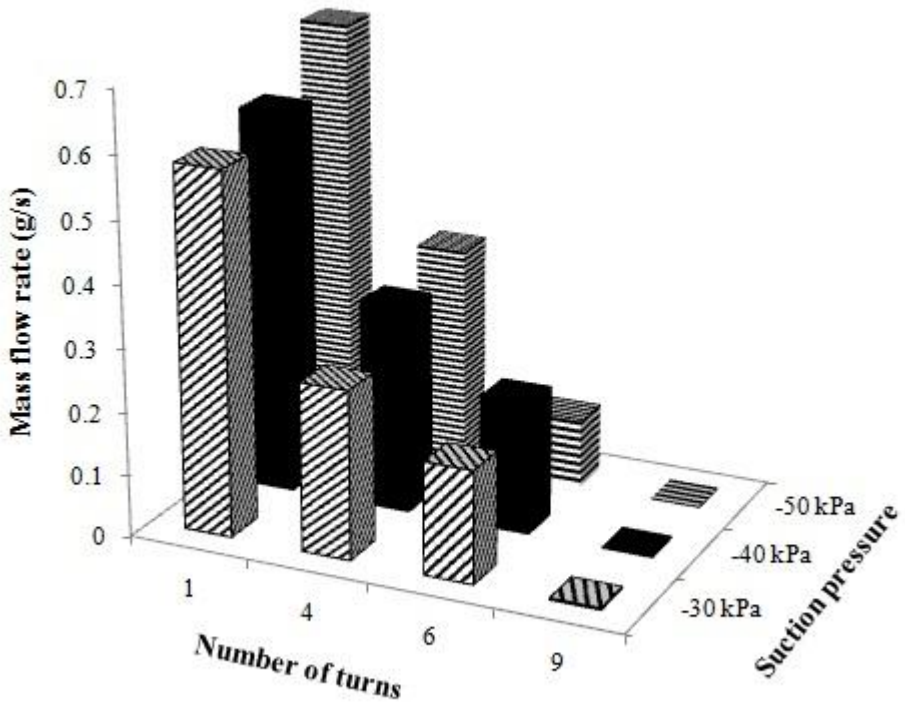

Figure 34. Mass flow rate is shown as a function of suction pressure and number of turns of the crystal flow rate knob applied in the static mode. Data represent the average of three replicate measurements. Error bars are not shown to simplify the presentation. The magnitude of the error bars in these data is similar to those shown in Figure 33A.

Crystal Velocity

Average crystal particle velocity was measured as a function of crystal flow rate and suction pressure, as shown in (Figure 35). These data show that velocity varied with crystal flow rate (two-way ANOVA, $P < 0.05$) but did not depend on suction pressure (two-way ANOVA, $P > 0.05$). More specifically, particle velocity was generally slower at higher particle flow rates (i.e., smaller number of crystal flow rate knob turns). Particle velocities ranged from approximately 1 m/s to 3.5 m/s under the conditions used in this study (which generally span the range of conditions enabled by the microdermabrasion machine).

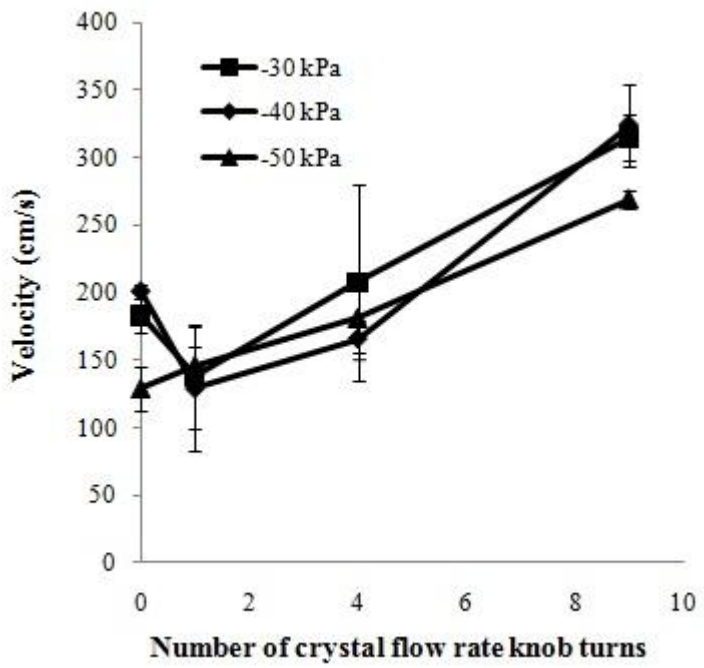

Figure 35. Average crystal particle velocity shown as a function of the number of turns of the crystal flow rate knob at different suction pressures. Data represent the average of 20 particle measurements ± standard deviation.

Closer examination of the video images used to determine particle velocity shows that the slower particle speed at higher particle flow rates appears to be due to the higher density of particles in the handpiece, which results in larger numbers of particle-particle collisions, thus reducing the particles' speed. The videos also show evidence of particles breaking apart upon collision, which increases particle number and decreases particle size.

Discussion and conclusion

This study provides the first detailed characterization of the physical operating parameters of this or, to our knowledge, any microdermabrasion machine. The mass flow rate, particle flow rate, and particle velocity were determined over most of the range of operating conditions enabled by the machine. The mass flow rate and particle flow rate increased as the opening of the crystal flow rate valve increased (i.e., at decreasing crystal flow rate knob turns). Mass flow rates ranged up to more than 0.7 g/s and particle flow rates ranged up to more than 2 x 10^6 particles/s. Crystal flow rate was found to be independent of time and suction pressure. Particle velocity was shown to vary between 1.0 cm/s and 3.5 cm/s and to decrease at increasing crystal flow rate due primarily to increased number of particle-particle collisions.

Appendix C: In vitro Drug Delivery Apparatus Schematic

As stated in the Material and Methods section, the in vitro drug delivery experiments were carried using horizontal and vertical diffusion chambers (PermeGear, Hellertown, PA). The SR experiments were carried out using horizontal diffusion chambers that used a water circulator to flow water through the outer jacket of the chambers to maintain a constant temperature (37 °C). The constant temperature eliminated the effects of a thermal gradient on diffusion. The chambers were placed on stir plates to allow adequate mixing. A schematic of the horizontal chamber set up is shown in Figure 36. The skin is positioned between the donor and receiving chamber and the skin surface was exposed to the donor solution. The donor and receiving chambers were each filled with 3 mL of the drug solution and PBS, respectively. The receiving chamber solution was sampled every hour for 24 h and the fluorescence was measured using a spectrofluorometer. Fresh PBS was added to the receiving chamber at each sample time point. The horizontal chambers have a 3.4 mL capacity for both chambers, which allows large volumes of drugs to be used for the diffusion experiments. However they are not ideal for expensive molecules since a large volume is needed cover the skin surface.

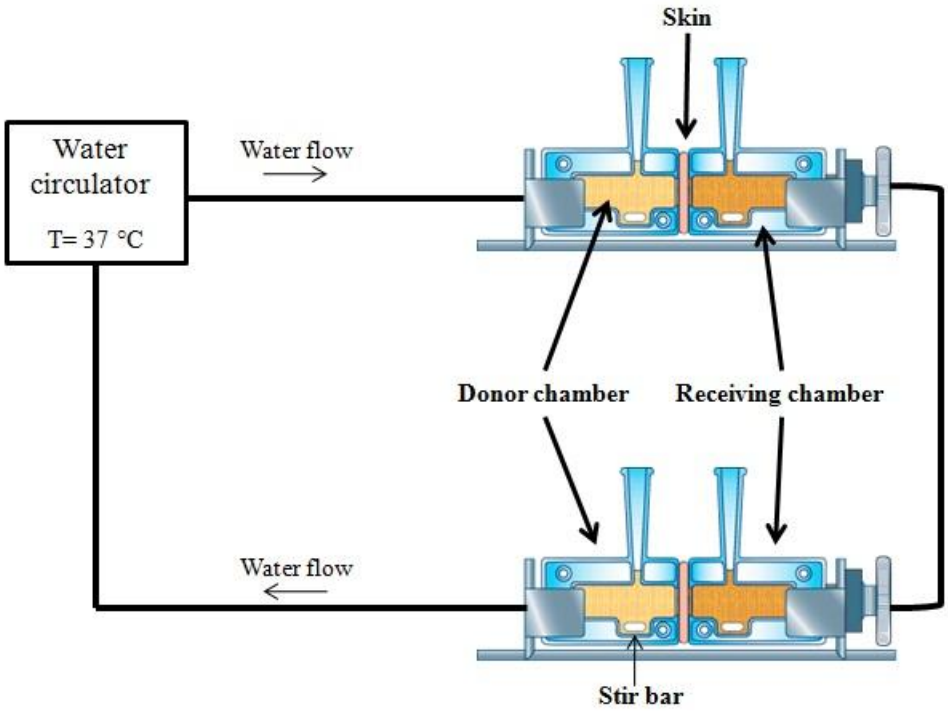

Figure 36. Schematic of the horizontal diffusion chamber drug delivery equipment. Pictures adapted from www.permegear.com.

The BSA, influenza vaccine, and mask experiments were carried out using vertical Franz cell diffusion chambers. The vertical chambers allowed smaller donor chamber volumes. The vertical and horizontal chambers function in the same manner, except the vertical chambers are placed individually in a heating block to maintain the temperature (37 °C). A schematic of the vertical chamber equipment setup is shown in Figure 37. The skin was loaded in the chambers using the same protocol as the horizontal chambers. One hundred microliters of the drugs were loaded in the donor chamber and 5 mL of PBS was added to the receiving chambers. The donor chamber was covered with parafilm to prevent the donor solution from evaporating. The receiving chamber for the BSA and influenza studies was not sampled since it was determined during preliminary experiments that BSA does not penetrate the entire thickness of the dermis

over the timescales using in this study. The receiving chamber for the sulforhodamine mask experiment was sampled every hour for 12 h. The receiving chamber for the insulin delivery mask study was sampled every 6 h for 54 h. For both experiments all of the PBS from the receiving chamber was removed and the amount of drug in the solution was quantified with a spectrofluorometer. Fresh PBS was added to the chamber at each sampling point.

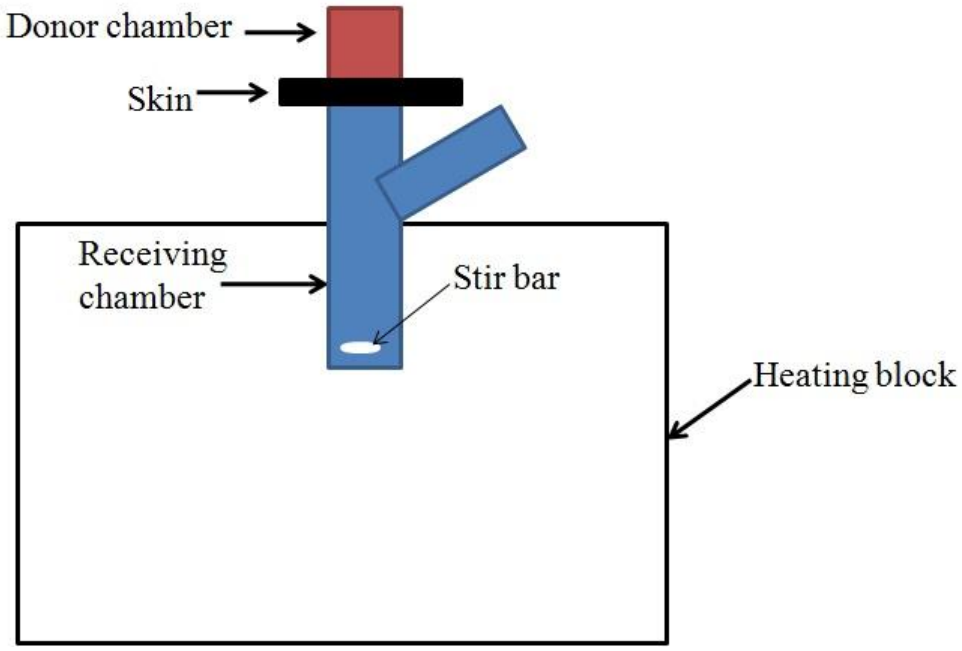

Figure 37. Schematic of the vertical diffusion chamber equipment setup.

.

Appendix D: Influenza A Drug Delivery Study

The goal of this experiment was to evaluate MDA as an immunization method for delivering influenza A vaccine to guinea pigs after a single vaccination.

Material and methods

Eight hairless guinea pigs (IAF strain, Charles River Laboratories, Wilmington, MA) were divided equally into two groups. Blood was collected from the animals one day prior to the experiment for baseline antibody measurements. One group received an intramuscular (IM) injection of 10 µg of PR8 inactivated influenza A virus. The second group was anesthetized with ketamine-xylaxine and abraded using the setting -40 kPa for 10 passes (1 pass/sec) at half of the crystal flow rate. After abrasion, a transdermal patch was placed on the animal and filled with 200 µL of 15 µg of PR8 inactivated influenza virus solution. The patch was removed after 24 h and the skin was wiped cleaned. Blood was collected 15 and 30 days after immunization for ELISA and the Hemagglutinin Inhibition (HAI) assay.

ELISA Protocol

ELISA was used to detect antibodies in the animal serum that were produced in response to the vaccination. The assay was conducted by first coating each of the wells of the 96-well plate with 100 µL of inactivated purified PR8 virus (5 ng/mL). The wells for the standard curve were coated with 100 µL of 2 µg/µL antibody solution. The plate was incubated over night at 4 °C. After incubation, the plate was washed three times with PBS. The wells were filled with 200 µL of blocking buffer, comprised of PBS and 3 % BSA, and the plate was incubated for 1 h at 37

°C. At the end of the incubation period, the plate was washed three times with PBS. One microliter of guinea pig serum and 100 µL of the primary antibody in a 1:100 dilution ratio were added to the wells. The primary antibody was diluted in PBS. Primary antibody standards were also added in concentrations ranging from 1 to 1000 ng/mL. The plate was incubated for 1.5 hours at 37 ^{o}C. After the incubation the plate was washed three times with PBS. One hundred microliters of the secondary antibody was added in a dilution ratio of 1:1000. The plate was incubated for 90 min at 37 °C. The plate was washed three times using PBS and 100 µL of an enzyme solution was added to each well for one minute. After 1 min, 50 µL of H_3P0_4 stop solution was added to the wells to stop the enzymatic reaction. The absorbance of the wells was measured at 450 nm using a plate reader.

Hemagglutinin Inhibition Protocol

The HAI assay was carried out to test the quality of the antibodies in the sera that were produced in response to the influenza immunization. Prior to the assay, the serum was separated from the blood by centrifugation. To begin the assay, 10 µL of serum was mixed with 30 µL of receptor destroying enzyme and incubated in a 56 °C water bath for 1 h to deactivate the complement. After the incubation, the serum mixture was cooled to reach room temperature and 60 µL PBS was added to the solution to bring the concentration of the serum to a 1:10 dilution ratio. Twenty-five microliters of PBS was added to each of the wells and then sera was added to all wells in serial dilutions from column 1 to column 12 by adding 25 µL to each well from the previous well. The plate was mixed and incubated at room temperature for 15 to 30 min. After incubation, 50 µL of 0.5% Red Blood Cells (RBCs) was added to each well. A positive control (25µL PBS + 50 µL of RBCs) and negative control (25µL virus + 50 µL of RBCs) was also

added to the plate. The plate was incubated for 1 h or until positive control formed a pellet. The value for HAI is when pellet becomes less than a complete pellet. Seroprotective results must have a 1:40 or greater ratio.

Results

The ELISA and HAI results indicated that the guinea pigs immunized using microdermabrasion did not have seroprotection against the PR8 vaccine. However, we did not challenge the guinea pigs with a lethal dose of influenza A to confirm the results. The HAI assay determined that the negative control (naïve) and microdermabrasion treated groups had a value of 10. The intramuscular group on day 15 and 30 had a HAI value of 80 and 160, respectively. HAI seroprotection in humans is determined to be significant if the value is over 40. Using a one-way ANOVA it was determined that microdermabrasion treated group was not significantly different ($p<0.05$) than the negative control, but was different that the intramuscular injection ($p>0.05$).

Discussion

Based on the results, it was shown that using MDA to immunize guinea pigs was not effective in eliciting a protective immune response after a single vaccination. Several studies have used transcutaneous methods to deliver vaccines, however, most vaccinations require multiple boosts, penetration enhancers, or adjuvants to illicit a protective immune response [63, 78]. Penetration enhancers alter the SC structure to increase the skin's permeability to hydrophilic molecules [21]. Adjuvants are compounds, such as cholera toxin, that stimulate an

immune response. They have been used with vaccines and have been shown to make them more immunogenic [78].

Conclusion

Microdermabrasion was not effective in immunizing guinea pigs using a single vaccination in this study. Multiple boosts may be needed to provide a strong immune response against influenza. Removing the epidermis may also increase the potency of the vaccine as compared to only removing the stratum corneum, as we done in this study.

REFERENCES

1. Prausnitz, M.R. and R. Langer, *Transdermal drug delivery.* Nature Biotechnology, 2008. **26**(11): p. 1261-1268.

2. Prausnitz, M.R., S. Mitragotri, and R. Langer, *Current status and future potential of transdermal drug delivery.* Nature Reviews Drug Discovery, 2004. **3**(2): p. 115-124.

3. Barry, B.W., *Breaching the skin's barrier to drugs.* Nature Biotechnology, 2004. **22**(2): p. 165-167.

4. Park, J.H., M.G. Allen, and M.R. Prausnitz, *Polymer microneedles for controlled-release drug delivery.* Pharmaceutical Research, 2006. **23**(5): p. 1008-1019.

5. Sullivan, S.P., N. Murthy, and M.R. Prausnitz, *Minimally invasive protein delivery with rapidly dissolving polymer microneedles.* Advanced Materials, 2008. **20**(5): p. 933-938.

6. Gill, H.S., D.D. Denson, B.A. Burris, and M.R. Prausnitz, *Effect of microneedle design on pain in human volunteers.* Clinical Journal of Pain, 2008. **24**(7): p. 585-594.

7. Fang, J.Y., W.R. Lee, S.C. Shen, Y.P. Fang, and C.H. Hu, *Enhancement of topical 5-aminolaevulinic acid delivery by erbium : YAG laser and microdermabrasion: a comparison with iontophoresis and electroporation.* British Journal of Dermatology, 2004. **151**(1): p. 132-140.

8. Lee, W.R., S.C. Shen, K.H. Wang, C.H. Hu, and J.Y. Fang, *Lasers and microdermabrasion enhance and control topical delivery of vitamin C.* Journal of Investigative Dermatology, 2003. **121**(5): p. 1118-1125.

9. Park, J.H., J.W. Lee, Y.C. Kim, and M.R. Prausnitz, *The effect of heat on skin permeability.* International Journal of Pharmaceutics, 2008. **359**(1-2): p. 94-103.

10. Kendall, M., *Engineering of needle-free physical methods to target epidermal cells for DNA vaccination.* Vaccine, 2005.

11. Plotkin, S., Offit, Paul, Orenstein, Walter, *Vaccines*. 5 ed. 2007: Saunders Book Company. 1748.

12. Gill, H.S., S.N. Andrews, S.K. Sakthivel, A. Fedanov, I.R. Williams, D.A. Garber, F.H. Priddy, S. Yellin, M.B. Feinberg, S.I. Staprans, and M.R. Prausnitz, *Selective removal of stratum corneum by microdermabrasion to increase skin permeability.* European Journal of Pharmaceutical Sciences, 2009. **38**(2): p. 95-103.

13. Lee, W.R., R.Y. Tsai, C.L. Fang, C.J. Liu, C.H. Hu, and J.Y. Fang, *Microdermabrasion as a novel tool to enhance drug delivery via the skin: An animal study.* Dermatologic Surgery, 2006. **32**(8): p. 1013-1022.

14. Bhalla, M., Thami Gurvinder P., *Microdermabrasion: Reappraisal and Brief Review of Literature.* American Society of Dermatological Surgury, 2006. **32**: p. 809-814.

15. Fujimoto, T., K. Shirakami, and K. Tojo, *Effect of microdermabrasion on barrier capacity of stratum corneum.* Chemical & Pharmaceutical Bulletin, 2005. **53**(8): p. 1014-1016.

16. Crotty, S. and S.L. Reynolds, *The new insulins.* Pediatric Emergency Care, 2007. **23**: p. 903-905.

17. *Transdermal Delivery of Drugs*, ed. A.F. Kydonieus, Berner, Bret. Vol. I. 1987, Boca Raton: CRC Press, Inc 205.

18. Davis, S.P., W. Martanto, M.G. Allen, and M.R. Prausnitz, *Hollow metal microneedles for insulin delivery to diabetic rats.* Ieee Transactions on Biomedical Engineering, 2005. **52**(5): p. 909-915.

19. Gill, H.S. and M.R. Prausnitz, *Coated microneedles for transdermal delivery.* Journal of Controlled Release, 2007. **117**(2): p. 227-237.

20. *Transdermal Drug Delivery*. 2 ed. Drugs and the Pharmaceutical Sciences, ed. R. Guy, Hadgraft, Jonathan. Vol. 123. 2003, New York: Marcel Dekker. 369.

21. Amsden, B.G. and M.F.A. Goosen, *Transdermal Delivery of Peptide and Protein Drugs: An Overview.* Aiche Journal, 1995. **41**(8): p. 1972-1997.

22. Frerichs, D.M., L.R. Ellingsworth, S.A. Frech, D.C. Flyer, C.P. Villar, J. Yu, and G.M. Glenn, *Controlled, single-step, stratum corneum disruption as a pretreatment for immunization via a patch.* Vaccine, 2008. **26**(22): p. 2782-2787.

23. Look, J.L., B. Butler, M. Al-Khalili, Y.H. Lai, V. Frolov, C. Zhang, J. Yang, D. Smyla, A. Mayo, J. Yu, M. Guebre-Xabier, S. Frech, L. Ellingsworth, R. Seid, and G. Glenn, *The adjuvant patch: A universal dose sparing approach for pandemic and conventional Vaccines.* Biopharm International, 2007. **20**(8): p. A34-A45.

24. Redelmeier, T., Schaefer, Hans, *Skin Barrier: Pinciples of Percutaneous Absorption*. 1996, Basel: Karger. 310.

25. Elsner, P., Berardesca, Enzo, Wilhelm, Klaus-Peter, *Bioengineering of the skin: skin biomechanics*. 2001, London: CRC Press. 276.

26. Freinkel, R., Woodley, David, *The Biology of the Skin*. 2000, New York: Parthenon. 432.

27. Lew, B.L., Y. Cho, and M.H. Lee, *Effect of serial microdermabrasion on the ceramide level in the stratum corneum.* Dermatologic Surgery, 2006. **32**(3): p. 376-379.

28. Shim, E.K., D. Barnette, K. Hughes, and H.T. Greenway, *Microdermabrasion: A clinical and histopathologic study.* Dermatologic Surgery, 2001. **27**(6): p. 524-530.

29. Glenn, G.M., C.P. Villar, D.C. Flyer, A.L. Bourgeois, R. McKenzie, R.M. Lavker, and S.A. Frech, *Safety and immunogenicity of an enterotoxigenic Escherichia coli vaccine patch containing heat-labile toxin: Use of skin pretreatment to disrupt the stratum corneum.* Infection and Immunity, 2007. **75**(5): p. 2163-2170.

30. Mkrtichyan, M., A. Ghochikyan, N. Movsesyan, A. Karapetyan, G. Begoyan, J.M. Yu, G.M. Glenn, T.M. Ross, M.G. Agadjanyan, and D.H. Cribbs, *Immunostimulant adjuvant patch enhances humoral and cellular immune responses to DNA immunization.* DNA and Cell Biology, 2008. **27**(1): p. 19-24.

31. Hendriks, F.M., D. Brokken, C.W.J. Oomens, and F.P.T. Baaijens, *Influence of hydration and experimental length scale on the mechanical response of human skin in vivo, using optical coherence tomography.* Skin Research and Technology, 2004. **10**(4): p. 231-241.

32. Pailler-Mattei, C., S. Pavan, R. Vargiolu, F. Pirot, F. Falson, and H. Zahouani, *Contribution of stratum corneum in determining bio-tribological properties of the human skin.* Wear, 2007. **263**: p. 1038-1043.

33. Pedersen, L. and G.B.E. Jemec, *Mechanical properties and barrier function of healthy human skin.* Acta Dermato-Venereologica, 2006. **86**(4): p. 308-311.

34. (CDC), C.f.D.C.P., *Update on Vaccine-Derived Polioviruses -- Worldwide, January 2006-August 2007.* MMWR: Morbidity & Mortality Weekly Report, 2007. **56**(38): p. 996-1001.

35. Roush, S.W. and T.V. Murphy, *Historical comparisons of morbidity and mortality for vaccine-preventable diseases in the United States.* Jama-Journal of the American Medical Association, 2007. **298**(18): p. 2155-2163.

36. Mikszta, J.A., J.B. Alarcon, J.M. Brittingham, D.E. Sutter, R.J. Pettis, and N.G. Harvey, *Improved genetic immunization via micromechanical disruption of skin-barrier function and targeted epidermal delivery.* Nature Medicine, 2002. **8**(4): p. 415-419.

37. Wermeling, D.P., S.L. Banks, D.A. Huclson, H.S. Gill, J. Glupta, M.R. Prausnitz, and A.L. Stinchcom, *Microneedles permit transdermal delivery of a skin-impermeant medication to humans.* Proceedings of the National Academy of Sciences of the United States of America, 2008. **105**(6): p. 2058-2063.

38. Chen, D., K.F. Weis, Q. Chu, C. Erickson, R. Endres, C.R. Lively, J. Osorio, and L.G. Payne, *Epidermal Powder Immunization Induces both Cytotoxic T-Lymphocyte and Antibody Responses to Protein Antigens of Influenza and Hepatitis B Viruses.* J. Virol., 2001. **75**(23): p. 11630-11640.

39. Herndon, T., Gonzalez, Salvador, Gowrishankar, TR, Anderson, R, Weaver, James, *Transdermal microconduits by microscission for drug delivery and sample acquisition.* Biomed Central, 2004. **2**: p. 11.

40. Cryan, S.-A., N. Sivadas, and L. Garcia-Contreras, *In vivo animal models for drug delivery across the lung mucosal barrier.* Advanced Drug Delivery Reviews, 2007. **59**(11): p. 1133-1151.

41. Dunkin, C.S.J., J.M. Pleat, P.H. Gillespie, M.P.H. Tyler, A.H.N. Roberts, and D.A. McGrouther, *Scarring occurs at a critical depth of skin injury: Precise measurement in a graduated dermal scratch in human volunteers.* Plastic and Reconstructive Surgery, 2007. **119**(6): p. 1722-1732.

42. Davidson, J.M. *Animal models for wound repair*. in *Special Symposium on Proteolysis and Tissue Repair, at the 7th Annual Meeting of the European-Tissue-Repair-Society*. 1997. Cologne, Germany.

43. Hantash, B.M., L.M. Zhao, J.A. Knowles, and H.P. Lorenz, *Adult and fetal wound healing.* Frontiers in Bioscience, 2008. **13**: p. 51-61.

44. Coulombe, P.A., *Wound epithelialization: Accelerating the pace of discovery.* Journal of Investigative Dermatology, 2003. **121**(2): p. 219-230.

45. Hinman, C.D., H. Maibach, and G.D. Winter, *Effect of Air Exposure and Occlusion on Experimental Human Skin Wounds.* Nature, 1963. **200**(490): p. 377-&.

46. Silverman, R.A., J. Lender, and C.A. Elmets, *Effects Of Occlusive and Semiocclusive Dressings on the Return of Barrier Function to Transepidermal Water Loss in Standarized Human Wounds.* Journal of the American Academy of Dermatology, 1989. **20**(5): p. 755-760.

47. Visscher, M., S.B. Hoath, E. Conroy, and R.R. Wickett, *Effect of semipermeable membranes on skin barrier repair following tape stripping.* Archives of Dermatological Research, 2001. **293**(10): p. 491-499.

48. Gupta, J. and M.R. Prausnitz, *Recovery of Skin Barrier Properties After Sonication In Human Subjects.* Ultrasound in Medicine and Biology, 2009. **35**(8): p. 1405-1408.

49. Williams, A., *Transdermal and Topical Drug Delivery*. 2003, London: Pharmaceutical Press. 242.

50. Arora, A., M.R. Prausnitz, and S. Mitragotri, *Micro-scale devices for transdermal drug delivery.* International Journal of Pharmaceutics, 2008. **364**(2): p. 227-236.

51. Banga, A.K., *Microporation applications for enhancing drug delivery.* Expert Opinion on Drug Delivery, 2009. **6**(4): p. 343-354.

52. Baxter, J. and S. Mitragotri, *Needle-free liquid jet injections: mechanisms and applications.* Expert Review of Medical Devices, 2006. **3**(5): p. 565-574.

53. Prausnitz, M.R., Mikszta JA, Cormier M, Andrianov AK., *Microneedle-based vaccines.* Current Topics in Microbiology and Immunology, 2009. **333**: p. 369-93.

54. Song, J.Y., H.A. Kang, M.Y. Kim, Y.M. Park, and H.O. Kim, *Damage and recovery of skin barrier function after glycolic acid chemical peeling and crystal microdermabrasion.* Dermatologic Surgery, 2004. **30**(3): p. 390-394.

55. Rajan, P. and P.E. Grimes, *Skin barrier changes induced by aluminum oxide and sodium chloride microdermabrasion.* Dermatologic Surgery, 2002. **28**(5): p. 390-393.

56. Freedman, B., Rueda-Pedraza, Eugenia, Waddell, Sharon, *The epidermal and dermal changes associated with microdermabrasion.* Dermatol Surg, 2001. **27**: p. 1031-1034.

57. Karimipour DJ, K.S., Johnson TM; Orringer JS, Hamilton T, Hammerberg C, Voorhees JJ, Fisher G, *Microdermabrasion with and without aluminum oxide crystal abrasion: A comparative molecular analysis of dermal remodeling.* Journal of the American Academy of Dermatology, 2006. **54**(3): p. 405-410.

58. Martanto, W., S.P. Davis, N.R. Holiday, J.W. Wang, H.S. Gill, and P. M.R., *Transdermal Delivery of Insulin Using Microneedles in Vivo.* Pharmaceutical Research, 2004. **21**(6): p. 947-952.

59. Prausnitz, M.R., *Microneedles for transdermal drug delivery.* Advanced Drug Delivery Reviews, 2004. **56**(5): p. 581-587.

60. Gupta, J., E.I. Felner, and M.R. Prausnitz, *Minimally Invasive Insulin Delivery in Subjects with Type 1 Diabetes Using Hollow Microneedles.* Diabetes Technology & Therapeutics, 2009. **11**(6): p. 329-337.

61. Kim, Y.C., P.J. Ludovice, and M.R. Prausnitz, *Transdermal delivery enhanced by magainin pore-forming peptide.* Journal of Controlled Release, 2007. **122**(3): p. 375-383.

62. *Transdermal Delivery of Drugs*, ed. A.F. Kydonieus, Berner, Bret. Vol. III. 1987: CRC Press, Inc. 160.

63. Skountzou, I., F.-S. Quan, J. Jacob, R.W. Compans, and S.-M. Kang, *Transcutaneous immunization with inactivated influenza virus induces protective immune responses.* Vaccine, 2006. **24**(35-36): p. 6110-6119.

64. Lin, Y. and Z.J. Sun, *Current views on type 2 diabetes.* Journal of Endocrinology, 2010. **204**(1): p. 1-11.

65. Santamaria, P., *The Long and Winding Road to Understanding and Conquering Type 1 Diabetes.* Immunity, 2010. **32**(4): p. 437-445.

66. Apovian, C.M., R.M. Bergenstal, R.M. Cuddihy, Y. Qu, S. Lenox, M.S. Lewis, and L.C. Glass, *Effects of Exenatide Combined with Lifestyle Modification in Patients with Type 2 Diabetes.* The American Journal of Medicine, 2010. **123**(5): p. 468.e9-468.e17.

67. Henkin, R.I., *Inhaled insulin-Intrapulmonary, intranasal, and other routes of administration: Mechanisms of action.* Nutrition, 2010. **26**(1): p. 33-39.

68. Brown, M.B., G.P. Martin, S.A. Jones, and F.K. Akomeah, *Dermal and transdermal drug delivery systems: Current and future prospects.* Drug Delivery, 2006. **13**(3): p. 175-187.

69. Spencer, J.M. and E.S. Kurtz, *Approaches to document the efficacy and safety of microdermabrasion procedure.* Dermatologic Surgery, 2006. **32**(11): p. 1353-1357.

70. Berrutti, L.E., A.J. Singer, and S.A. McClain, *Histopathologic effects of cutaneous tape stripping in pigs.* Academic Emergency Medicine, 2000. **7**(12): p. 1349-1353.

71. Tanaka, M., Y.X. Zhen, and H. Tagami, *Normal recovery of the stratum corneum barrier function following damage induced by tape stripping in patients with atopic dermatitis.* British Journal of Dermatology, 1997. **136**(6): p. 966-967.

72. Rizzi, S.C., Z. Upton, K. Bott, and T.R. Dargaville, *Recent advances in dermal wound healing: biomedical device approaches.* Expert Review of Medical Devices, 2010. **7**(1): p. 143-154.

73. Jahoda, C.A.B. and A.J. Reynolds, *Hair follicle dermal sheath cells: unsung participants in wound healing.* Lancet, 2001. **358**(9291): p. 1445-1448.

74. Davies, D.J., Ward, R.J., Heylings, J.R., *Multi-species assessment of electrical resistance as a skin integrity marker for in vitro percutaneous absorption studies.* Toxicology in Vitro, 2004. **18**: p. 351-358.

75. Kim, H.S., S.H. Lim, J.Y. Song, M.Y. Kim, J.H. Lee, J.G. Park, H.O. Kim, and Y.M. Park, *Skin barrier function recovery after diamond microdermabrasion.* Journal of Dermatology, 2009. **36**(10): p. 529-533.

76. Milewski, M., N.K. Brogden, and A.L. Stinchcomb, *Current aspects of formulation efforts and pore lifetime related to microneedle treatment of skin.* Expert Opinion on Drug Delivery, 2010. **7**(5): p. 617-629.

77. Banks, S.L., R.R. Pinninti, H.S. Gill, K.S. Paudel, P.A. Crooks, N.K. Brogden, M.R. Prausnitz, and A.L. Stinchcomb, *Transdermal Delivery of Naltrexol and Skin Permeability Lifetime after Microneedle Treatment in Hairless Guinea Pigs.* Journal of Pharmaceutical Sciences, 2010. **99**(7): p. 3072-3080.

78. Glenn, G.M., D.N. Taylor, X.R. Li, S. Frankel, A. Montemarano, and C.R. Alving, *Transcutaneous immunization: A human vaccine delivery strategy using a patch.* Nature Medicine, 2000. **6**(12): p. 1403-1406.

VITA

Samantha Nacole Andrews was born on November 18, 1980 in Fort Walton Beach, FL. She grew up in neighboring city of DeFuniak Springs, FL where she attended Walton County Schools. After graduating from Walton Senior High School in 1999, she attended the University of Florida (UF) and majored in Materials Science and Engineering and minored in premedical science. In 2004, she graduated from UF, with honors, with a Bachelor of Science Degree in Materials Science and Engineering and was accepted into the joint Biomedical Engineering Ph.D. program at the Georgia Institute of Technology and Emory University. Her thesis topic was Microdermabrasion for Transdermal Drug Delivery. She defended her thesis on August 17, 2010 and obtained her Ph.D. in Biomedical Engineering in December 2010.